UNIVERSITÀ DEGLI STUDI DI PADOVA

MASTER THESIS 2012:13

STRUCTURAL AND FLUYD-DYNAMIC ANALYSIS OF AN AXIAL COMPRESSOR WITH ADJUSTABLE INLET GUIDE VANES

By

Pachera Matteo
(Matriculation Number 1034265)

Thesis supervisors:
Prof. Dr.-Ing Pavesi Giorgio (Università degli studi di Padova)
Prof. Dr.-Ing. F.K. Benra (Universität Duisburg – Essen)

Università degli studi di Padova
Faculty for Engineering
Department of Industrial Engineering

Universität Duisburg – Essen, Campus Duisburg
Faculty for Engineering
Department of Mechanical Engineering
Institute for Energy and Environmental Engineering
Department of Turbomachinery

Contents

Acknowledgements

Vorrei sinceramente ringraziare il Professor Pavesi per l'aiuto e l'interesse mostrato nei confronti del mio lavoro di tesi, vorrei inotre ringraziare tutti i compagni che negli anni dell'universitÃ mi sono stati vicini in particolare Giacomo, Maicol, Alberto, Federico, Ettore e Francesco, gli amici che ho trovato in collegio Stefano, Enrico, Francesco, Andrea, Marco, Roberto, Nicola, Anthony, Alberto, Dario, Marco, Luca, Guido, Federico, Don, Principe e tutti coloro che hanno condiviso con me quattro magnifici anni. Vorrei ringraziare gli amici che sin dalle scuole superiori mi sono stati vicini Matteo, Simone, Mirko e Marco e anche quelli trovati negli ultimi anni: Davide, Maicol, Tomas, Cosmin, Paola, Annapaola, Caterina, Jari, Alessandra e Andrea.

Ich will mich auch bei meinen deutschen Freunden und Kollegen bedanken. Am Lehrstuhl f*ür* Str*ö*mungsmaschinen habe ich gelernt sowohl wissenschaftlich als auch praktisch zu arbeiten. Professor Benra, Doktor Dohmen, Sebastian Schuster, Clemens Domnick, Jan Schnitzler, Pradeep Nagabhushan, Alexander Kefalas, Botond Barabas und Stefan Clauss haben mir immer geholfen und viel deutsch beigebracht. In Duisburg habe ich auch eine neue Familie gefunden: Kenneth, Socrat, Nicole, Clark, Gustavo, Antonio, Bernardo, Breno, Poncho, Cesar, Ivan, Patricia, Guillaume, Selcen, Victor und Yann.

Vorrei infine ringraziare la mia famiglia che mi ha sostenuto moralmente

e materialmente in un persorso che mi ha reso prima di tutto una persona più matura e completa. A mia mamma che in questi anni mi ha sempre spinto a dare il massimo facendomi ottenere grandi soddisfazioni, a mio papà che mi ha trasferito la passione per il fuoristrada, ad Umberto che mi ha trasferito la sua passione per la montagna e per i viaggi e ai miei fratelli che mi hanno aiutato e sopportato per tutti questi anni. Inoltre voglio ricordare i miei nonni e i miei zii che sempre hanno saputo apprezzare il mio impegno e il mio lavoro.

Chapter 1

Introduction

A compressor is a mechanical device that increases the pressure and the energy of a gas[1]. Nowadays there are several types of compressors, but two main categories can be defined: Turbo-compressors and positive displacement compressors. The positive displacement compressors work isolating a finite volume of gas and reducing its available volume therefore rising the pressure. These can be in turn divided in Reciprocating compressors, where the compression is made by a piston, and Rotary compressors, where the compression is made with a screw, lobes or a scroll. The turbo-compressors on the other hand work with a continuous fluid field, where the energy exchange is obtained deflecting the flow. This machines can be divided regarding on the shape of the meridional channel in axial machines or centrifugal.

1.1 Introduction to the turbo-machinery theory

A turbo-compressor is a rotating machine composed by one or more stages[2] [3], these are in turn composed by a rotor and a stator. A rotor is a rotating

blades row fixed on the shaft while a stator is a static blade row fixed on the chasing of the compressor. In a compressor's stage the energy exchange is occurs only in the rotor. The blades receive the flow and due to their geometry these can decrease the circumferential component of the relative velocity, increasing the circumferential component of the absolute velocity. In the static row the fluid's energy doesn't change, but the velocity decreases increasing and balancing the static pressure at the outflow of the stage.

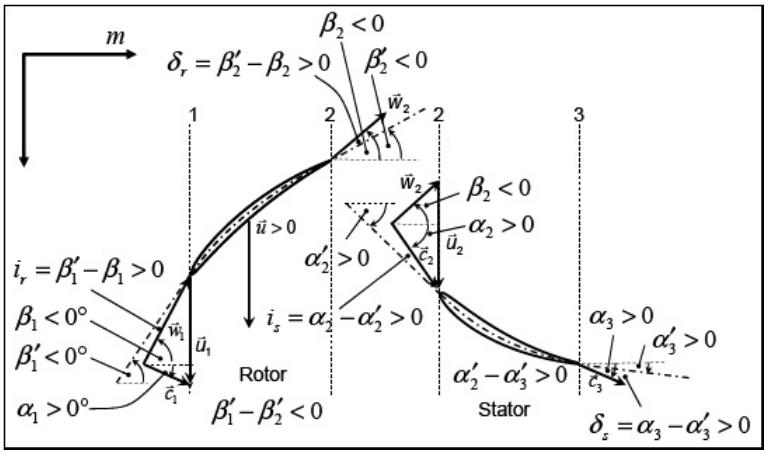

Figure 1.1: velocity triangle in an axial compressor's stage

The energy exchange can be written, using the Euler's pump and turbine equation, as $\Delta H_{tot} = c_{\theta\,out} \cdot u_{out} - c_{\theta\,in} \cdot u_{in}$, where c_θ is the circumferential component of the absolute speed at the inflow and at the outflow of a rotor and $u = \omega \cdot R$ is the tangential speed of the compressor. This formula explains the different contribution to the energy exchange. Regarding to the shape of the meridional section the axial machines have almost a constant radius thus the energy exchange is the result of the flow deflection. In the centrifugal machines the energy exchange is mainly a result of the radius variation, where due to the machine shape the radius increase and $u_{out} > u_{in}$. The

centrifugal machines thanks to their geometry, can exchange more energy and reach higher pressure ratio than the a axial machine's stage, where the work exchange is limited by the maximum flow deflection thus the stage's pressure ratio is limited by 1.2-1.3. However the centrifugal compressors present a modest usable mass flow, while the axial compressors allows greater flow rate. So, in order to reach high pressure ratio with high mass flow, the axial compressor are composed by several stages, stacked along the machine axis. A simple analysis of the compressor behaviour can be developed applying the thermodynamic equations. For a rotor is possible to write the first Low of thermodynamics for an open system:

$$\dot{m} \cdot (H_{out} + \frac{1}{2} \cdot c_{out}^2 - H_{in} + \frac{1}{2} \cdot c_{in}^2) = \dot{Q} - P \tag{1.1}$$

The power, P, is positive when the fluid gives its energy to the surroundings while the heat flux $\dot{Q}$ is positive when the fluid receives heat from the surroundings. Considering the Euler's equation, $P = \dot{m} \cdot (c_{\theta\, out} \cdot u_{out} - c_{\theta\, in} \cdot u_{in})$ and supposing an adiabatic process, it's possible to define a new thermodynamic variable, the Rothalpy, I:

$$I_{out} = H_{out} + \frac{1}{2} \cdot w_{out}^2 - \frac{1}{2} \cdot u_{out}^2 = I_{in} = H_{in} + \frac{1}{2} \cdot w_{in}^2 - \frac{1}{2} \cdot u_{in}^2 \tag{1.2}$$

This equation is anyway true also if the process is irreversible and there are energy losses. For a stator the exchanged power is equal to zero, if effect of the shaft is neglected, and the process is supposed to be adiabatic so the first law of thermodynamic can be written as the conservation of the total enthalpy:

$$H_{out}^0 = H_{out} + \frac{1}{2} \cdot c_{out}^2 = H_{in}^0 = H_{in} + \frac{1}{2} \cdot c_{in}^2 \tag{1.3}$$

The role of the stator in the stage is then to transform the kinetic energy in enthalpy, rising the static pressure through the stage.

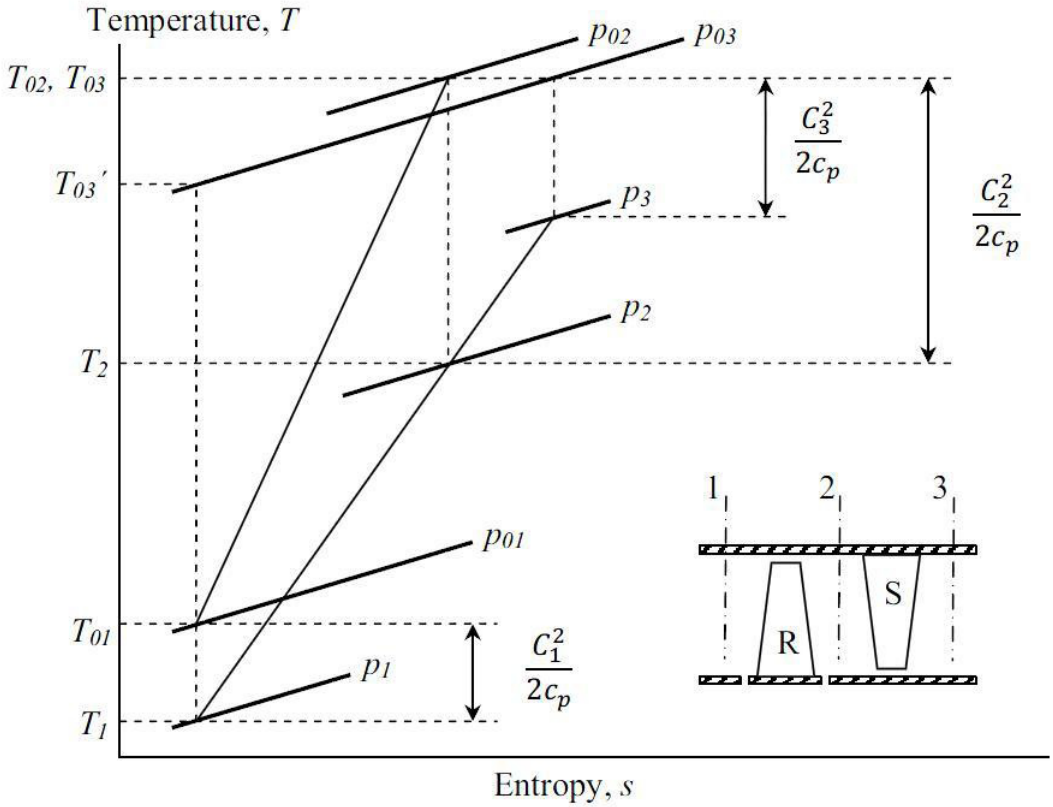

Figure 1.2: Entropy temperature diagram for a compressor stage

The overall performance of the stage can be summarized with some parameter. The pressure ratio is defined as the ratio between the total pressure at the outlet and the total pressure at the inlet:

$$\pi_c = \frac{P^0_{out}}{P^0_{in}} \tag{1.4}$$

The compressor's isentropic efficiency can be defined as the ratio between the work made by a ideal machine without losses and the real machine in order to reach the same static pressure a the outlet of the compressor.

$$\eta_{iso} = \frac{H^0_{out\,iso} - H^0_{in}}{H^0_{out\,real} - H^0_{in}} = \frac{\left(\frac{P_{out}}{P_{in}}\right)^{\frac{\gamma}{\gamma-1}} - 1}{\left(\frac{T_{out}}{T_{in}}\right) - 1} \tag{1.5}$$

The isentropic process is a particular adiabatic process where the energy degradation due to the fluidynamic losses are null. From the thermodynamic equations is possible to define a relation between the inlet and outlet flow characteristics.

$$\frac{p_{out}}{p_{in}} = \frac{T_{out}}{T_{in}}^{\left(\frac{\gamma}{\gamma-1}\right)} \tag{1.6}$$

The isentropic efficiency compares the ideal isentropic work with the real work in the machine. But this definition prevent to separate the losses source, fluid dynamic and thermodynamic. Thereby the isentropic efficiency is not only depending on the fluid-dynamic design, but also influenced by the pressure ratio and the Enthalpy exchange. Different compressors with the same fluid-dynamic design and with different pressure ratio show different isentropic efficiency, preventing the possibility of a correct comparison of the performance. Therefore also another efficiency parameter can be introduced, the polytropic efficiency, this is defined as the ratio between the work in a reversible process and the work in real machine, where the fluid conditions are the same a the begin and at the end of the process.

$$\eta_{pol} = \frac{H^0_{out\,pol} - H^0_{in}}{H^0_{out\,real} - H^0_{in}} = \frac{\left(\frac{P_{out}}{P_{in}}\right)^{\frac{n}{n-1}} - 1}{\left(\frac{T_{out}}{T_{in}}\right) - 1} \tag{1.7}$$

The politropic process is a reversible process which present also heat flux, so the relation between temperature and pressure can be written as:

$$\frac{p_{out}}{p_{in}} = \frac{T_{out}}{T_{in}}^{\left(\frac{n}{n-1}\right)} \tag{1.8}$$

The politropic efficiency allows to evaluate only the fluid-dynamic losses preventing the influence of the thermodynamic losses. The operating conditions of the compressor can also be defined with some non-dimensional parameter,

the flow coefficient, ϕ and the stage loading coefficient ψ.

$$\psi = \frac{\Delta H_{tot}}{U^2} \tag{1.9}$$

$$\phi = \frac{C_a}{U} \tag{1.10}$$

These parameters allow to study the machine behaviour independently from its dimensions. In the compressor the energy exchange is the sum of two contributions, $H_{tot} = H + \frac{1}{2} \cdot c^2$, the kinetic part and the internal energy part. In order to analyse the compressor behaviour we can define the degree of reaction R as follow:

$$R = \frac{\Delta H_{rotor}}{\Delta H^{\circ}_{stage}} = \frac{H_{out} - H_{in}}{H_{out} + \frac{1}{2} \cdot c^2_{out} - H_{in} - \frac{1}{2} \cdot c^2_{in}} \tag{1.11}$$

Increasing the degree of reaction the machine increases the fluid's static pressure instead keeping the same energy exchange. Decreasing the degree of reaction it's easier to reach high work exchange, but the velocity in the machine are high and also the losses get greater, so the efficiency drop down.

Chapter 2

Compressor's description

The examined compressor is an axial machine made up of four stage and inlet guide vanes at the begin[4]. The compressor design starts carrying out a parametric study according with the project's constrains. The boundary condition can be summarized as follow:

No.	Parameter	Value
1	Rotational speed, ω	11500 [RPM]
2	Hub radius R_{hub}	0.1152 [m]
3	Tip radius R_{tip}	0.187735 to 0.2 [m]
4	No. of stages, N	4
5	Inlet circumferential speed c_u	0 [m/s]
6	Maximum engine power	< 1 [MW]

Parameters like the inlet velocity, the mass flow and the pressure ratio at the design point are not defined as constrains, but they are the result of the preliminary design. The compressor's stages are designed with a constant hub radius and decreasing the shroud radius. This allows to use a cylindrical shaft for the machine reducing the compressor's manufacturing cost. Over the previous constrains there are also some other limits in the compressor's

design, the compressor musts be subsonic, so the tip speed of the air musts be lower than the speed of sound for the design conditions. For the energy exchange definition the mean deflection has to be lower than 20° and also the diffusion factor, DF, and de Halle Number,dH, defined as follow, are restricted:

$$DF = 1 - \frac{V_{out}}{V_{in}} + \frac{\Delta c_u}{2\sigma V_{in}} \leqslant 0.6 \tag{2.1}$$

$$dH = \frac{V_{out}}{V_{in}} \geqslant 0.72 \tag{2.2}$$

According with this boundary conditions the parametric design establishes the compressor's parameters:

No.	Parameter	Value
1	Mass flow rate, $\dot{m}$	14.5 [kg/s]
2	Pressure ratio π_c	1.86
3	No. of stator's blades	0.187735 to 0.2 [m]
4	No. of rotor's blades	4
5	Inlet circumferential speed c_u	0 [m/s]

The inflow conditions for the machine are:

Total pressure inlet,P_{in}° = 101325 [Pa]

Temperature inlet, P_{in}° =288.15 [K]

Density inlet, ρ= 1.225 [kg/m^3]

Axial velocity inlet, c_a = 154.11 [m/s]

Circumferential velocity inlet, c_u = 0 [m/s]

For the stage design all the stage are designed with the same axial and circumferential speed at the inflow and a the outflow of every stage, so the flow features are repeated at the mean radius, simplifying the machine's manufacturing.

Once the design of the stage is made for the mean radius, the next step has to define the three-dimensional distribution of the flow, analysing the flow-field features along the blade's span. As constrain of the project requests to use a free vortex scheme so the axial speed will be constant also along the blade. It's possible form the equations of thermodynamic and the equilibrium equation for the flow to get the velocity profile for the inlet and outlet section of the stage. The first equation is the radial equilibrium for a flow particle supposing an axial-symmetric flow field:

$$\frac{1}{\rho} \cdot \frac{dp}{dr} = \frac{c_u^2}{r} \tag{2.3}$$

The second equation is the first low of Thermodynamic in the differential formulation, Gibb's equation, derived along the radial direction:

$$\frac{dH}{dr} = T \cdot \frac{ds}{dr} + \frac{1}{\rho} \cdot \frac{dp}{dr} \tag{2.4}$$

The third equation is the total enthalpy's definition derived along the radial direction:

$$\frac{dH_{tot}}{dr} = \frac{dH}{dr} + c_\theta \cdot \frac{dc_\theta}{dr} + c_a \cdot \frac{dc_a}{dr} \tag{2.5}$$

Combining together the previous equations and neglecting the losses, $ds = 0$, it's possible to write the following equation:

$$\frac{dH_{tot}}{dr} = \frac{c_\theta^2}{r} + c_\theta \cdot \frac{dc_\theta}{dr} + c_a \cdot \frac{dc_a}{dr} \tag{2.6}$$

Solving this equation it's possible to determinate the velocity distribution in the stage. This solution impose the fixed value of the axial velocity and of the work exchanged along the span.

$$\frac{dH_{tot}}{dr} = 0 \tag{2.7}$$

$$\frac{dc_a}{dr} = 0 \tag{2.8}$$

Solving the obtained equation:

$$\frac{c_\theta^2}{r} + c_\theta \cdot \frac{dc_\theta}{dr} = 0 \tag{2.9}$$

We get the following result:

$$c_\theta \cdot u = Const. \tag{2.10}$$

The velocity distribution is hyperbolic with the radius, at the hub most of the work is obtained with the flow deflection while at the tip the work exchange is mainly done by the tangential velocity. Also the degree of reaction is not constant along the span blade.

$$R(r) = 1 - \frac{c_{\theta\,out} + c_{\theta\,in}}{2\omega r} = 1 - \frac{1 - R_{rm}}{(r/r_m)^2} \tag{2.11}$$

Where R_{rm} is the degree of reaction at the mean radius, the work exchanged in the stage is the same along the blade but the pressure and kinetic contribution are variable.

The last step for the compressor design is the profile definition, the velocity and pressure profile are defined in the stage's inflow and outflow, but is necessary to define the profile that can deflect the flow for the request angle. At this step the aspect ratio of the blade and the number of blades are already defined, these are important in order to avoid resonant forces to use for rotor a stators the number of blades must be prime. The design variable for the profile definition are the incidence angle and the profile shape. The incidence angle is defined as $i = \alpha_1 + \alpha_1'$ and it change the flow deflection increasing the work exchanged, but the pressure losses increase too. The incidence angle is imposed at $0°$ and the inlet angle of the fluid will correspond to the solid angle of the blade. At the trailing edge the finite difference of the

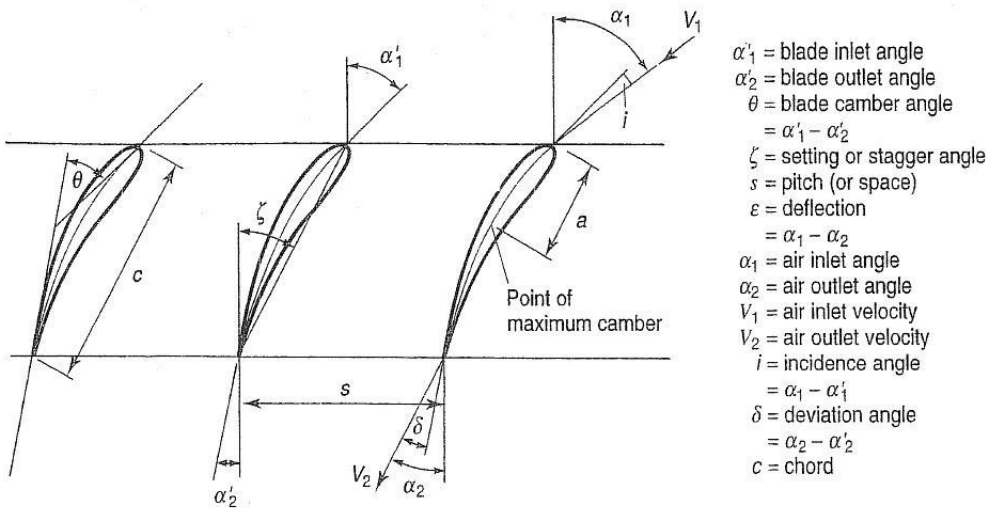

Figure 2.1: Blade cascade's features

pressure between pressure side and suction side deflect the streamline from the pressure side to the suction side, decreasing the deflection. There solid angle is defined knowing the flow deflection and the flow angle $\alpha_2 = \alpha'_2 + \delta$. To define the deflection δ the Carter's rule is used:

$$\delta = m\theta \frac{1}{\sqrt{\sigma}} \tag{2.12}$$

Where σ is the solidity defined as the ratio between the blade's cord and the blade to blade spacing, $\theta = \alpha'_1 - alpha'_2$ is the stagger angle and m is a coefficient. The profile used for the blade are from the NACA 65 Series, this profiles normally present a sharp trailing edge, but this become a limit for the blade manufacturing. So the profiles are modified and trailing edge present a rounded shape where the curvature radius is 0.666 of the curvature radius at the trailing edge. When all the single profiles are defined the three-dimensional blade has to be build up, stacking the different layers.

The profile stacking is important blade's life, since the centrifugal forces and the aerodynamic forces can generate high torque value. With this aim the stacking line is defined as strait radial line without any curvature.

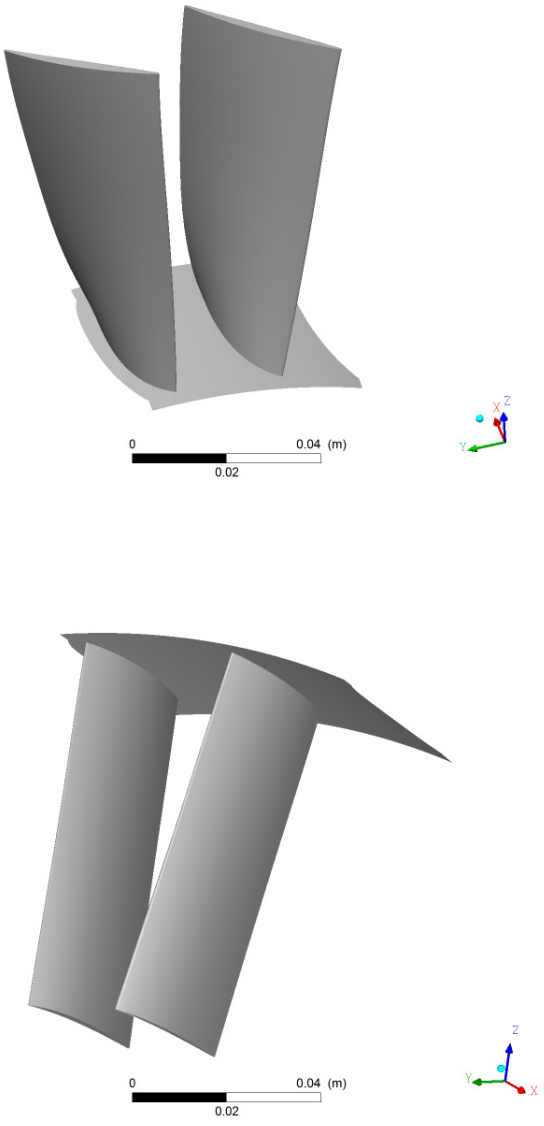

Figure 2.2: Two rotor's blades (above) and two stator's blades (below) of the first stage

Chapter 3

Numerical investigation

The compressor analysis has been carried out with the support of the Computation Fluid Dynamic, CFD. The theory behind the CFD is the fluid dynamic combined with the numerical resolution methods. The fluid behaviour is governed some physical principles, the mass is conserved, the Newton's second law and the energy is also conserved[5]. The flow description is made using the Eulerian specification where the flow characteristics are monitored in a fixed control volume. Considering a control volume where the flow can run, the accumulation of the mass in it is equal to the net flux trough the surfaces of the domain. The conservation of the mass can be expressed by the continuity equation:

$$\int_{C\,V} \left[\frac{\partial \rho}{\partial t} + \nabla \cdot (\rho \vec{v}) \right] dV = 0 \tag{3.1}$$

The equilibrium of the forces in a infinitesimal volume require the balance of the inertia, surface forces and volume forces.

$$\frac{d}{dt} \int_{C\,V} \rho \vec{v} dV = \int_{C\,V} \rho \vec{g} dV + \int_{C\,S} \sigma \cdot \vec{n} dS \tag{3.2}$$

Where the σ is the stress tensor defined as $\sigma = -pI + \tau$, τ is the viscous stress, parallel to the element's faces, while p is the pressure, normal to the

element's faces. In the differential form the newton equation can be written as:

$$\frac{\partial \rho \vec{v}}{\partial t} + \nabla \cdot (\rho \vec{v} \otimes \vec{v}) = \rho \vec{g} - \nabla p - \nabla \cdot \tau \tag{3.3}$$

The energy equilibrium for a infinitesimal volume is described by the first low of thermodynamic, where the energy accumulation is balanced by the heat transfer and by the work exchanged. The heat transferred to the control volume is the sum of the internal heat sources and the diffusive heat transfer:

$$s = \rho q dV + \kappa \nabla T dS \tag{3.4}$$

The work done is the sum of the surface forces and of the volume forces:

$$w = \rho \vec{g} \cdot \vec{v}\, dV + \vec{v} \cdot (\sigma \cdot \vec{n})\, dS \tag{3.5}$$

The fluid energy is the sum of the kinetic energy and of the specific internal energy:

$$\frac{d}{dt} \int_{C\,V} \rho E \, dV = \int_{C\,V} \frac{\partial (\rho E)}{\partial t} \, dV + \int_{C\,S} \rho E \, \vec{v} \cdot \vec{n} \, dS \tag{3.6}$$

Writing the balance energy balance in the differential form we get:

$$\frac{\partial (\rho E)}{\partial t} + \nabla \cdot (\rho E \, \vec{v}) = \nabla \cdot (\kappa \nabla T) + \rho q - \nabla \cdot (\rho v) + \tag{3.7}$$

$$+ v \cdot (\nabla \cdot \tau) + \nabla v : \tau + \rho g \cdot v \tag{3.8}$$

The previous equations define a differential problem where the unknown quantities are ρ, $\vec{v}$, e, p, τ, T, there are more than the equation in the system, so it's necessary to introduce other equations, for a ideal gas there is a relation between T, p, ρ and e:

$$\frac{p}{\rho} = RT \tag{3.9}$$

$$u = c_v(T - T_{ref}) \tag{3.10}$$

These equation are the ideal gas low and the caloric equation of state where the c_c and R are two constants. For the newtonia fluid the stress tensor is written as follow:

$$\tau = (\lambda \nabla \cdot \vec{v})I + 2\mu\, D(\vec{v}) \tag{3.11}$$

Where D is the deviatoric part of the tensor and is defined as:

$$D(\vec{v}) = \frac{1}{2}\left(\nabla\vec{v} + \nabla\vec{v}^T\right) \tag{3.12}$$

The problem can be summarized in a compact form using some new vectorial variables:

$$U = \begin{pmatrix} \rho \\ \rho\vec{v} \\ \rho E \end{pmatrix} \; F = \begin{pmatrix} \rho\vec{v} \\ \rho\vec{v} \otimes \vec{v} + p \cdot I - \tau \\ (\rho E + p)\vec{v} - \kappa\nabla T + \tau \cdot \vec{v} \end{pmatrix} \; Q = \begin{pmatrix} 0 \\ \rho\vec{g} \\ \rho(q + \vec{g} \cdot \vec{v}) \end{pmatrix} \tag{3.13}$$

With the new variables the problem written in the differential form is:

$$\frac{\partial U}{\partial T} + \nabla \cdot \vec{F} = Q \tag{3.14}$$

The Navier-Stokes equations is a three-dimensional differential problem, so there is an analytical solution for the equation, but until now the solution has not been founded jet and the problem is still open. Instead an analytical solution the problem is solved as an algebraical problem, the partial derivatives of the equations can be approximated by linear combinations of function values at the grid points,(mesh points).

3.1 Turbulence modelling

The turbulent flows represent the most difficult and tricky part of the numerical analysis. When the flow become locally unstable and the effects

of the viscosity are negligible respect to the fluid's inertia, the flow show high fluctuations in the pressure field and in the velocity field. Hence this flow is time-dependent, completely three-dimensional and with high Reynolds number. The turbulent flow present a wide range of frequency and length scale, the eddies develop in the flow field and change their size with energy exchange, this process is usually a reversible Reversible process. However when the eddies length scale is comparable with the molecular mean free path , the energy dissipated into heat by molecular viscosity, and the process become irreversible. For a long time the turbulent flow was supposed to be stochastic thereby impossible to study and predict with equation as done for the free shear flow. Nowadays is known the motion in a turbulent flow is not chaotic, but controlled by physical equation, but these request a greater computational power. So only the effect of the turbulent flow on the mean flow is modelled, ignoring the complete resolution of the turbulent flow field. Normally the numerical simulations run in the steady state form, so the computational time can be strongly reduced, but this hypothesis is not valid for the turbulent flow. Hence the solution to this problem is to count only the averaged effect of the turbulent flow using some models:

1. Zero equation, Algebraical model
2. One-Equation Models
3. Two-Equation Models
4. Second-Order Closure Models

The two equations models are the most used because they can predict the flow feature with a adequate accuracy and their computational cost is acceptable. These models present two variables for the turbulence solution. The first is always the turbulent kinetic energy, k, defined as the mean kinetic energy associated with eddies in turbulent flow per unit mass. The

second term is depending on the model, nowadays there are two common model, $k-\omega$ model[6] and $k-\epsilon$ model[7]. The other variables are ϵ defined as the dissipation, or rate of destruction of turbulence kinetic energy per unit time, and ω defined either as the rate at which turbulent kinetic energy is dissipated or as the inverse of the time scale of the dissipation. The three variables are related to each other and to the length scale, l, as follow:

$$\omega = c \cdot \frac{k^{\frac{1}{2}}}{l} \tag{3.15}$$

Where l is a constant value. These two models work in different manner and their result's accuracy is different depending also on the flow feature. The $k-\epsilon$ model has been shown to be useful for free-shear layer flows with relatively small pressure gradients. Similarly, for wall-bounded and internal flows, the model gives good results only in cases where mean pressure gradients are small; accuracy has been shown experimentally to be reduced for flows containing large adverse pressure gradients. Normally the $k-\epsilon$ model don't analyse correctly the details of the turbulent motion. The simulation show a false stability on the flow delaying the stall conditions. While The $k-\omega$ model has been shown to reliably predict the law of the wall when the model is used to resolve the viscous sub-layer, thereby eliminating the need to use a wall function, except for computational efficiency. The two models show a well agreement with the experimental results for different flow condition, so the better solution is obtained combing the two models. The use of a $k-\omega$ formulation in the inner parts of the boundary layer makes the model directly usable all the way down to the wall through the viscous sub-layer, hence the SST $k-\omega$ model[8] can be used as a Low-Re turbulence model without any extra damping functions. The SST formulation also switches to a $k-\epsilon$ behaviour in the free-stream and thereby avoids the common $k-\omega$ problem that the model is too sensitive to the inlet free-stream turbulence

properties. Authors who use the SST $k-\omega$ model often merit it for its good behaviour in adverse pressure gradients and separating flow. The SST $k-\omega$ model does produce a bit too large turbulence levels in regions with large normal strain, like stagnation regions and regions with strong acceleration. This tendency is much less pronounced than with a normal $k-\epsilon$ model though. As follow are listed the parameters used for the SST $k-\omega$ model: Kinematic Eddy Viscosity:

$$\nu_T = \frac{a_1 k}{max(a_1\omega, SF_2)} \tag{3.16}$$

Turbulence Kinetic Energy

$$\frac{\partial k}{\partial t} + U_j\frac{\partial k}{\partial x_j} = P_k - \beta\cdot k\omega + \frac{\partial}{\partial x_j}\left[(\nu + \sigma_k\nu_T)\frac{\partial k}{\partial x_j}\right] \tag{3.17}$$

Specific Dissipation Rate

$$\frac{\partial \omega}{\partial t} + U_j\frac{\partial \omega}{\partial x_j} = \alpha S^2 - \beta\cdot\omega^2 + \frac{\partial}{\partial x_j}\left[(\nu + \sigma_k\nu_T)\frac{\partial \omega}{\partial x_j}\right] + \tag{3.18}$$

$$+(2-F_1)\sigma_{\omega 2}\frac{1}{\omega}\frac{\partial k}{\partial x_i}\frac{\partial \omega}{\partial x_i} \tag{3.19}$$

Closure Coefficients and Auxiliary Relations

$$F_2 = \tanh\left[\left[max\left(\frac{2\sqrt{k}}{\beta\omega y}, \frac{500\nu}{\omega y^2}\right)\right]^2\right] \tag{3.20}$$

$$P_k = min\left(\tau ij\frac{\partial U_i}{\partial x_j}, 10\beta * k\omega\right) \tag{3.21}$$

$$F_1 = \tanh\left\{\left\{min\left[max\left(\frac{2\sqrt{k}}{\beta\omega y}, \frac{500\nu}{\omega y^2}\right), \frac{4\sigma_{\omega 2}k}{CD_{k\omega}y^2}\right]\right\}^4\right\} \tag{3.22}$$

$$CD_{k\omega} = max\left(2\rho\sigma_{\omega 2}\frac{1}{\omega}\frac{\partial k}{\partial x_i}\frac{\partial \omega}{\partial x_i}, 10^{-10}\right) \tag{3.23}$$

$$\phi = \phi_1 F_1 + \phi_2(1 - F_2) \tag{3.24}$$

$$\alpha_1 = \frac{5}{9}\,,\ \alpha_2 = 0.44 \tag{3.25}$$

$$\beta_1 = \frac{3}{40}\,,\ \beta_2 = 0.0828 \tag{3.26}$$

$$\beta* = \frac{9}{100} \tag{3.27}$$

$$\sigma_{k1} = 0.85\,,\ \sigma_{k2} = 1\sigma_{\omega 1} = 0.5\,,\ \sigma_{\omega 2} = 0.856 \tag{3.28}$$

3.2 Resolution scheme of the governing equations in CFX

Previously the Navier-Stokes equation were shown and explained, they define nonlinear partial differential equations. So the computer require a linearisation before to solve the system of equation, now algebraical. The fluid domain is divided in several cells, here i found the solution of the Navier-Stokes problem so the solution is not a continuous function, but defined only in some points. The discretization problem is solved using a hybrid finite-volume/finite-element method. The finite volume satisfies the different strict global conservations, the finite element method is use to evaluate the variation within the each element. Once the algebraical system of equations

is defined the solution is obtained solving all the equations simultaneously across the vertex or the nodes.

3.3 Numerical model for the flow in the compressor

The numerical analysis introduce some hypothesis and simplification due to reduce the computational cost of the simulation, but limiting the reliability of the result. The first hypothesis is the "steady state simulation" instead of "transient flow simulation". In a steady state simulation the solution is not depend on the time and the flow condition are reached after a relate long time. In many practical flow is assumed to be steady after initial unsteady flow development. When the simulation don't converge to the solution the reason could be numerical or physical. If the flow is unsteady and time dependent in some region of the machine, the steady state solution can't reach the convergence. The Total enthalpy is the model hypothesis used for the thermal exchange throughout the flow including the effects of the conduction convection, this models the conservation of the thermal energy and the kinetic energy through the compressor. This is preferred to the Thermal energy model because the contribution of the velocity is not negligible due to the Mach number greater than 0.3. The machine's model is simplified version of the real one, here only a one blade for every row is simulated, this require some observation on the domain interface. The periodic interface allow to simulate only one blade channel with a strong saving of computational time, the rotational connection require to define the machine axis and to have the same mesh on the periodic faces. It's supposed the flow is the same for every blade channel, preventing a not-axisymmetrical distribution of the

flow, which appends when the flow get unstable. The rotor and the stator are refereed to a rotating and to a stationary reference coordinate system, but they have to be matched together. In these simulation the stage interface is used, the flow on the outflow surface is averaged along the circumference. With this model it's supposed the interaction between the two components mixes the flow at the interface and the incoming flow has the same features for every point on the same circumference. For the compressor the blades row are fixed at the root to the shaft or to the casing, but the other surface has a relative speed compared with the blade. In the rotor the shroud surface rotates with a speed equal to $-\omega$ in the relative frame, so that means the casing in the stationary frame don't rotate. In the stator the hub rotate with a speed equal to ω hence this surface belongs to the shaft.

In order to simplify the meshing process, which use a structured mesh, the geometry of the real machine is different from the simulated one. The first group of simulations used a blade without fillet where the root of the blade was fixed to the shaft or to the casing without fillet, creating a 90° angle. The second group of simulations used a blade with constant radius fillet, 2 mm, so the connection between the blade and the casing or the shaft become smooth. In the real compressor the blade are made with fillet in order to avoid structural failure caused by fatigue stress. So the first group of simulations don't overlap the real geometry, but also the second geometry doesn't exactly copy the real machine. In the real machine all the stator blades can move so they are not directly fixed to the casing, but they are fixed with a shaft to the moving system. In the real machine there is a fillet in the stator blades but it has a variable radius and only near the shaft. For the rotor the real machine is made with a constant radius so the simulated geometry and the real geometry, except for the modelling and manufacturing

errors, are the same.

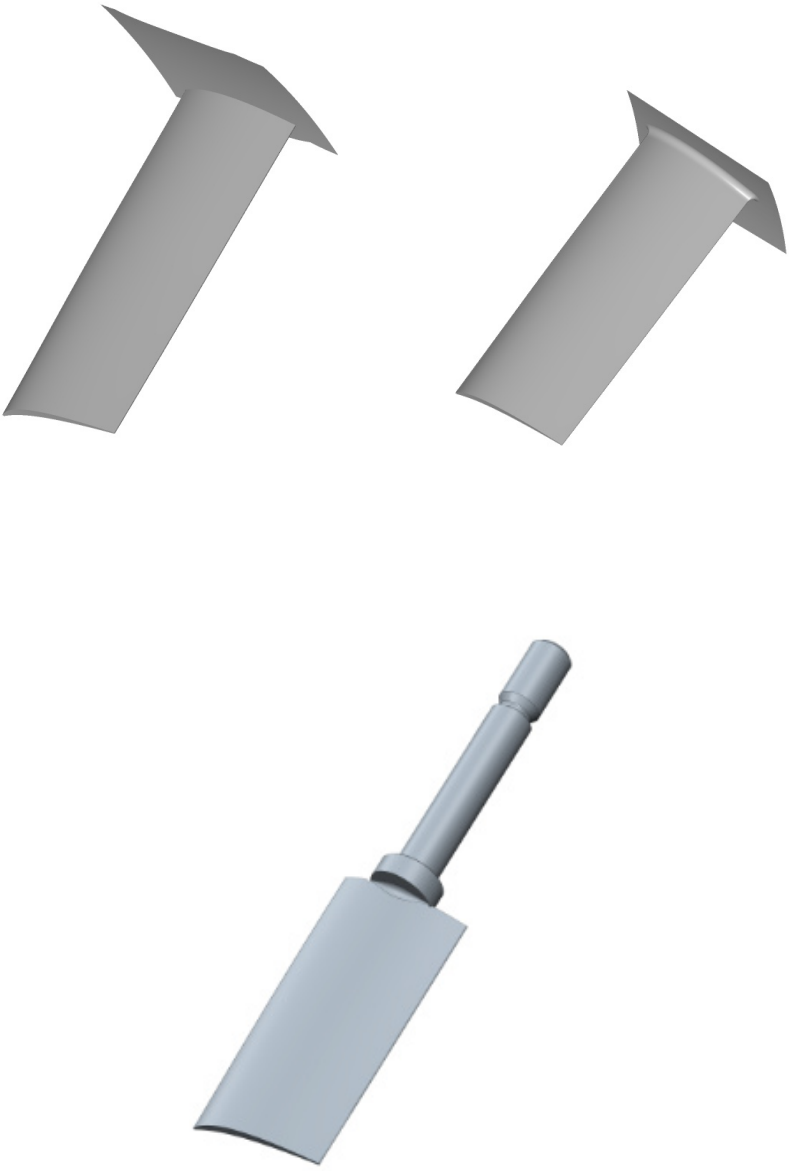

Figure 3.1: Comparison of the blade's geometry: the blade without fillet (top, let), the blade with constant radius fillet (top, right), real blade with a non-constant fillet (bottom)

3.4 Numerical model for the flow in the compressor

The simulations requires the usage of some boundary condition, these are constrains of the problem's solution. The boundary condition are defined at the inlet face and at the outlet face. The inlet face is placed at the inflow of the IGV row where it's supposed the flow aspirated by the machine. While the outlet is placed at the outflow if the fourth stator where it's supposed the flow is ousted. If in the inlet and in the outlet region the velocity is opposite to the allowed direction the solver put a wall surface in these region. When this happen the boundary surfaces have to be chanced, moving their position or using the opening option which allows also reverse flow.

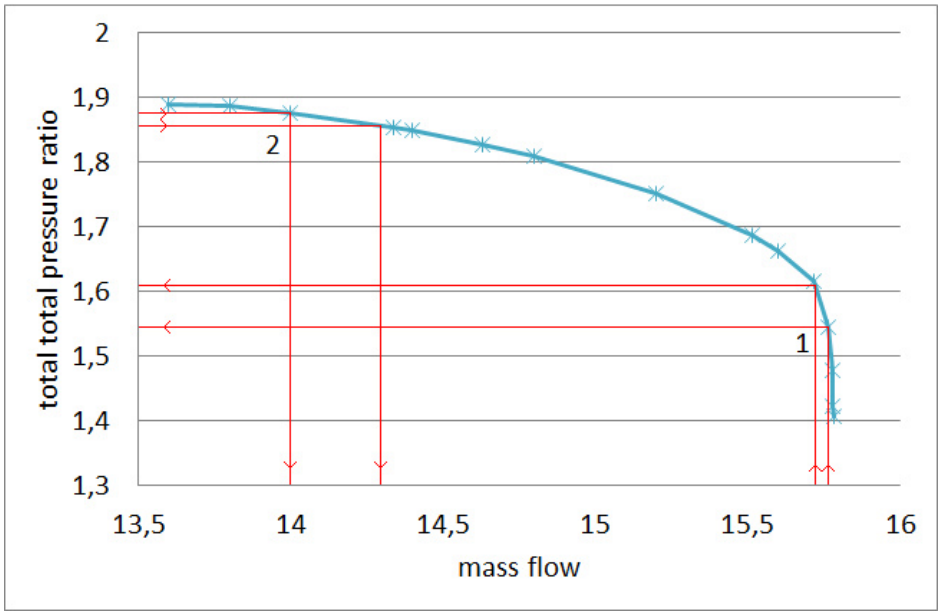

Figure 3.2: Compressor's map for the IGV 00 configuration and error propagation using mass flow outlet as Boundary condition, 1, and using the static pressure as boundary condition, 2.

The points on the compressor map are obtained with two different set-up of the boundary condition. For the points next to the choke where the slope of the compressor map is vertical the total pressure at the inlet and the static pressure at the outlet are fixed, while for the point next to the surge limit where the slope of the map is zero the mass flow outlet is fixed rather than the static pressure. The two different boundary condition are used to reduce the error propagation according with the shape of the compressor map. When the mass flow at the outlet is fixed as boundary condition the result of in the compressor map is the total pressure at the outlet and the total total pressure ratio, while when the static pressure is fixed the total pressure at the outlet is almost defined and the result of the simulation is the mass flow. So it's important to understand how in the different zones of the map the error propagates through the simulation. The formula of the Propagation of uncertainty[9] explains the propagation of the error form the variables to the function based on them:

$$\Delta f = \Delta f(x_1, x_2, ..., x_n, \Delta x_1, \Delta x_2, ..., \Delta x_n) = \left(\sum_{i=1}^{n} \left(\frac{\partial f}{\partial x_i} \Delta x_i \right)^2 \right)^{\frac{1}{2}} \quad (3.29)$$

For the compressor map two form can be written $\pi_c = f(\dot{m})$ or $\dot{m} = g(\pi_c)$ where $f = g^{-1}$, so there is only a variable for the two different functions. Whether in the analytical study the two writing are the same in a numerical analysis this in no more valid. For the points next to the surge line where the map has a vertical slope the static pressure outlet as boundary condition allows to write the map as $\dot{m} = g(\pi_c)$ and the error become:

$$\Delta \dot{m} = \frac{\partial g}{\partial \pi_c} \Delta \pi_c \quad (3.30)$$

The partial derive of g is almost zero and this reduce the error propagation in the map, the same happens next to surge where the slope is zero so the mass

flow at the outlet as boundary condition define the map points as $\pi_c = f(\dot{m})$ and the error become:

$$\Delta\pi_c = \frac{\partial f}{\partial \dot{m}}\Delta\dot{m} \tag{3.31}$$

Here the derive of f is also almost zero reducing the error propagation in the map definition. For the points in the halfway zone the solution are reached independently on the boundary condition showing a good agreement in the result.

Chapter 4

Mesh independence study

At the beginning of the analysis on the axial compressor is necessary to define the usable mesh for the investigation. The choice of the mesh's size is a deal between the quality of the prediction and the computational cost request for the simulations. A fine mesh allows better prediction of the machine's behaviour, but the computational cost isn't bearable for the available computational resources and for the required time. A coarse mesh is faster and doesn't require large computational resources, however the result's quality is poor and its prediction isn't trustworthy. Therefore is necessary to find a balance between the quality of the mesh and the time request by the simulation's resolution. The mesh independence study is a manner to find how the result is influenced by the size of the mesh and the coarsest mesh which can be used in the numerical investigation. Increasing the numbers of elements the monitored variables tend to an asymptotic value, hence the results are studied due to find the finest mesh whose properties are depending on the mesh, but with a feeble influence.

4.1 Preliminary mesh independence study

Before to start the numerical investigation a preliminary mesh independence study is carried out, but this study is partial because the compressor map is not known jet so the simulations are done only for the design point instead of the complete map.

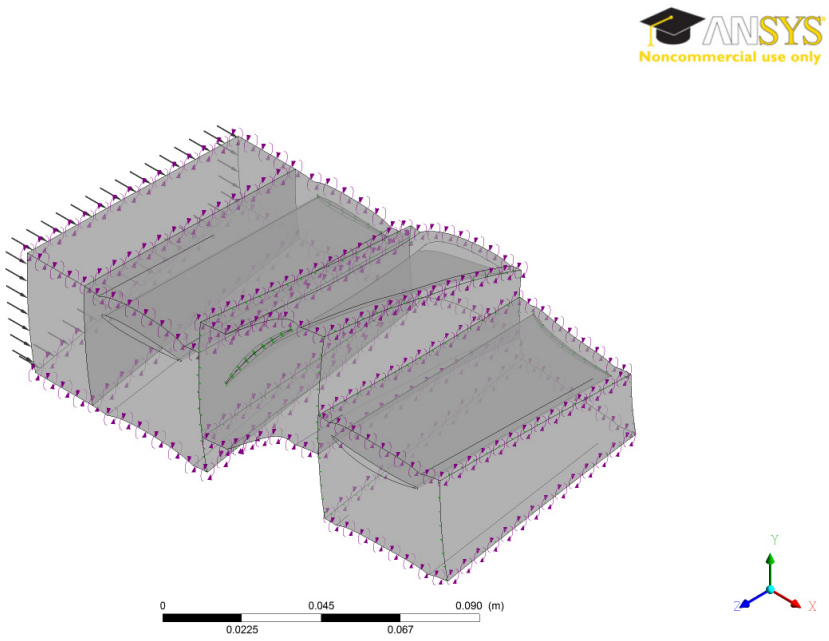

Figure 4.1: Percentage different for the total total pressure ratio, red line, and for the total static pressure ratio, blue line

Only the first stage and the Inlet Guide Vanes (IGV) are simulated saving time for the calculation and for the mesh generation. The mesh are created using the Ansys program Turbogrid and their features are summarized in the following table:

N.	Mesh 1	Mesh 2	Mesh 3	Mesh 4
N. Elem. IGV	70238	155128	304660	661978
N. Elem. R1	99600	195770	363008	679502
N. Elem. S1	85533	149968	274400	464417
N. Elem. Total	255371	500866	942068	1805897

The third mesh was already done and used for some previous investigation but from this model the other meshes are generated paying attention to the y^+ of the simulation and to the number of elements. The y^+ musts be below 70 on the wall surface because this allows a greater convergence and is request for the correct estimation in the boundary layer with the $k-\epsilon$ SST model. The number of elements, according to a good mesh quality, have to be one quarter half and the double number of the elements in the third mesh. For all the meshes also the convergence criteria is investigated, comparing for every mesh the results with different value of the maximum residual value allowed in the mesh domain, 10^{-3}, 10^{-4} and 10^{-5}. For the four mesh the simulation has the same boundary condition and the same set-up, the total pressure inlet is the atmospheric pressure 101325 [Pa] and the outlet condition is the mass flow 14,75 [kg s^{-1}]. The monitored parameters are the total pressure ratio and the static pressure ratio since the main aim of the study is the compressor map, total pressure ratio vs mass flow which is fixes as constrain. The relative difference for the pressure ratio are calculated referring to the value of the finest mesh:

$$\Delta\pi_c\% = \frac{\pi_c - \pi_{c\ finest\ mesh}}{\pi_{c\ finest\ mesh}} \cdot 100 \tag{4.1}$$

The picture show an asymptote for high value of the number of elements, but the difference between the finest mesh and the coarsest is small, less than 0.30%, so the finest mesh is chosen for the numerical investigation, but now it's necessary to compare the results also for different convergence criteria.

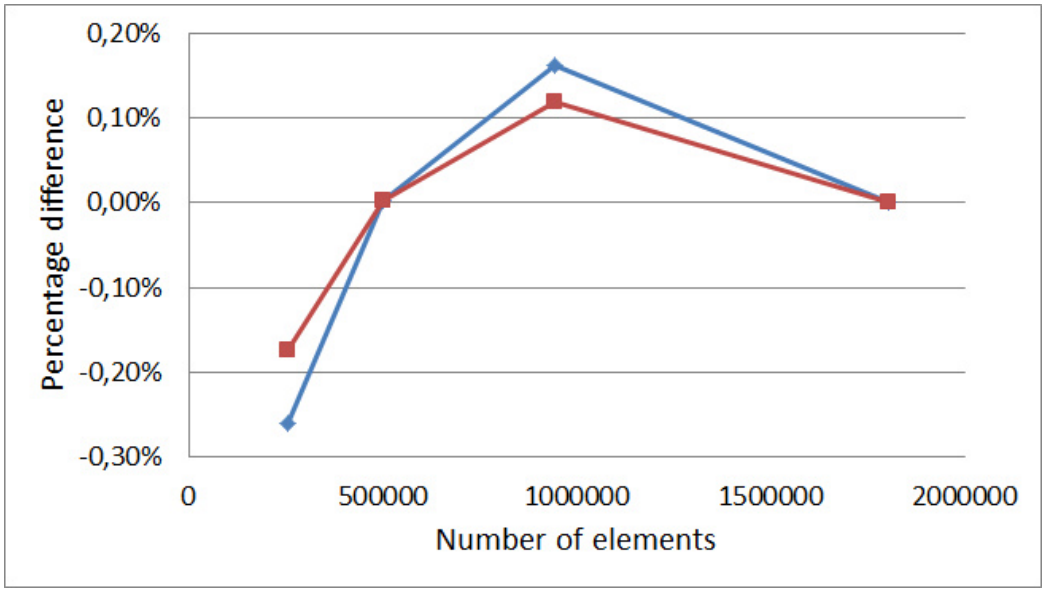

Figure 4.2: Percentage different for the total total pressure ratio, red line, and for the total static pressure ratio, blue line

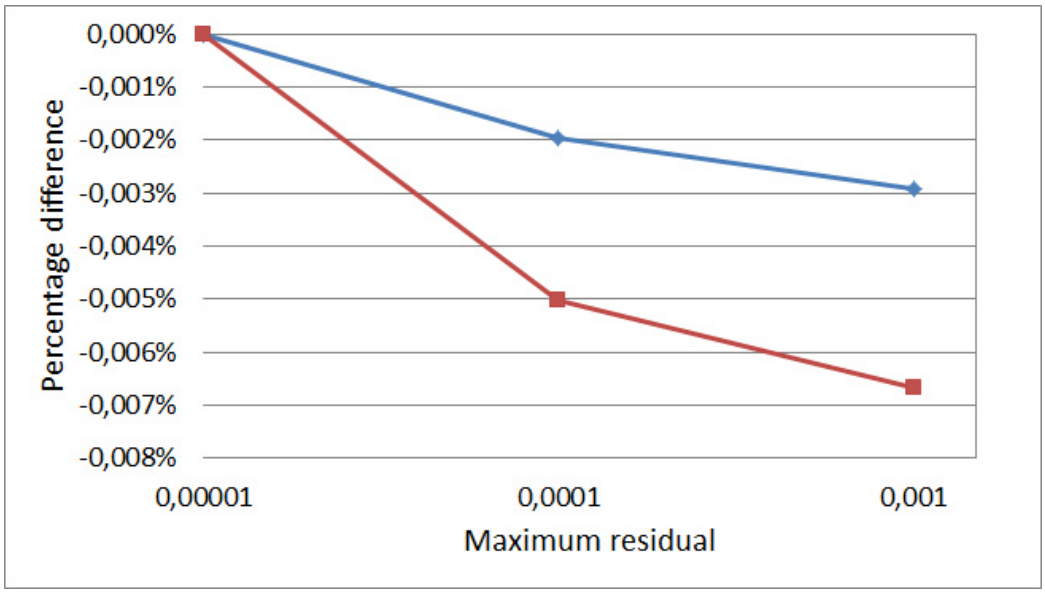

Figure 4.3: Percentage different for the total total pressure ratio, red line, and for the total static pressure ratio, blue line

The results here founded are in well agreement and the difference is less than 0.01%, almost zero. For the simulations the used convergence criteria is Maximum residual in the entire domain less than 10^{-3} with the coarsest mesh which has about one quarter of the elements of the initial mesh. Once the mesh's size is calculated the mesh are made also for the other stage and for the different IGV configurations. It's important to highlight the mesh created in Turbogrid use as geometrical model the points of the different layer in the blade, so the geometry could be not identical to the geometry created in the CAD model, because the algorithms for the surface creation are different in the two programs.

4.2 Mesh independence study along the operating line

Once the compressor map is generated a new mesh independence is carried out because the well agreement between the results at the design point doesn't assume a good agreement all along the operating line. In this study the entire compressor is simulated with the 00 IGV's angle. The study is also carried out comparing the simulation with the fillets and without in order to find the effect of the geometrical configurations. In the this section the result are compared only for the same geometrical configuration while the comparison between the two configurations is made later. The mesh data for the model without fillet are summarized in the following table:

N.	Mesh 1	Mesh 2	Mesh 3
N. Elem. IGV	70238	143191	393394
N. Elem. R1	109896	176120	421691
N. Elem. S1	94359	177454	308240
N. Elem. R2	96956	176399	408672
N. Elem. S2	89889	181618	312112
N. Elem. R3	101137	179553	438620
N. Elem. S3	93545	181859	315500
N. Elem. R4	110412	187348	429360
N. Elem. S4	114990	159447	420266
N. Elem. Total	881422	1562989	3447855

While the features of the mesh with fillet are summarized in the following table

N.	Mesh 1	Mesh 2	Mesh 3	Mesh 4
N. Elem. IGV	49756	89782	175240	385153
N. Elem. R1	53232	99564	198851	398464
N. Elem. S1	48356	90794	176751	387197
N. Elem. R2	52872	100874	187730	388932
N. Elem. S2	45028	86978	172782	381232
N. Elem. R3	51636	100314	184250	411172
N. Elem. S3	44254	82874	167282	370707
N. Elem. R4	51636	10874	189038	379062
N. Elem. S4	49672	92474	175865	405032
N. Elem. Total	445442	844528	1627769	3506951

For the different mesh are simulated the same operating points in order to allow to compare the simulations with different mesh and to understand how the mesh influence the result. It's important to know, given the complexity

of the geometry and the numerous elements, the mesh is not depending only on the number of the elements but also on the elements distribution and on the mesh quality. These parameters are controlled in both of the geometry models, but according to the availability of more elements finer meshes have a better quality. Looking at the map of the compressor the first important difference is the change of the surge limit, for finest mesh the last stable point move to lower mass flow increasing the operating range of the compressor.

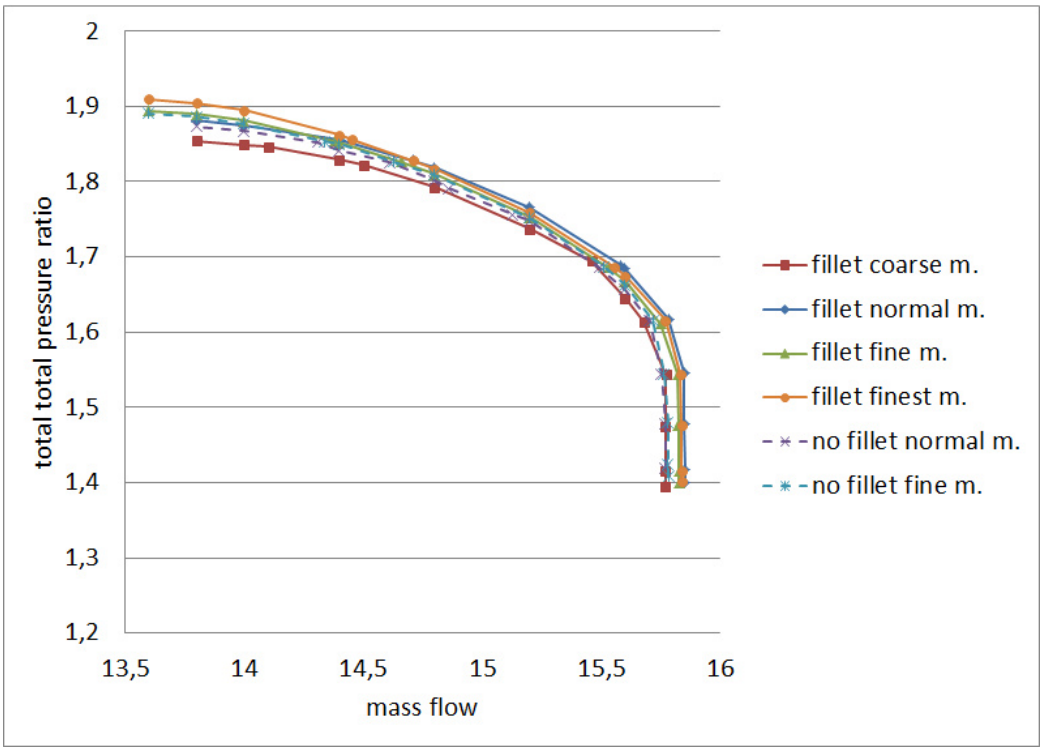

Figure 4.4: Compressor operating line for the IGV 00 °$configuration$

For the different operating points when the mass is fixed as boundary condition at the outlet the pressure ratio is monitored while the static pressure is the boundary condition the mass flow is monitored. With the different operating points is possible to make a diagram showing the trend of the percentage difference as function of the operating point and of the number of

element. For the simulations with the fillet included in the geometrical model the comparison is made between four mesh and is presented in the following picture:

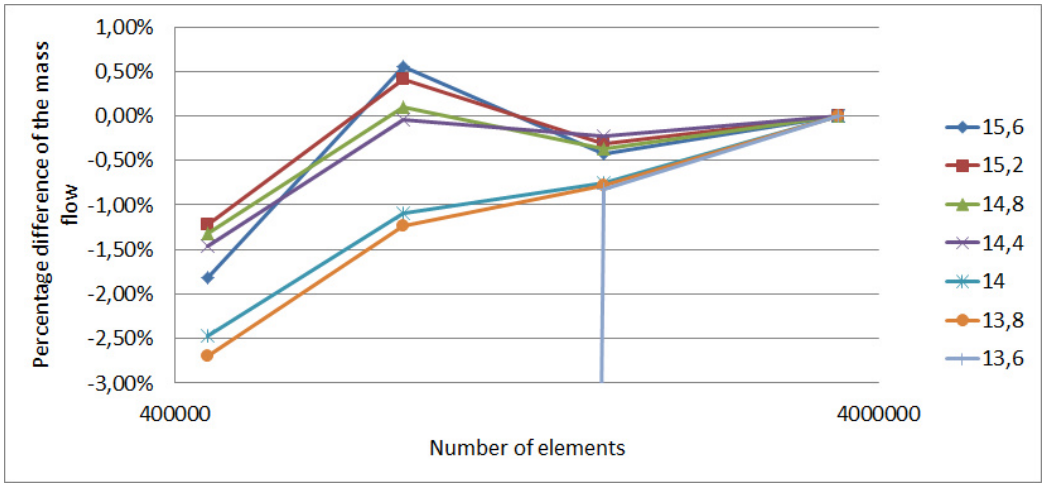

Figure 4.5: Percentage difference of the pressure ratio as function of the mesh size for the different operating points

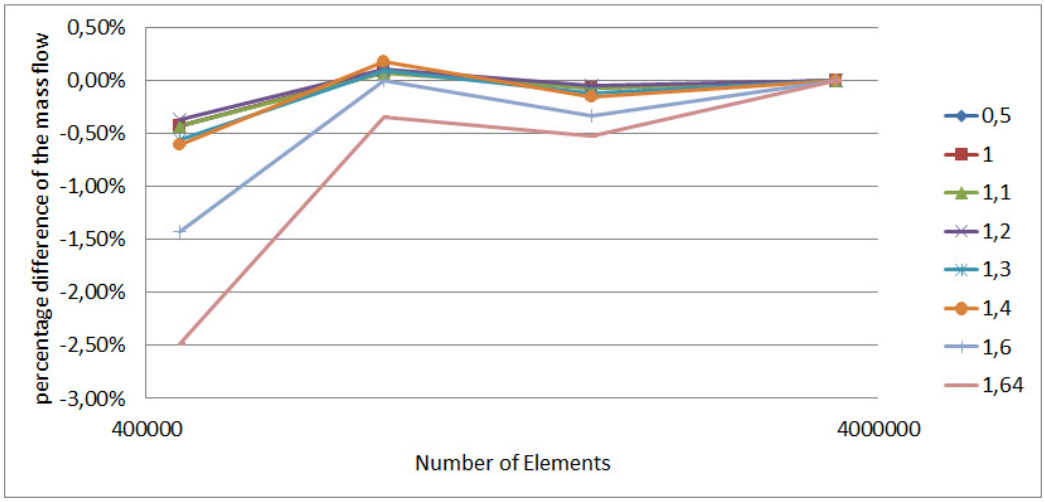

Figure 4.6: Percentage difference of the mass flow as function of the mesh size for the different operating points

Watching on the trend of the two curve they show how for the points next to the choke line the difference between the different meshes is small while approaching the surge line and the high pressure operating points the difference increase. In the simulation with the mesh 1 and the mesh 2 the last stable point is obtained with a mass flow outlet of 13.8 [kg s^{-1}] while for the mesh 3 and the mesh 4 also the simulation with a mass flow outlet of 13.6 [kg s^{-1}] can reach the convergence confirming the trend founded in the other points. The difference of the results for the different mesh are acceptable for the point far from the surge line where the difference of the result is always lower than 0.50 % referring to the mesh 4, but approaching the surge line the flow become more unstable and the mesh has a deep effect on the result. For the geometrical model without fillet the mesh independence is carried out with only three mesh and also for these simulation the percentage difference of the result is monitored.

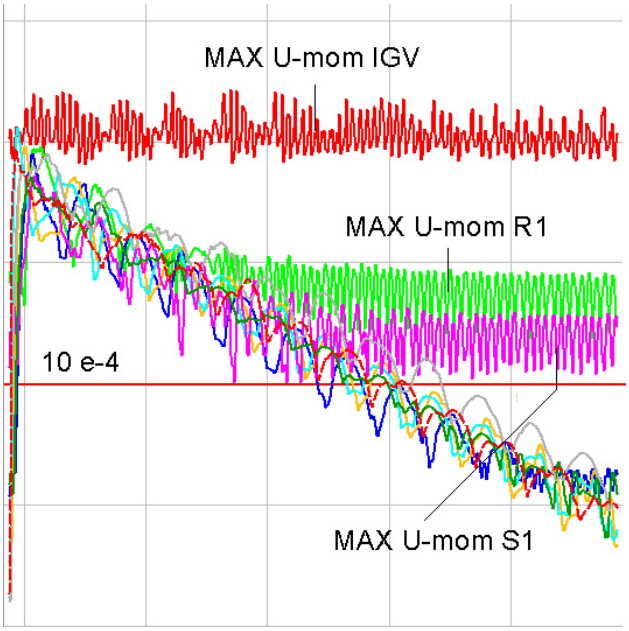

Figure 4.7: Maximum residual in the compressor.

For the mesh without fillet the result are presented only for two of the three mesh because the third one has convergence problems. In the simulated operating points, where the mass flow at the outlet and the total pressure inlet are defined as boundary conditions, the residual in the IGV stage keep staying over the convergence value 10^{-4}. The simulations are ran with double precision which avoid avoids any problem with the high aspect ratio of the mesh. The convergence process is presented in the following picture with also the flow field feature in the IGV where the compressor is simulated with a mass flow equal to 14.4 [kg s^{-1}].

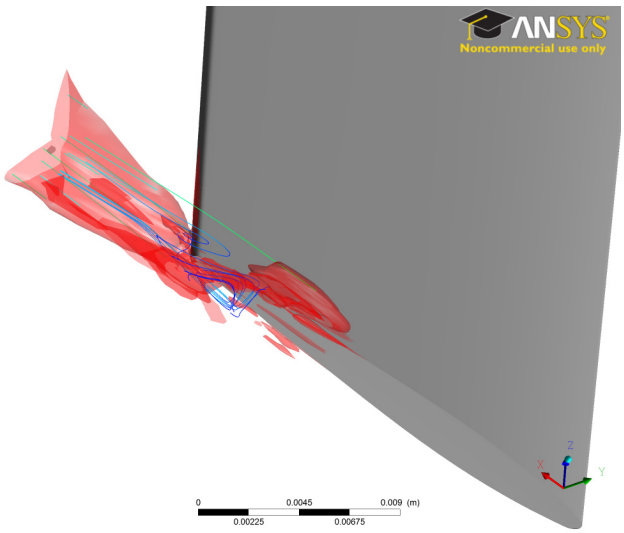

Figure 4.8: Isosurface where the U-Mom residual are equal to 10^{-4} and streamline near the high residual zone.

The high residual zone at the trailing edge of the blade near the tip clearance, here the flow is not stable and a small vortex grows there. The vortex is time depending and this prevent to find a solution with a stationary simulation. Comparing the results for the two mesh in the same way used for the other geometrical configuration the results show the same trend. Approaching the surge line the percentage difference of the residual increase,

the last stable point have 13.6 [kg s^{-1}] as mass flow for the fine mesh while 13.8 [kg s^{-1}] for the normal mesh. So the same conclusions made for the other geometrical model can be extended also to the geometry without fillet.

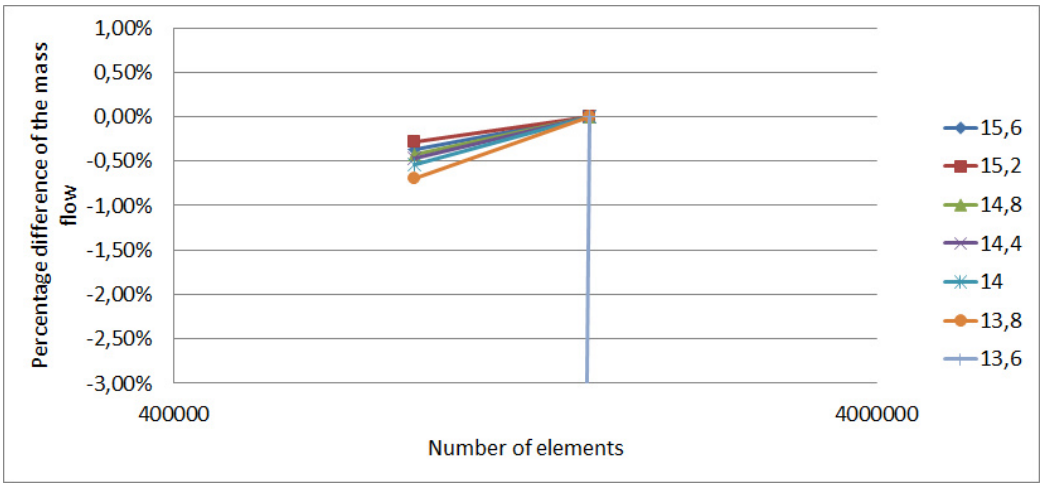

Figure 4.9: Percentage difference of the pressure ratio as function of the mesh size for the different operating points

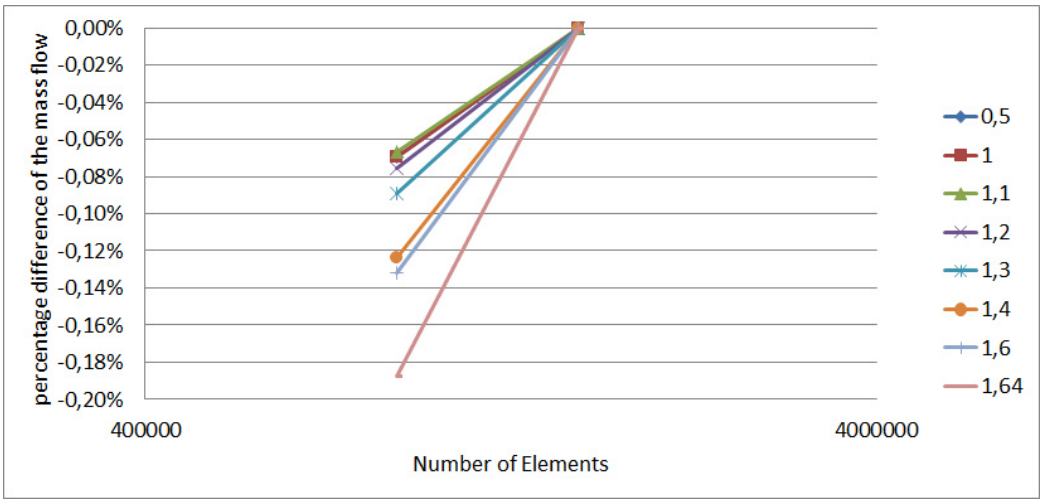

Figure 4.10: Percentage difference of the mass flow as function of the mesh size for the different operating points

According with the time limits and with the computational power the result of the coarse mesh are used and this mesh is the base model also for the other mesh with the different position also if the error is increasing approaching the surge line. The flow near the surge is very complex and the used model with steady state simulation and with mixing plane at the stage interface can introduce an uncertainty greater that the one on the mesh hence the simulations in that region can give us only qualitative information regard the flow in the pre-stall region.

Chapter 5

Compressor map for the geometry without fillet

The performances of a compressor are normally illustrated as a map where the pressure ratio is plotted as function of the mass flow. The compressor's operating line describes the machine's performances for a fixed inlet condition, rotational speed and geometrical configuration. When the geometry changes, like in the studied compressor, the operating lines become as many as the geometrical configurations. In the compressor the IGV and the stator's blades can change their orientation while the rotor blade are fixed, in the following pages the the behaviour of the axial compressor is studied moving only the IGV blades. These are rotated only for some specific angles: -15°, -10°, -5°,10°, 20° and 30° while 00° is the design configuration. The sign of the stagger angle is positive when the flow direction produced by the IGV is concordant with the rotational speed. The machine's configurations with negative IGV's angles have greater loads on the first rotor increasing the pressure ratio, while the configurations with positive IGV's angles have lower load on first rotor decreasing the overall pressure ratio. The geometry's

parameters and the rotational speed of the compressor are fundamental parameters for the machine's flexibility. Nowadays the compressors, especially if used in aeronautic engines, need a wide range of operating conditions, keeping high efficiency value and avoiding the not-stable operations over the surge line. Using different IGV's orientations the compressor is no more forced to work only along a single operating line, but it can move its operating line with more degree of freedom. The variable-geometry compressors give a lot of new opportunities for the compressor usage, but a deep analysis of the machine's behaviour is required. A new geometrical configuration changes the matching between the stages thus the compressor doesn't work any more as supposed in the design condition.

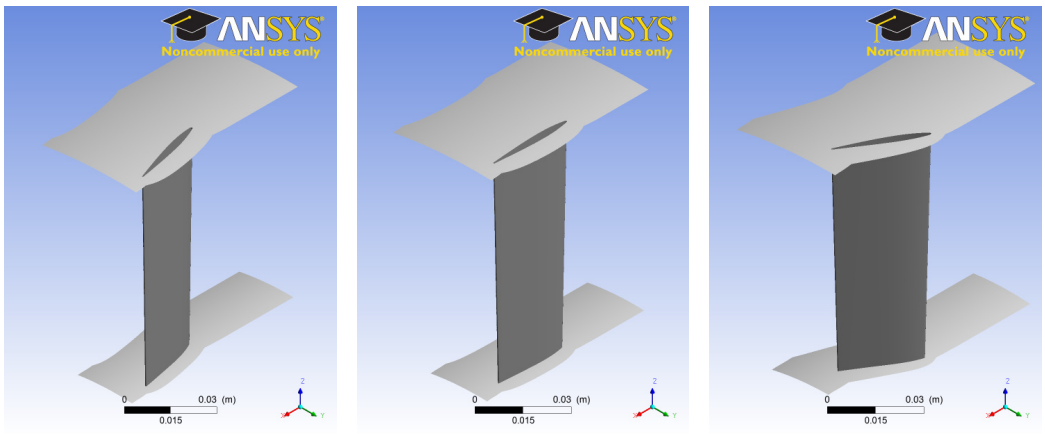

Figure 5.1: Some IGV without fillet for -15° (left), 00° (center) and 30° (right) configurations

The compressor's map contains all the operating lines and defines also the limits of the compressor's usage range, surge line and choke line. The surge line indicates the maximum pressure ratio and the minimum mass flow with which the compressor can still work in a stable manner. This is obtained

enveloping the last stable point for every IGV's orientation. On the other side of the operating line, the choke line defines the maximum mass flow which can pass thought the compressor, the choke happens when the Mach number is equal to 1 at the throat section of the compressor. The position of the operating lines is the result of the machine's geometry, increasing the loading on the stages normally the compressor works with greater pressure ratio and greater mass flow. For a single stage the energy exchange is written using the first law of thermodynamic and Euler's formula.

$$c_{\theta\,out} \cdot u_{out} - c_{\theta\,in} \cdot u_{in} = \frac{kR}{k-1} T_{in} \cdot (\pi^{\frac{k-1}{k\eta_{pol}}} - 1) \tag{5.1}$$

When the machine has an axial configuration the previous relation become:

$$c_{ax\,in}[\tan(\alpha_{out}) \cdot \frac{\rho_{in}}{\rho_{out}} \cdot \frac{A_{in}}{A_{out}} - \tan(\alpha_{in})] \cdot u = \frac{kR}{k-1} T_{in} \cdot (\pi^{\frac{k-1}{k\eta_{pol}}} - 1) \tag{5.2}$$

Supposing that the polytropic efficiency, the density ratio and the outflow flow direction are nearly constant, the pressure ratio is function of the inlet velocity and of the inlet angle. Defining the inlet the mass flow and inlet speed as constant, the exchanged work and the pressure ratio increase when the inlet angle α_{in} is reduced moving the operating point above in the compressor map. Reducing the IGV's angle the compressor's operating line move to the right in the map flow because the choke and the stall occur with greater mass flow. This when the compressor is choked is limited by the available mass flow thought the throat section.

$$\dot{m} = A \cdot \rho \cdot \sqrt{KRT} \tag{5.3}$$

With greater pressure ratio and greater energy exchange also the density and the temperature increase hence the choke limit move to greater mass flow reducing the IGV's angle. The surge line is influenced by the incidence angle which in turn depends on the IGV orientation and on the mass flow.

The incidence increase reducing the IGV's angle and reducing the mass flow, the critical condition are reached with a greater mass flow since the blade are already loaded by the IGV.

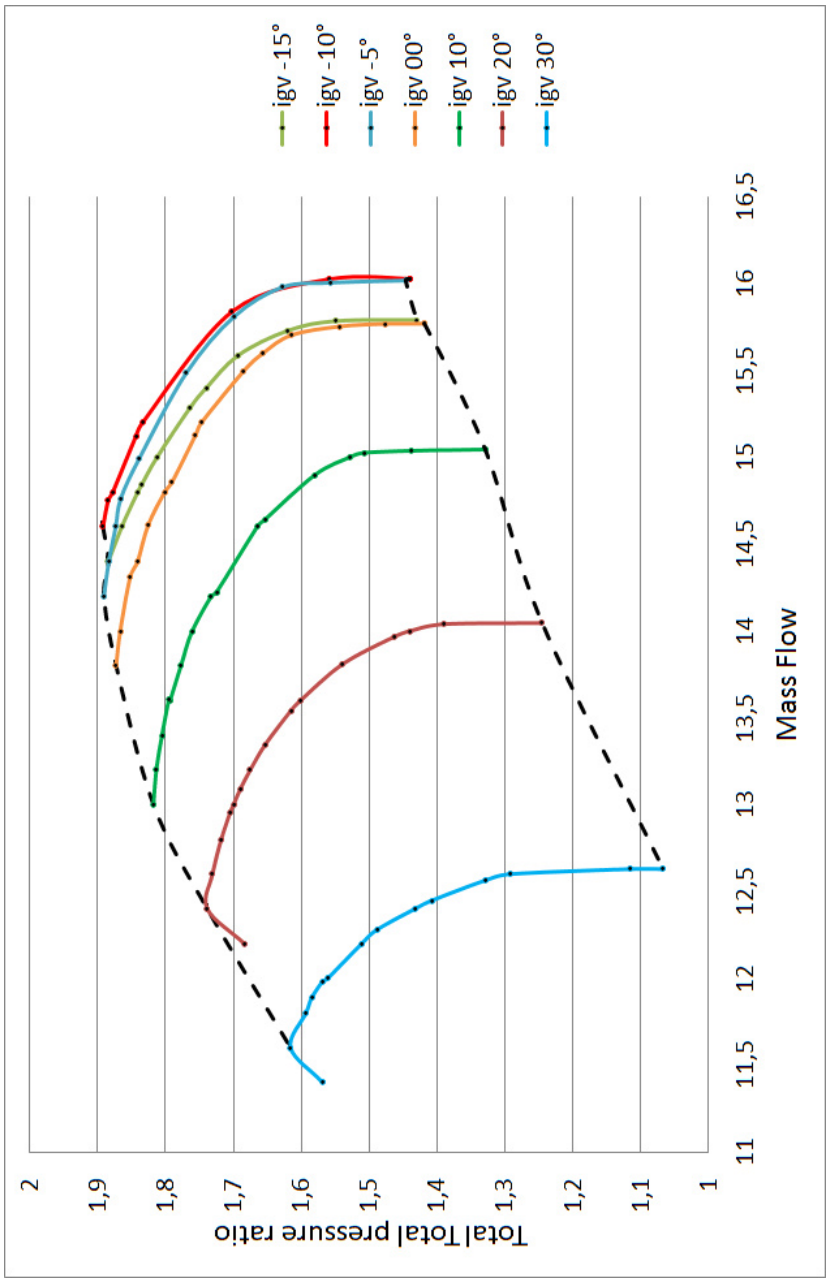

Figure 5.2: Compressor map for the different IGV configurations

This explanation is simplified and it doesn't count all the effects of the losses and the matching between the stages, but it can give a simple guide line to understand the compressor map. In the compressor map the maximum mass flow is obtained with the -10° configuration , while the minimum mass flow is obtained with the +30°. The maximum pressure ratio is also obtained with the -10° configuration, contrary to the initial forecast which supposed that the -15° one could reach the highest pressure ratio and highest mass flow. The machine performance are summarized and compared with the machine in the basic configuration, where the IGV's angle is equal to 00°.

	maximum π_c	minimum $\dot{m}$	maximum $\dot{m}$
Basic configuration	1.873	13.8 [kg s^{-1}]	15.851 [kg s^{-1}]
Studied configuration	1.8924	11.8 [kg s^{-1}]	16.191 [kg s^{-1}]
Performance improvement	+1.04%	-14.49%	+2.14%

The compressor map summarize the compressor's performance, but in order to understand how the IGV's orientation changes the machine's operation is necessary to study the flow field in the different stages.

5.1 Compressor's operating lines with negative IGV's angle

The negative IGV orientation allows to increase the incidence angle on the first rotor increasing the pressure ratio and the enthalpy exchange. The position of the -5° and -10° operating line are expected with greater pressure ratio and greater mass flow but the -15° operating line shows a unusual position crossing the two previous operating lines. The IGV's angle in the latter is to big and the compressor's performances degenerate moving the operating line down to lower pressure ratio. The IGV orientation has the

deeper effect on the first stage, here the pressure ratio and the enthalpy difference are plotted as function of the mass flow.

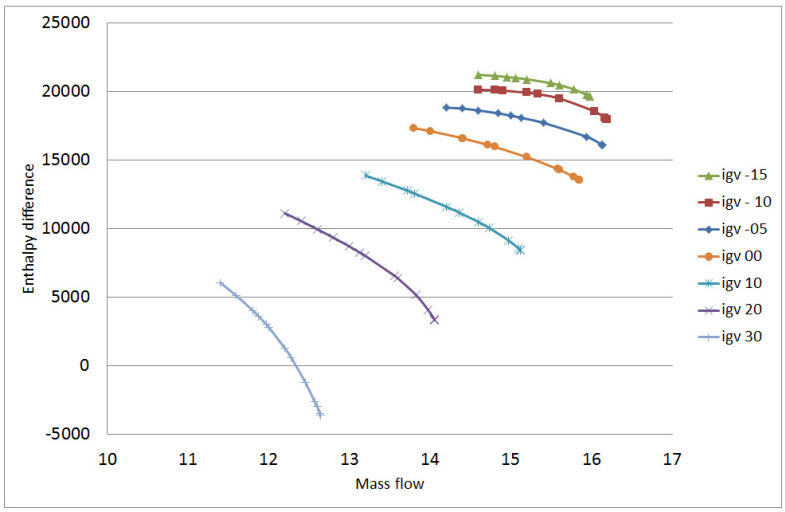

Figure 5.3: Total enthalpy difference map thought the first stage

In the enthalpy map decreasing the IGV's angle the exchanged work increase and the -15° operating line overlie the all the other line.

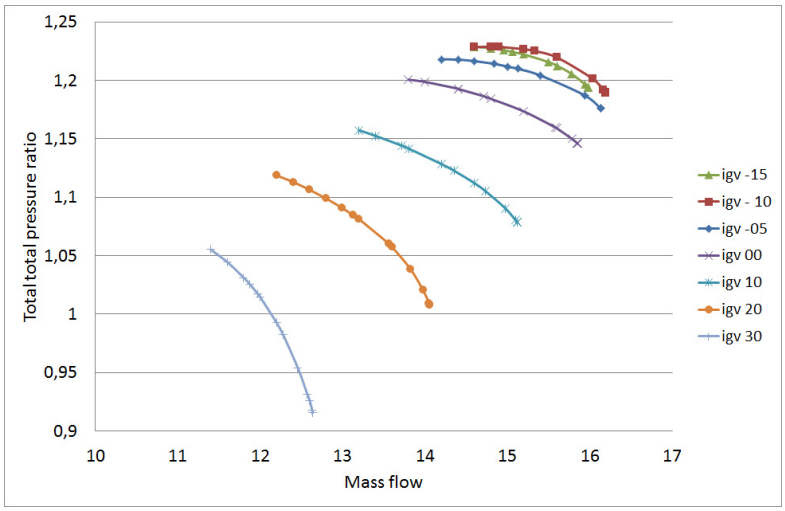

Figure 5.4: Total total pressure ratio map thought the first stage

In the pressure ratio map the operating the operating line of the -15° lie

under the -5° and -10° operating lines. The pressure ratio and the enthalpy exchange give two different informations because the enthalpy difference evaluates the amount of work exchanged between the machine and the flow. The enthalpy difference counts only the flow deflection through the Euler's pump and turbine equation, $\Delta H = c_{\theta\,out} \cdot u_{out} - c_{\theta\,in} \cdot u_{in}$, if the process is adiabatic. Decreasing the the value of the $c_{\theta\,in}$ as result of the IGV orientation the work can increase also if the $c_{\theta\,out}$ decrease because of the greater deflection at the blade's trailing edge. The deflection depends on the incidence with a linear relation for the profile before the stall, but the deflection change is always lower than the incidence change, thus the energy exchange becomes greater decreasing the IGV angle. On the other hand the pressure ratio is greater for the -10° configuration hence the pressure losses are different in the first stage for the different configurations. In the first rotor when the IGV has the -15° orientation there is a vortex on the suction side of the blade, this vortex affects the pressure ratio deteriorating the flow energy. If the incidence is too big on a profile this falls to stall because the flow on the suction side decelerates too much near the trailing edge in order to be in equilibrium with the flow coming from the pressure side. So the flow on the suction side in no more attached on the blade and generate a vortex, which is mainly located near the blade root in the hub. The vortex distribution is the result of the new matching between the stages, at the first rotor's inlet the flow angle is almost constant along the span of the blade because the IGV is designed to work as bi-dimensional profile giving a uniform direction to the fluid. Along the span when the IGV has a negative angle the circumferential component of the absolute speed is opposed to the rotor speed hence is negative:

$$\beta_{in} = \arctan\left(\frac{u - c_{\theta\,in}}{c_{ax}}\right) \tag{5.4}$$

When the IGV angle is negative the circumferential component is negative

hence β_{in} increases, the solid angle of the blade was designed for the 00 configuration where the velocity inlet $c_{\theta\, in}$ is 0.

$$\beta_{in\, blade} = \arctan\left(\frac{u}{c_{ax}}\right) \tag{5.5}$$

So the incidence angle obtained as the difference between the fluid angle and the blade angle is.

$$i_{in} = \arctan\left(\frac{u - c_{\theta\, in}}{c_{ax}}\right) - \arctan\left(\frac{u}{c_{ax}}\right) \tag{5.6}$$

The incidence is plotted for a generic velocity distribution showing how it decreases from the root to the tip and explaining why the vortex is mainly located near the blade root.

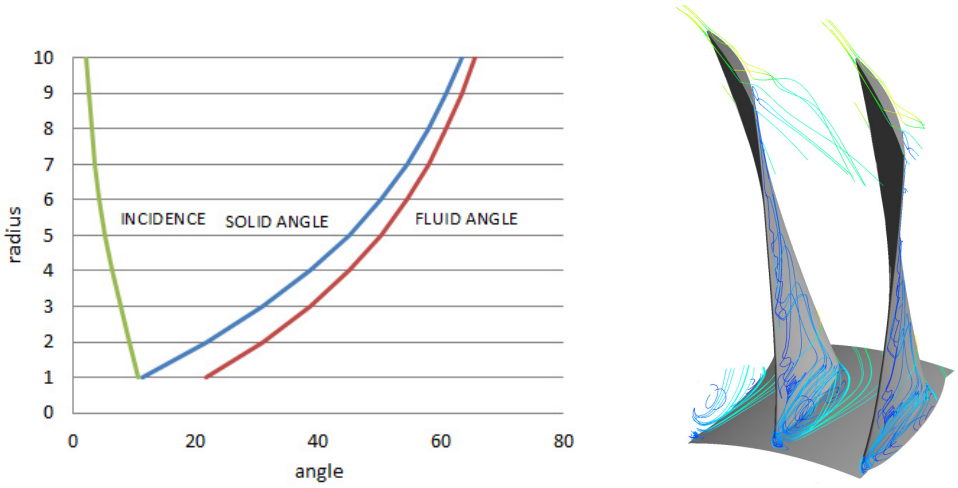

Figure 5.5: Incidence angle along the blade for a negative IGV's orientation (left) and vortex in the first rotor for the -15° configuration (right)

The vortex lie on the suction side of the blade also when the machine is not stalled and it works in a steady manner. The rotating stall is detected when in one part of the blade channel there is a vortex, stalled cell, which moves in the row along the circumferential direction with a speed different

from the rotational speed of the machine. In the -15° configuration the vortex on the suction side doesn't trigger the stall because this phenomena is mainly connected with the flow near the tip clearance. The stall topic is presented in the next chapter, but here is already possible to assert that the compressor stall is almost independent on the flow condition near the root of the rotor blade.

In order to understand how the IGV affect the behaviour of the machine the results, obtained with the same boundary condition but different geometries, are compared. At the inlet the total pressure is 101324[Pa] the temperature is 288.15 [K] and at the outflow the mass flow is fixed at 14.8[kg s^{-1}]. The main effect of the IGV is on the first rotor because as seen the incidence angle change, but change also the loading of the blade along the span. The total pressures at the rotor inlet are different in the four configurations and comparing the pressure distribution is clear how the IGV blade with stagger equal to -15° are already stalled and generate wide wake behind the blade.

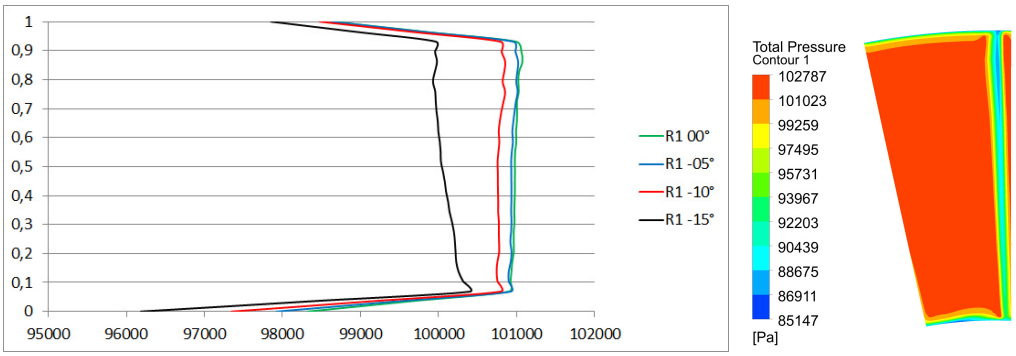

Figure 5.6: Total pressure at the first rotor inflow (left) and total pressure distribution in behind the IGV in the -15° configuration (right)

The pressure losses are mainly located near the shroud this is the conse-

quence of three dimensional flow since the incidence angle is constant along the blade span. The total pressure drop near the hub and the shroud are the consequence of the boundary layer on the hub and on the shroud surface. In the first rotor the pressure ratio profiles at the outlet surface show the effect of the losses in in the blades row, decreasing the IGV angle the pressure distribution increase except in the most loaded configuration where in the blade's middle height the pressure decrease:

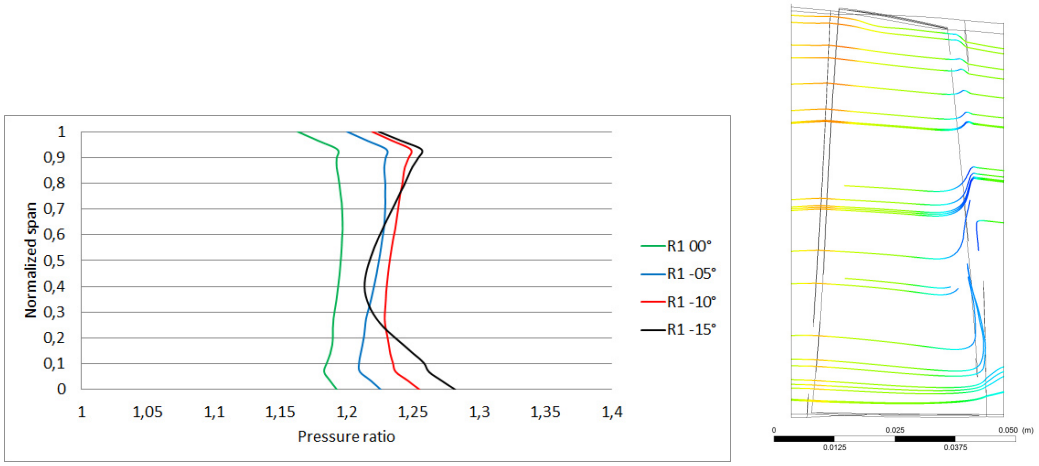

Figure 5.7: Pressure ratio along the first rotor blade (left) and stream line in the first rotor for the -15° configuration (right)

The vortex in the rotor is near the hub, but in the picture show the main pressure loss in the middle span at the rotor outflow because the three dimensional flow in the rotor moves the low pressure flow from the hub to the middle span region.

If the pressure ratio is affected by the vortex and the pressure losses on the suction side, the enthalpy exchange depends only on the inlet and outlet velocity. The axial speed is almost uniform at the inlet for all the configurations, but it decreases in the -15° configuration in the middle blade

region because the flow in that region moves along the blade span to the blade tip, hence the speed has a radial direction.

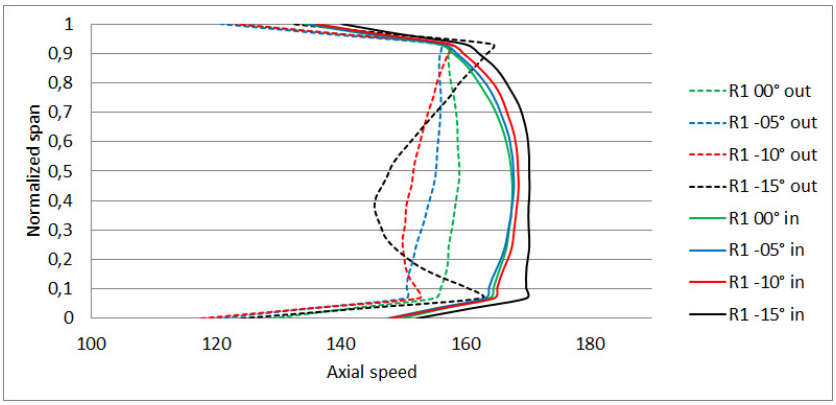

Figure 5.8: Axial speed distribution in the first rotor

The circumferential speed at the inflow is the result of the IGV flow field so the distribution is linear along the span while the outlet velocity are the result of the exchanged work in the rotor. In -15° configuration the effects of the vortex and the secondary flow increase near the hub the circumferential speed.

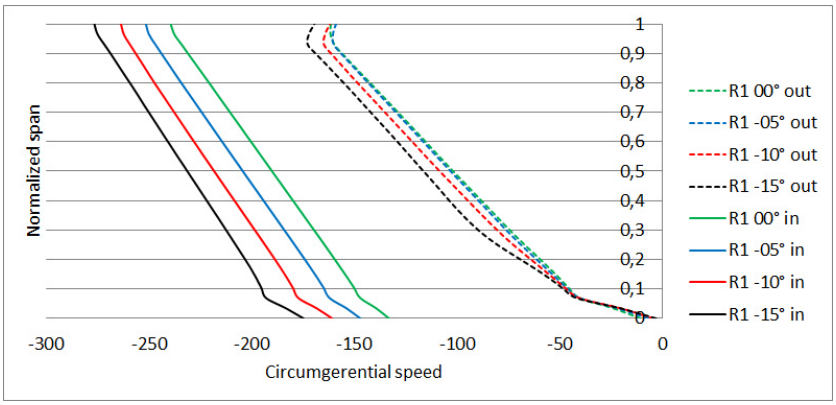

Figure 5.9: Circumferential speed distribution in the first rotor

The flow angle distribution is depending on the blade deflection, on the

incidence and on the solid angle distribution. The deflection increases with the profile load hence with the IGV's load, but for the -15° configuration at the outflow the angle is increased because the meridional speed is deflected in radial direction. In the hub region out of the boundary layer the deflection is greater because the incidence in also bigger, moving to the tip blade the incidence become smaller and the outflow angle are more close for the different configurations.

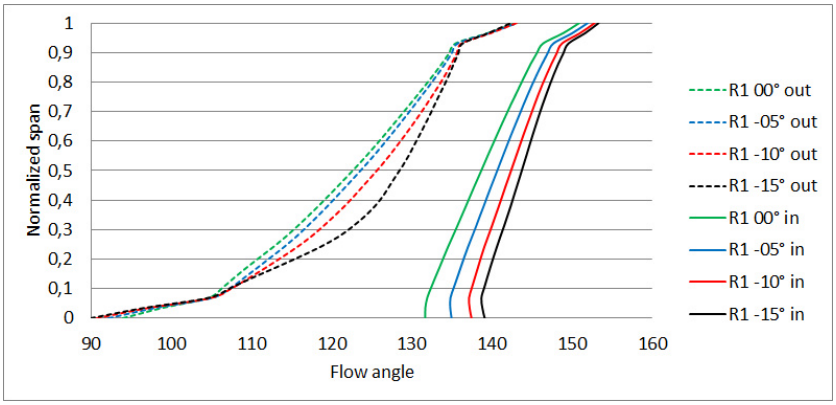

Figure 5.10: Pressure distribution along the compressor for the -15° (red line) and -10° (blue line)

The flow in the first rotor have effects also on the other stage because the new pressure and the enthalpy exchange distributions change the inlet condition to the rear stages. The pressure ratio in the rear stages follows the same trend of the one in the first rotor, the pressure ratio increases in the stages decreasing the IGV's angle except for the -15° configuration.

IGV	π_{cS1}	π_{cS2}	π_{cS3}	π_{cS4}
00°	1.1832	1.1708	1.1532	1.1324
-05°	1.2147	1.1773	1.1585	1.1368
-10°	1.2289	1.1788	1.1591	1.1373
-15°	1.2276	1.1785	1.158	1.1355

The losses and the incidence in the first rotor modify the pressure ratio, but they affect the density of the air and on its temperature too. In a rotor the total temperature in the relative frame is constant $c_pT + w^2/2 - u^2/2$ is constant but the total pressure is reduced by the losses. In the vortex the total pressure goes down while the static pressure is constant thus relative speed decreases and the temperature increases. Because of the temperature rise the constant static pressure the density is reduced and at the outflow the axial speed becomes greater. In the second rotor the different flow features are compared, they prove the previous reasoning about the effect of the axial speed. The axial mainly control the load on the blades since the circumferential speed is almost constant.

Inflow R2	00°	-05°	-10°	-15°
ρ [kg m^{-3}]	1.221	1.249	1.258	1.258
T [K]	290.5	293.6	295.4	296.1
c_{ax}	164.4	160.7	159.6	161.7
c_θ	-189.9	190.2	190.7	190.8
θ	138.8	139.5	139.7	139.3
Outflow R2	00°	-05°	-10°	-15°
ρ [kg m^{-3}]	1.350	1.381	1.390	1.371
T [K]	303.5	306.7	308.7	309.5
c_{ax}	158.8	155.4	154.3	156.0
c_θ	-100.6	-99.6	-98.6	-98.1
θ	121.3	121.5	121.4	121.0

Increasing the axial speed of the air the rear stages have lower incidence angles and become more unloaded. The deceleration of the air is not affected by the different axial speed or by the different pressure ratio thus the ratio between the inlet and the outlet speed is almost constant.

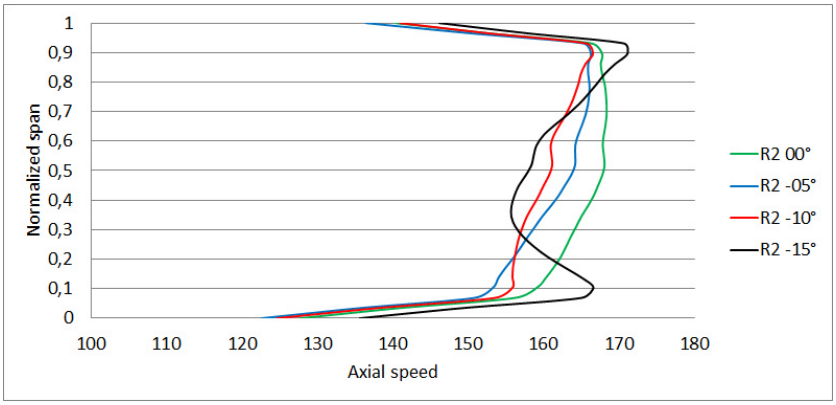

Figure 5.11: Axial velocity distribution at the second rotor inlet

If the flow deceleration doesn't chance between the configurations and the -15° one can't reduce the speed gap with the other configurations and the pressure ratio remains lower in all thee rear stages. The axial speed is not constant and it depends on the mass flow and on the density thus on the operating condition of the first stage. When the axial speed increases and the rotational speed is the same the incidence angle decrease unloading the stage. The pressure ratio increases decreasing the axial speed of the air also in the rear stages, the rear stages of the -15° configuration are thus affected by axial speed distribution of the first stage. In the different stage the speed

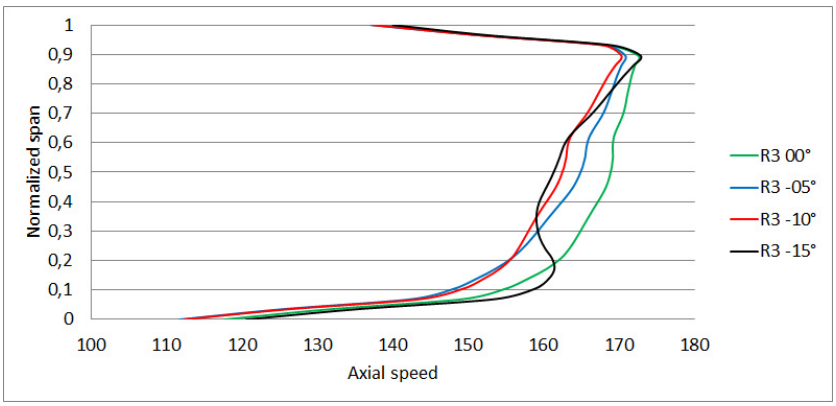

Figure 5.12: Axial velocity distribution at the second rotor inlet

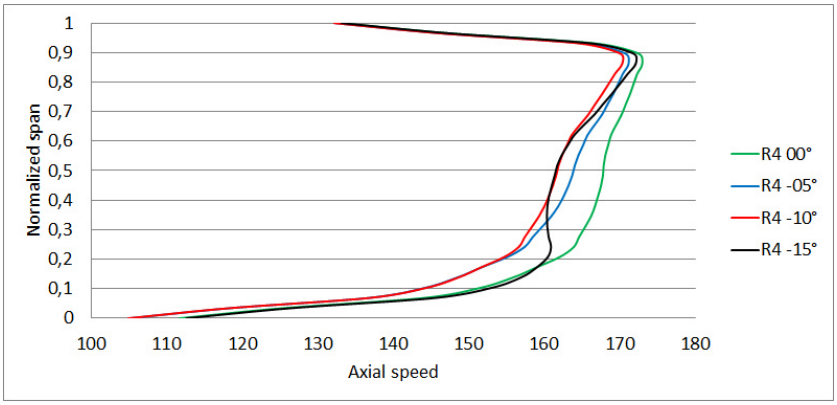

Figure 5.13: Axial velocity distribution at the second rotor inlet

profile is similar to the one at the first rotor outlet but this distribution is more equalized stage by stage. The stages damp the non-uniform axial speed profile and try to bring the compressor to the nominal work condition with a constant axial speed profile. The design axial distribution suppose a uniform axial speed all along the span obtained with a free vortex speed distribution.

5.2 Compressor's operating line with positive IGV's angle

When the IGV angle is positive the incidence angle on the first rotor decreases and the compressor is unloaded thus the pressure ratio and the mass flow are reduced, but the different orientations have not the same effect of the first rotor and on the rear stages. The circumferential velocity component induced by the IGV has the same direction of the rotor speed so the incidence angle is negative and as seen in the other configurations the its distribution is not constant along the blade. For positive IGV's angle the circumferential velocity is positive and the incidence increase from the blade's root to the clearance. It's easy to find the new incidence distribution for the new IGV

orientation evaluating the flow angles.

$$\beta_{in} = \arctan\left(\frac{u - c_{\theta\, in}}{c_{ax}}\right) \tag{5.7}$$

The solid angle of the blade was designed for the 00 configuration where the velocity inlet $c_{\theta\, in}$ is 0.

$$\beta_{inblade} = \arctan\left(\frac{u}{c_{ax}}\right) \tag{5.8}$$

So the incidence angle obtained as the difference between the fluid angle and the blade angle is.

$$i_{in} = \arctan\left(\frac{u - c_{\theta\, in}}{c_{ax}}\right) - \arctan\left(\frac{u}{c_{ax}}\right) \tag{5.9}$$

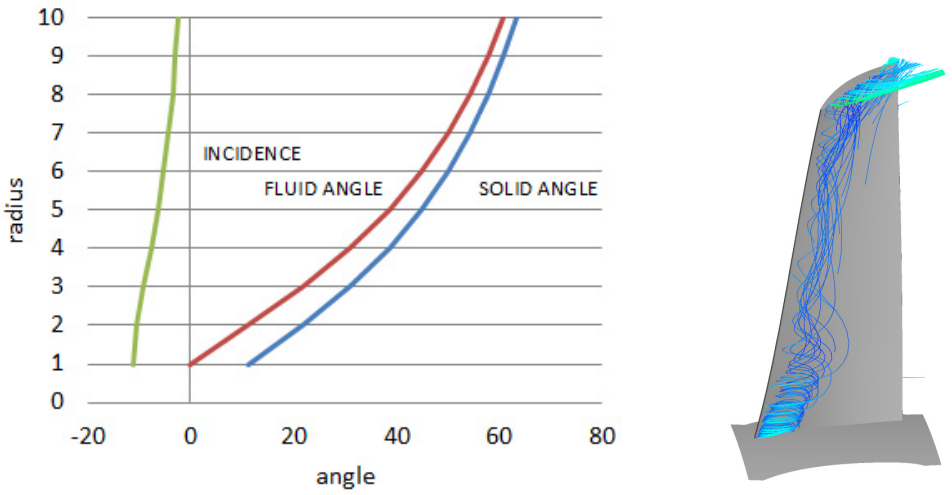

Figure 5.14: Angle distribution along the span when the IGV has a positive angle (left) vortex in on the pressure side +30° configuration (right)

The flow attach the blade on the suction side instead of the pressure side hence the flow when the incidence angle is too negative can't stay attached on the pressure side and generates a vortex, which is located near the hub

because of the angle distribution. The incidence angle depends also on the operating point because when the mass flow increase the axial speed grows as well and the incidence become more negative.

$$\tan(\beta_{R1\,in}) = \frac{u - c_{\theta\,in}}{c_{ax}} = \frac{u}{c_{ax}} - \tan(\alpha_{IGV\,out}) \tag{5.10}$$

The vortex on the pressure side surface is present in all the operating points for the +30° configuration, it is present only for the operating points near the choke line for the +20° configuration and it is absent in the +10° configuration. The flow field features are compared for the different IGV's orientation in order to understand how the velocity distribution change in the machine. The inlet condition of the first rotor are the result of the flow in the IGV thus the inlet angle distribution is linear along the span except for the boundary layer region near the hub and shroud.

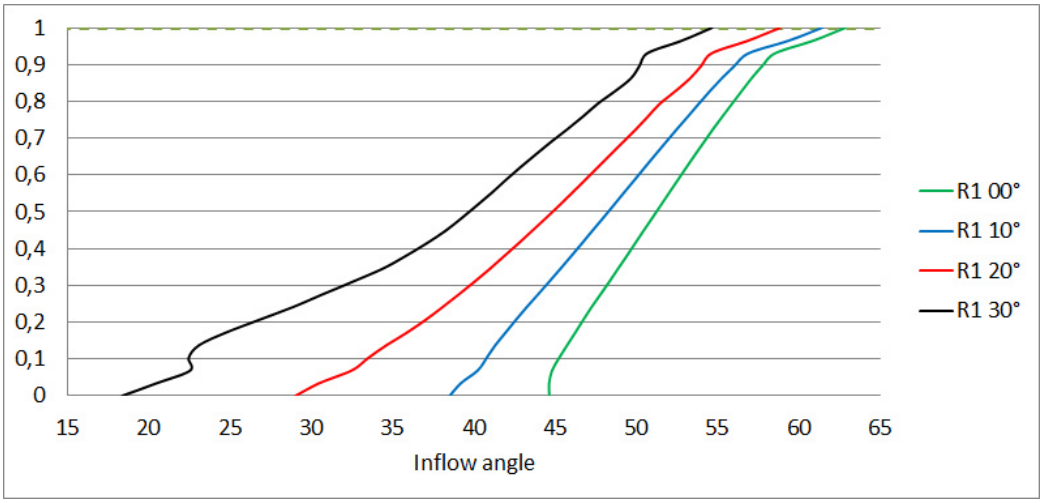

Figure 5.15: Angle distribution at the inlet of the first rotors

The angle distribution at the outflow is almost linear along the span but it's affected by the different incidence angle and by the vortex effect near the hub. The incidence angle is negative and increase from the hub to the shroud

so the outflow angle are similar in the different solutions near the rotor's tip. Near the shroud the different incidence and the vortex effect on the pressure side of the +30° configuration change more the flow distribution.

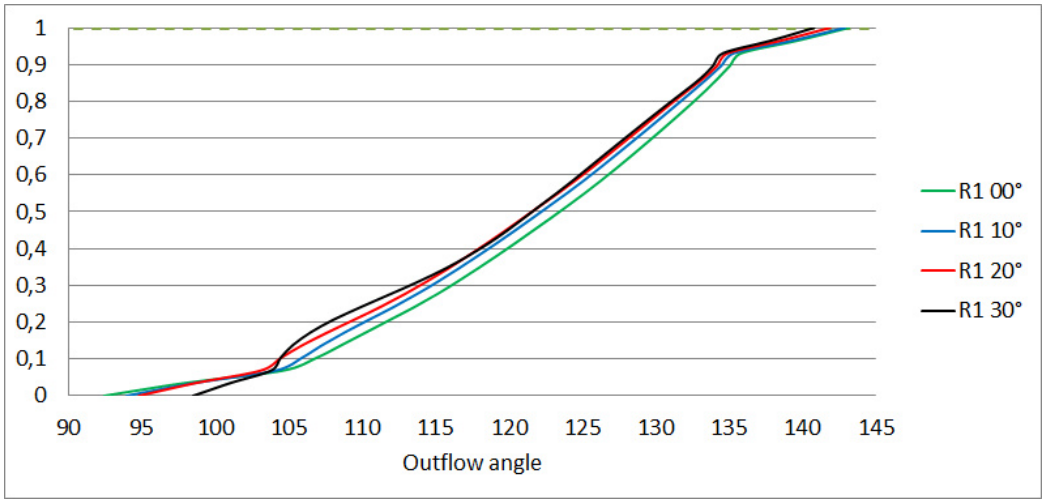

Figure 5.16: Angle distribution near the blade tip for the second and the third rotors

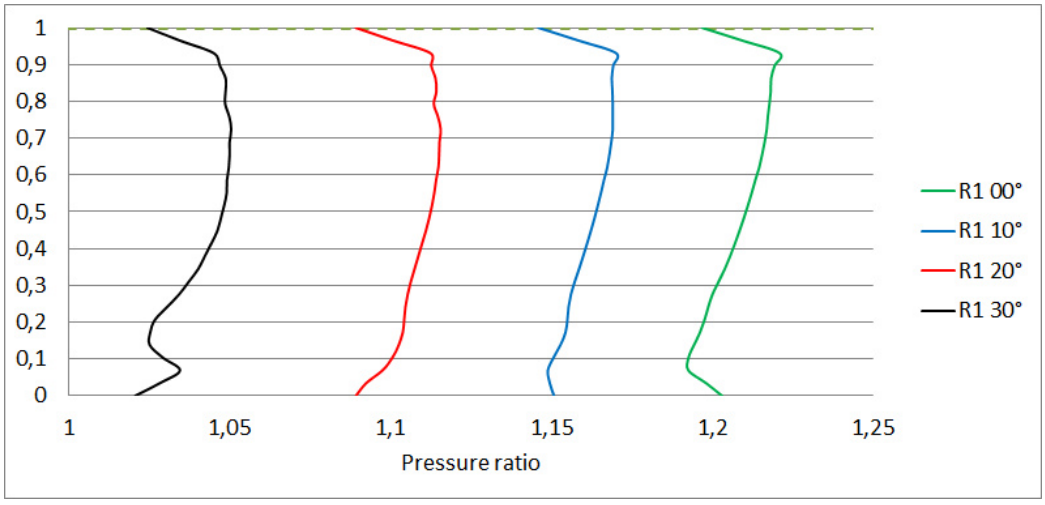

Figure 5.17: Angle distribution near the blade tip for the second and the third rotors

Also the pressure ratio is influenced by the inlet condition which decrease the exchanged work as seen in the previous section but at the same time the pressure ratio drop down near the hub because of the suction side vortex. The new compressor matching has effect not only in the first rotor but also in the rear stages with some unexpected results. Near the surge line for the negative positive IGV orientations the pressure ratio and the enthalpy exchange increase increasing the IGV angle. If a stage is working with higher enthalpy difference also the flow deflection has to be greater. In the second rotor the performance get better if the IGV angle increases, at the inflow the circumferential speed are grouped in a small range while the axial speed and the flow angle change consequently. At the outflow the flow deflection decreases increasing the IGV angle so the blade loading become bigger when the first stage is unloaded.

IGV angle	$v_{ax\,in}$	$v_{\theta\,in}$	θ_{in}	$v_{ax\,out}$	$v_{\theta\,out}$	θ_{out}	$\Delta\theta_{out}$
+10°	149.03	-187.83	141.24	144.20	-95.0	122.14	19.1
+20°	149.62	-187.87	141.13	144.13	-93.37	121.75	19.38
+30°	147.93	-187.70	141.42	142.05	-91.78	121.63	19.79

From the averaged deflection angle and from the averaged speed is possible to understand why the stage has different pressure ratio in the different configurations, but the velocity averaged value don't explain why the same blade with the same inlet condition can perform in different manners. In order to understand the cause of the different pressure ratio is necessary to analyse the distribution along the blade span of the pressure ratio and of the flow angle. For the +30° configuration the flow with greater incidence angle tends to move to the tip zone while near the hub the incidence angle is lower. The blade is more loaded in the tip region where the radius is greater so for the Euler's formula the enthalpy exchange become greater. In the hub region

the incidence decreases as the exchanged work but has modest weight. Using a incidence profile whit the same averaged conditions but greater incidence near the high radius zone the exchanged work is greater.

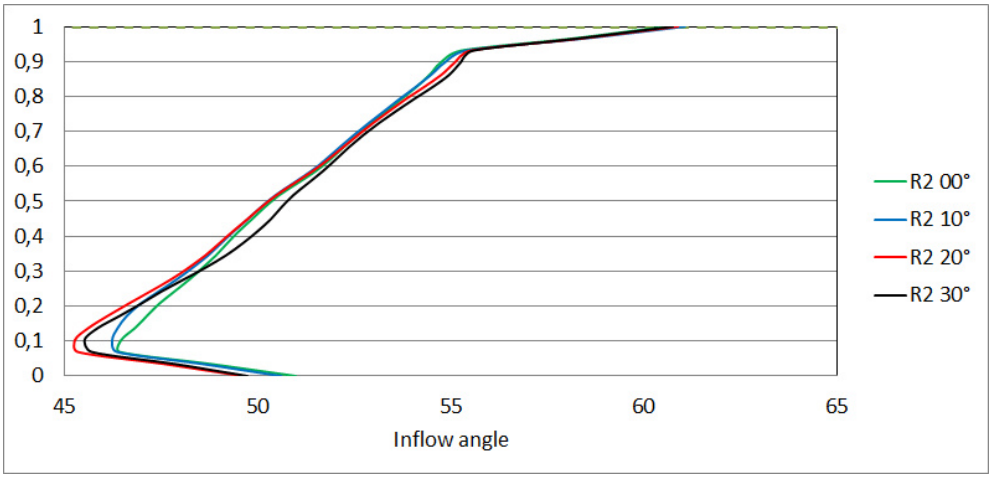

Figure 5.18: Angle distribution at the inlet of the second near the surge line

The total total pressure ratio distribution points out that the pressure ratio is greater all along the span increasing the IGV angle. The pressure ratio is influenced also by the inlet conditions and it's related to the enthalpy exchange though the following formula.

$$\frac{p_{out}}{p_{in}} = \left[\frac{k-1}{kRT^{\circ}_{in}}\Delta H^{\circ} + 1\right]^{\frac{k\eta_{pol}}{k-1}} \tag{5.11}$$

The total temperature at the inlet can change the pressure ratio using the same work amount. The temperature is always decreasing increasing the IGV because the first stage become always more unloaded.

The same analysis is carried out also on the third rotor in order to understand if also here the inlet angle distribution change the stage behaviour.

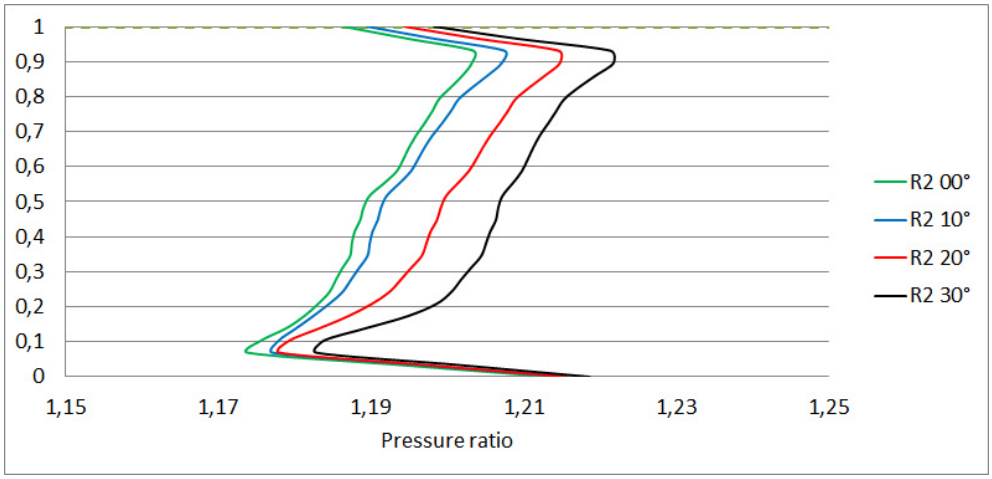

Figure 5.19: Pressure ratio in the second rotor

IGV angle	$v_{ax\,in}$	$v_{\theta\,in}$	θ_{in}	$v_{ax\,out}$	$v_{\theta\,out}$	θ_{out}	$\Delta\theta_{out}$
+10°	149.26	-183.98	140.74	144.34	-93.24	121.64	19.1
+20°	149.19	-183.90	140.73	143.91	-92.13	121.44	19.38
+30°	147.05	-183.78	141.12	141.62	-91.03	121.49	19.79

In this rotor the inlet angle change between the different configurations, but the angle distribution show how the 30° configuration has in the middle span the greater incidence thus the energy exchange is also greater. For the pressure ratio as seen for the second rotor there is the sum of two effects because the configuration with great IGV angle have greater energy exchange and have lower total temperature inlet. The two combined effects give as result the pressure ratio distribution.

The effect of the matching between the stages is damped thought the compressor and for the last stage the enthalpy difference and the pressure ratio don't change with the different IGV's angle. To understand why for the different IGV orientation there are different velocity profiles on the rear stages inlet is necessary to explain how the load on the blade change when it doesn't work in the nominal conditions. The angle distribution for the second

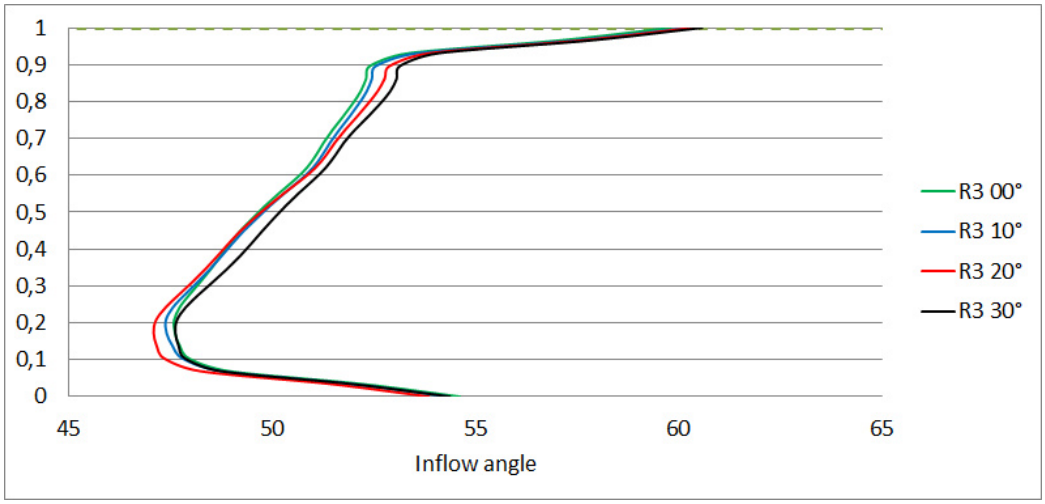

Figure 5.20: Angle distribution at the inlet of the third near the surge line

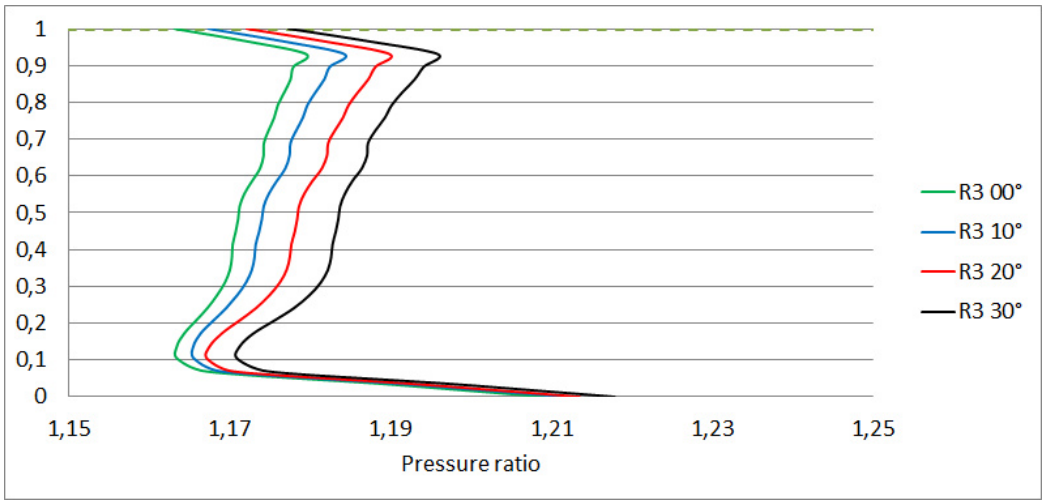

Figure 5.21: Pressure ratio distribution in the third near the surge line

rotor in the +30° has a greater incidence angle in the tip region while the angle in the hub region is smaller this is almost the same distribution founded at the outlet of the first rotor. Thought the machine the angle distribution can pass because the flow angle are the averaged along the circumferential direction. In the rotor the blade load supposing the radial flow are negligible the inlet angle in a stator is function of the outflow angle of the rotor:

$$\tan(\alpha_{in}) = \frac{c_\theta}{c_{ax}} = \frac{u}{c_{ax}} - \tan(\beta_{out}) \tag{5.12}$$

If in the rotor the angle β_{out}=$\beta_{out\,blade}$+δ is small because the profile is not loaded and the deflection is small the stator profile has a greater incidence angle a greater load on the blade and a greater deflection. So at the inlet of the successive rotor the relation is:

$$\tan(\beta_{in}) = \frac{w_\theta}{c_{ax}} = \frac{u}{c_{ax}} - \tan(\alpha_{out}) \tag{5.13}$$

The stator profile is more loaded and the angle α_{out} is also greater so the incidence angle on the successive rotor is lower and the load will be lower. As conclusion the pressure ratio distribution in the rotor is the reverse pressure ratio distribution of the stator. So the angle distribution in two successive rotor when the radial flow doesn't change it so much are almost the same. With the positive IGV's angles the incidence angle in the first rotor increases increasing the radius in the first rotor. In the second stage at the surge line the inlet average conditions are the same but the angle's trends are the same of the first rotor so increasing the IGV angle the incidence angle increase more on the tip and decreases on the blade root. The new angle distribution show greater deflection where the radius is bigger, thus the energy exchange can also be greater.

Chapter 6

Choke line definition

The maximum mass flow through the machine is limited by the mass flow in the throat section when Mach number equal to 1[10]. In all the IGV's configurations there are several zones with Mach number greater than 1, usually on the suction side of the rotor blades and one in the last stator. In the rotors there are some high speed zones, but the velocity along the blade increase and after decrease below the speed of sound. In the last stator the velocity on the outflow surface exhibit Mach number greater than 1 and the stator behave like a de Laval nozzle. The choked line is founded using the same boundary condition for all the configuration except for the +30 ° configuration. The total pressure inlet is equal to 101325 [Pa] the static pressure outlet is half of the pressure inlet 50662.5 [Pa].

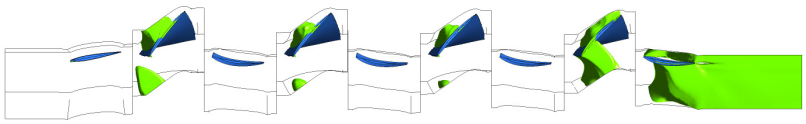

Figure 6.1: Isosurface in the entire compressor for the points with Mach number equal to 1

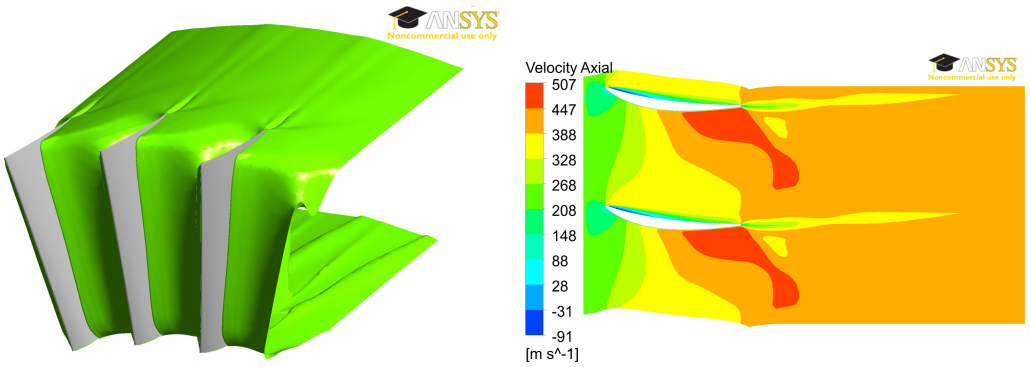

Figure 6.2: Throat surface in the fourth stator(left) and axial velocity distribution at the 0.5 span height(right)

For the simulated points close to the choke line the simulations don't satisfy the convergence criteria, maximum residual lower than 10^{-4}, but these keep swinging around an asymptotic value also the monitored flow features show the same behaviour defining a limit cycle. The map points are defined using the average value of the point in the limit cycle.

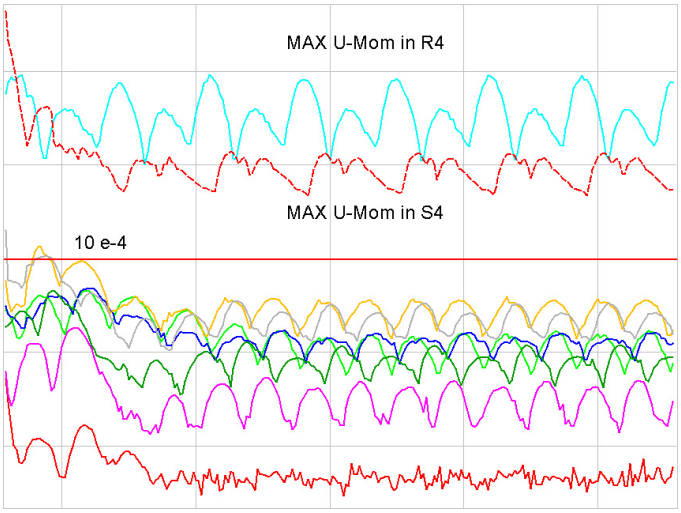

Figure 6.3: Maximum U residual in the different stage of the compressor at the choke line for the 00° configuration

The high residual in the compressor are not distributed in all the stages but they are located in the fourth rotor and in the fourth stator. The flow feature of the last stage are investigated in order to find a relation between the flow characteristic and the high residual zones. In the last rotor the residual are located near the root of the blade and in this zone a vortex lies on the suction side of the blade.

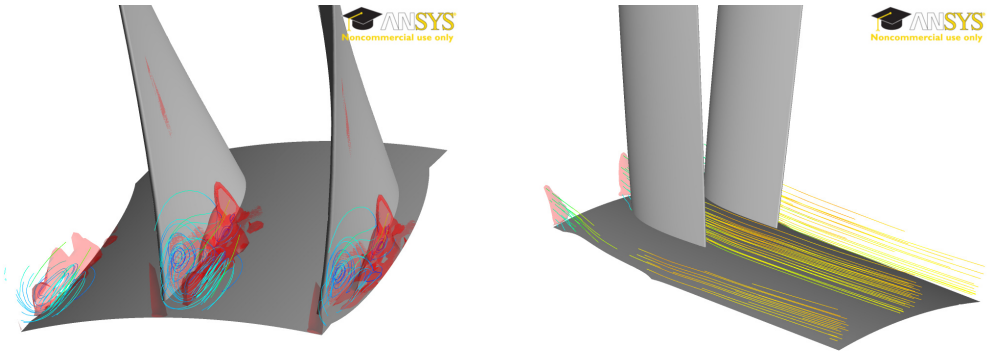

Figure 6.4: Isosurface with residual equal to 10^{-3} and streamline at the root of the blade in the last rotor (left) and in the last stator(right)

The high residual in the last rotor are directly connected with the vortex. The flow in the region is not steady, but time dependent and is not possible to find the converged solution with a steady state simulation. In the last stator there are also some high residual region, but the streamline starting form there don't show any vortex so the residual are the consequence of the flow motion in the previous rotor. Also if the simulation are not converged the result are still usable because the oscillation range of the monitored value is less than 1%, the mass flow for the different simulation at the choke line are summarized reporting the maximum value the minimum value and the averaged value used in the compressor map.

θ	$\min(\dot{m})$	$\max(\dot{m})$	$\bar{\dot{m}}$
-15°	15.791	15.793	15.792 ± 0.006 %
-10°	16.027	16.029	16.28 ± 0.006 %
-5°	16.018	16.02	16.019 ± 0.006 %
0°	15.77	15.771	15.771 ± 0.003 %
10°	15.044	15.045	15.045 ± 0.003 %
20°	14.045	14.048	14.047 ± 0.01 %
30°	12.627	12.632	12.63 ± 0.019 %

6.1 Compressor's choke for negative IGV's angle configurations

Watching the compressor map is clear how the IGV's angle influences the compressor's choke line with a non-linear effect. The mass flow in the choked condition is almost the same for the -5° and -10° configuration, $\dot{m} = 16.02$ [kg s^{-1}] and $\dot{m} = 16.03$ [kg s^{-1}], while in the -15° one is smaller $\dot{m} = 15.79$ [kg s^{-1}]. Theoretically if the stage are more loaded and the pressure increase more also the density and the temperature will increase thus the available mass flow in the choke condition could be greater supposing the same area.

$$\dot{m}_{choke} = \rho A \sqrt{KRT} \tag{6.1}$$

But this reasoning doesn't count the effect of the matching between the stages which changes the behaviour of the whole machine. Comparing the flow feature in the three configurations is possible to understand how the different loads and losses in the first stage can affect the choked flow in the last stator. The work exchanged in the different stages, calculated as total enthalpy difference between the inlet and the outlet, shows that the energy

exchanged in the first stage increases decreasing the IGV's angle, while the rear stages are working almost in the same manner.

Δ_H [J m^{-3}]	Stage 1	Stage 2	Stage 3	Stage 4
-5°	15988	13675	12402	5505
-10°	17738	13726	12396	5485
-15°	19090	13579,6	12298	5533
π_c	Stage 1	Stage 2	Stage 3	Stage 4
-5°	1.1818	1.1353	1.1121	0.9749
-10°	1.1822	1.1385	1.1143	0.9606
-15°	1.7376	1.1394	1.1153	0.9742

As founded also for the other operating points the enthalpy exchange in the first stage is controlled by the IGV outflow angle and increases increasing the blade load, but the pressure ratio is affected also by pressure losses. In the first rotor the pressure ratio also at the choke line for the -15° is beyond the expectations and is lower than the pressure ratio in the -10° and -5° configurations. At the choke line limit the low performance of the -15° configuration are already known since the previous analysis, but also the performance of the -10° configuration are unexpected because the mass flow limit is close to the -5° one. The choked mass flow is depending on the density and on the temperature.

$$\dot{m}_{choke} = \rho A\sqrt{KRT} = \frac{PA}{\sqrt{TKR}} \tag{6.2}$$

The temperature and the pressure at the throat area in the last stator are the result of the operating conditions in the previous stage. In the first rotor the greater pressure ratio is obtained with -10° configuration because it can balance a big incidence angle with acceptable losses. The total temperature

is the result of the first low of the thermodynamic:

$$H_{tot} - H_{tot\,0} = c_p \cdot (T_{tot} - T_{tot\,0}) \tag{6.3}$$

The total temperature is directly related to the energy exchange in the rotor, but the static temperature which influence the mass flow at the choke line is also depending on the kinetic load:

$$T = T_{tot} - \frac{1}{2}c^2 \tag{6.4}$$

If the flow speed decrease the static temperature rises the mass flow at the choke line decreases thus for the first rotor the losses and the work exchange are listed:

	T_{out} [K]	$T_{tot\,out}$ [K]	ΔP	P_{tot} [Pa]	ρ_{out} [kg m^{-3}]
-5°	286.1	304.1	1.604%	119529	1.175
-10°	287.9	305.8	2.326%	120676	1.817
-15°	289.1	307.1	3.031%	120432	1.174

The total temperature give the same information as the enthalpy exchange decreasing the IGV angle the flow energy increase but the ΔP indicate how the losses increases in the first rotor decreasing the inlet angle. This is evaluated as:

$$\Delta P = \frac{P_{tot\,rel\,in} - P_{tot\,rel\,out}}{P_{tot\,rel\,in}} \tag{6.5}$$

In the first rotor the density is a consequence of the pressure ratio and of the temperature and it has the maximum value with the -10° configuration.

$$\rho = \frac{P}{KRT} \tag{6.6}$$

The density affects the axial velocity in the stages hence it controls the row's load. In the rear stages the enthalpy difference is greater for the -10°

configuration but the pressure ratio is greater for the -5° one. The difference are the inlet conditions because the -5° configuration work with a lower inlet temperature so the pressure ratio also with a smaller enthalpy difference is bigger.

$$\frac{p_{out}}{p_{in}} = \left[\frac{k-1}{kRT^{\circ}_{in}}\Delta H^{\circ} + 1\right]^{\frac{k\eta_{pol}}{k-1}} \tag{6.7}$$

The different enthalpy exchange in the stages increases changes the temperature at the last stator inlet where the flow chokes. The rear stages work also with different pressure ratio because the -15° configuration is affected by the high axial speed, consequence of the vortex in the first stage. The -5° configuration works better because it can reduce the density gap with the -10° one having a greater density a the last stator inlet. At the last rotor outlet the flow features are:

c_θ	T [K]	c_{ax} [m s^{-1}]	ρ [kg m^{-3}]	$\dot{m}$ [kg s^{-1}]
-5°	310.3	219.9	1.308	16.02
-10°	311.9	220.4	1.305	16.03
-15°	312.94	221	1.284	15.79

The flow is almost the same for the two first configuration where the -10° is working better and is exchanging more work so the temperature is a little better but the -5° one has a greater density and this allows to recover the speed gap. The density and speed distribution confirm the results of the previous table the density in the -5° configuration show a greater density distribution in the region near the tip, this allows to increase the mass flow in that region. The different velocity distribution are the effect of the first stage matching on the rear stages because as seen before the velocity distribution in the first stage is reflected also in the rear stages.

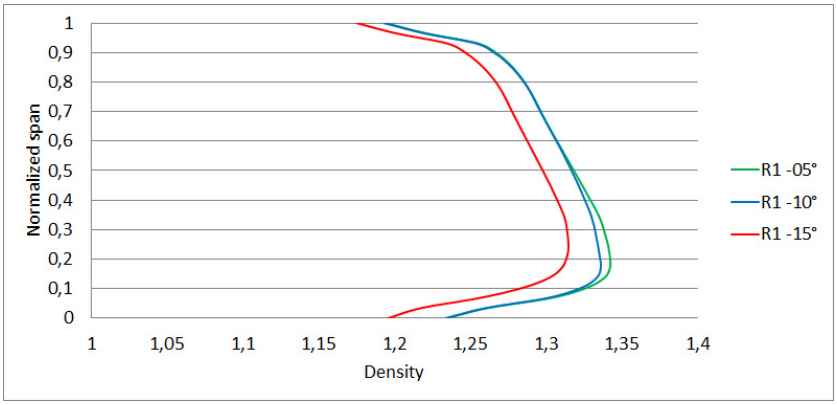

Figure 6.5: Comparison of the density distribution at the fourth rotor outflow

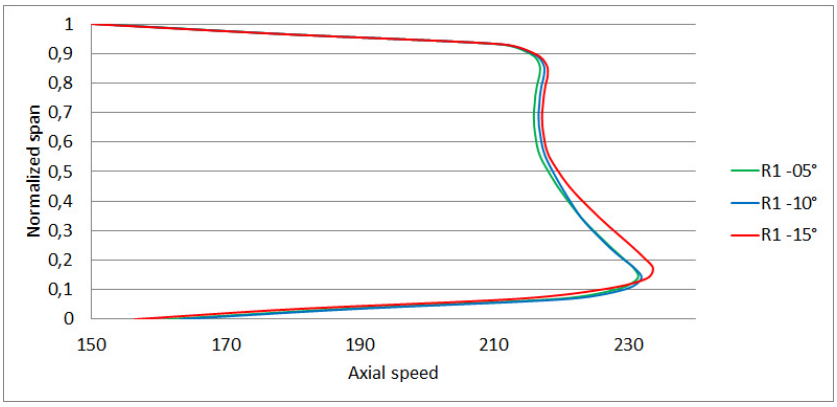

Figure 6.6: Comparison of the axial speed distribution at the fourth rotor outflow

6.2 Compressor's behaviour of the first stage for the +30 ° configuration

This configuration is the most unloaded set-up in the machine's configuration so the operating line of the compressor moves, with respect to the initial configuration, to lower pressure ratio and lower mass flow. Watching the maps of the the different stage monitoring the pressure ratio and the total enthalpy difference it's possible to understand how the new IGV angle influence the

first stage behaviour.

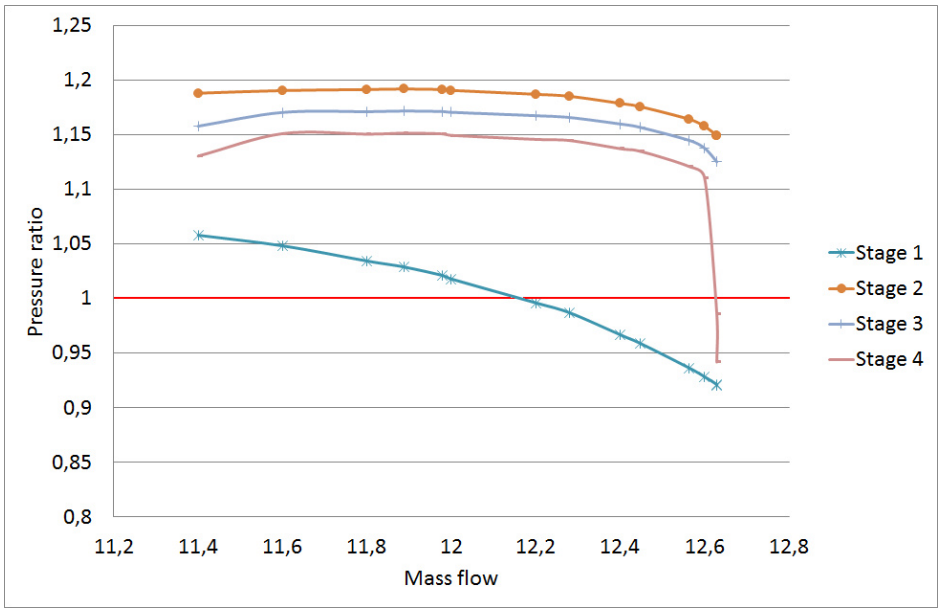

Figure 6.7: Pressure ratio map for +30° configuration

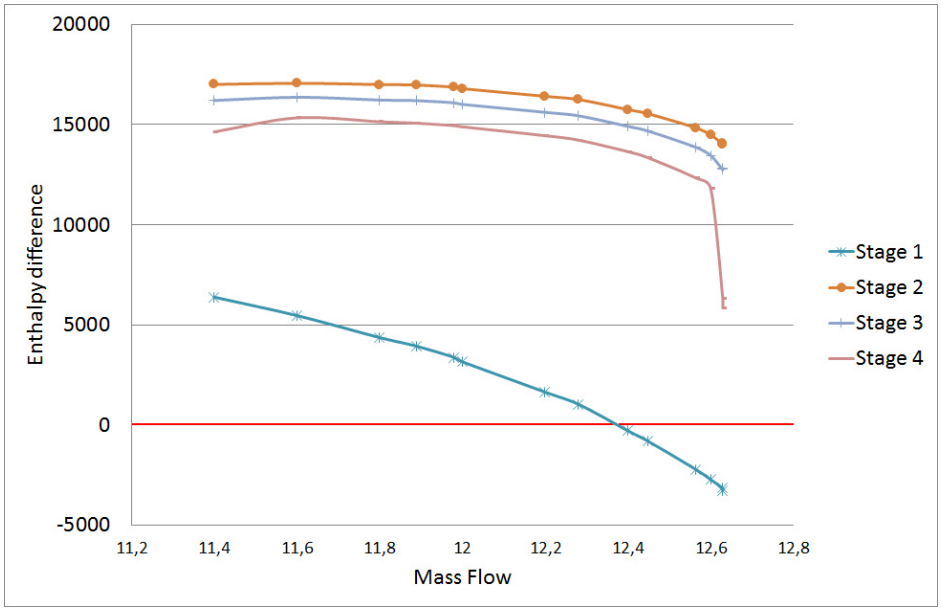

Figure 6.8: Enthalpy difference map for +30° configuration

The first stage in for high mass flow has a negative enthalpy difference and

the pressure ratio is less than one, so that means the first stage behaves like a turbine stage, decreasing the energy of the flow and transferring the work to the machine's shaft. Comparing the two maps is possible to define three different zones. The first stage behaves like a turbine with gas expansion, 1, the first stage behaves like a compressor, but with air expansion, 2, and the the first stage behaves like a compressor and with air compression, 1. The three zones are located in the following picture

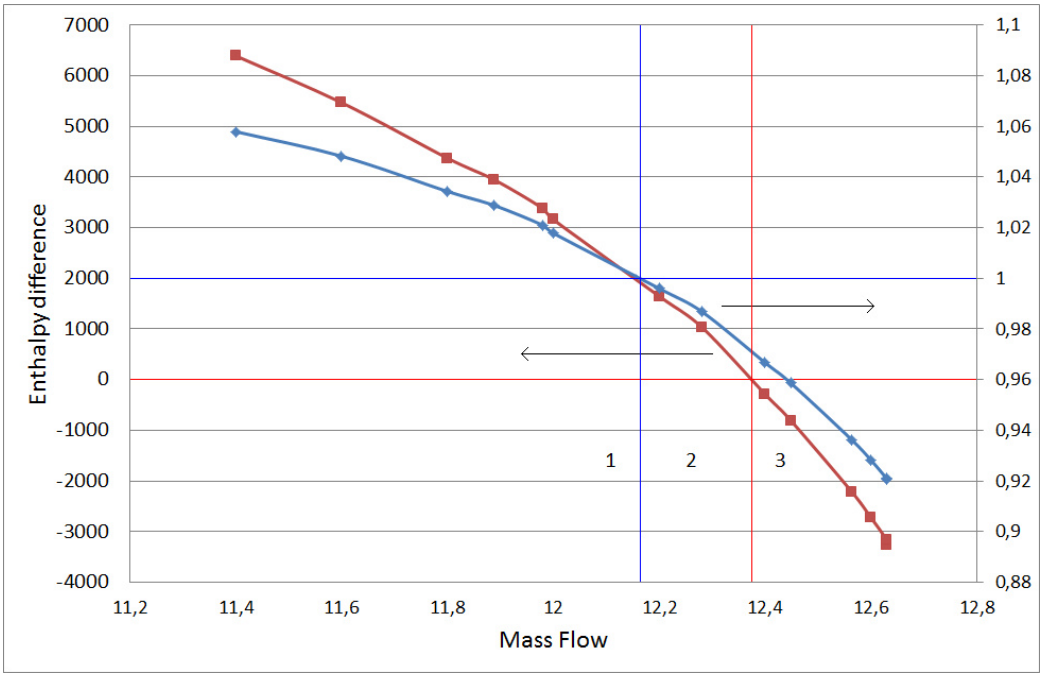

Figure 6.9: The three behaviour of the compressor are defined by the pressure ratio line (blue line) and by the enthalpy difference line (red line)

The explanation of this operating line is founded in analysing the flow field in the first rotor for three different operating points.

	Inlet	Outlet	ΔH_{tot} [J kg^{-1}]	π_c
Zone 1	P_{tot} = 101325 [Pa]	$\dot{m}$ = 11.8 [kg s^{-1}]	4371	0.936
Zone 2	P_{tot} = 101325 [Pa]	P = 131722.5 [Pa]	1038	0.987
Zone 3	P_{tot} = 101325 [Pa]	P = 111457.5 [Pa]	-2219	1.034

From the streamline plot it's clear how the IGV give to the flow at the first rotor an negative incidence angle so it presses on the suction side of the blade. The flow on the pressure side couldn't stay attached to the blade near the trailing edge and generate a vortex.

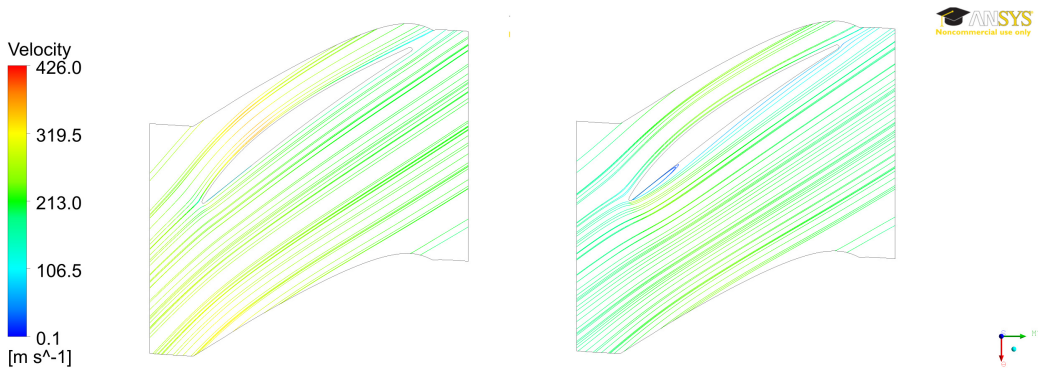

Figure 6.10: Streamline comparison between the 00° configuration (left) and the +30° one (right)

The circumferential velocity at the inlet and outlet of the first rotor explain the different behaviours of the machine:

	c_{ax} Inlet	c_{ax} Outlet	c_θ Inlet	c_θ Outlet	θ inlet	θ outlet
Zone 1	143.34	141.90	-118.48	-93.2	129.93	122.15
Zone 2	152.36	156.58	-112.75	-104.01	126.92	122.56
Zone 3	158.18	170.68	-108.84	-116.91	124.99	123.43

The the vortex has a strong effect on the axial velocity because the pressure losses decrease the pressure of the gas and also the density of the flow, thus

the flow in the rotor is accelerated instead of being decelerated. When the axial velocity in the rotor is strongly increased because of the flow expansion also the circumferential component will increase too in the rotating frame because the deflection is almost constant. The work exchanged in the rotor is $\Delta H_{tot} = c_{\theta\,out} \cdot u_{out} - c_{\theta\,in} \cdot u_{in}$, where the $c_{\theta\,out} = u_{out} + w_{\theta\,out}$. As seen in the table the outlet angle is not deeply influenced by the operating conditions, so the outlet circumferential velocity is proportional to the axial velocity. When the axial speed increases also the circumferential speed decreases reducing the exchanged work. The second parameter influencing the work is the inlet velocity this is influenced by the operating condition because the angle at the outside of the IGV are almost the same for all the operating points and the circumferential velocity changes because the axial velocity changes. Increasing the mass flow the circumferential component of the velocity at the IGV outlet increase $c_{\theta\,in}$ decreasing the exchanged work of the stage. The velocity in the first rotor explain the sign of the exchanged work in the machine, but to understand the pressure ratio of the first stage is necessary to analyse also the pressure losses in the machine which affect the total pressure. The behaviour of the first stage is depending on the inlet condition of the flow and on the outlet condition, the union of the two effects changes the working condition of the profile. The pressure side and the suction side change definition changing the operating point, only for the operating points near the surge line the incidence is big enough to have a normal behaviour of the profile. This difference occurs because the force on the blade change its direction hence the maximum averaged pressure on the blade changes side. When the two sides are inverted also the deflection will change direction and for the turbine behaviour it become negative. The total pressure in the rotating frame and the axial speed are compared in order to see the difference

in the flow for the different zones.

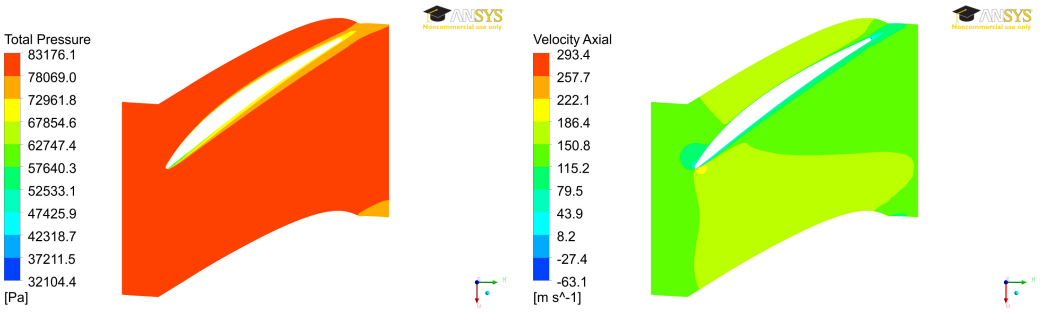

Figure 6.11: Blade to blade view for the zone 1 at 0.5 span height

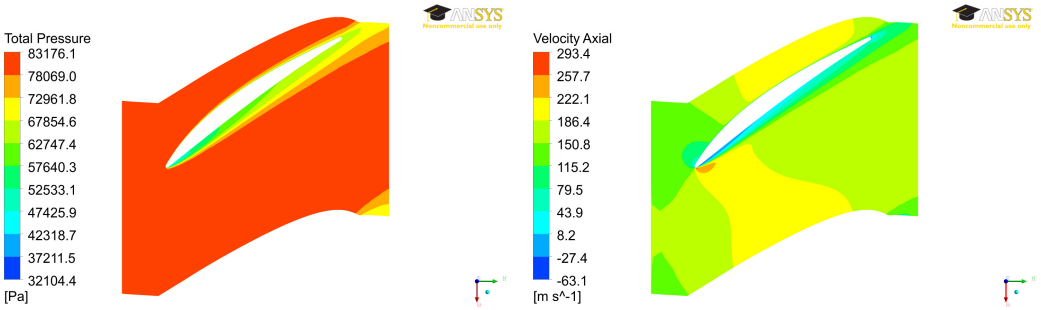

Figure 6.12: Blade to blade view for the zone 2 at 0.5 span height

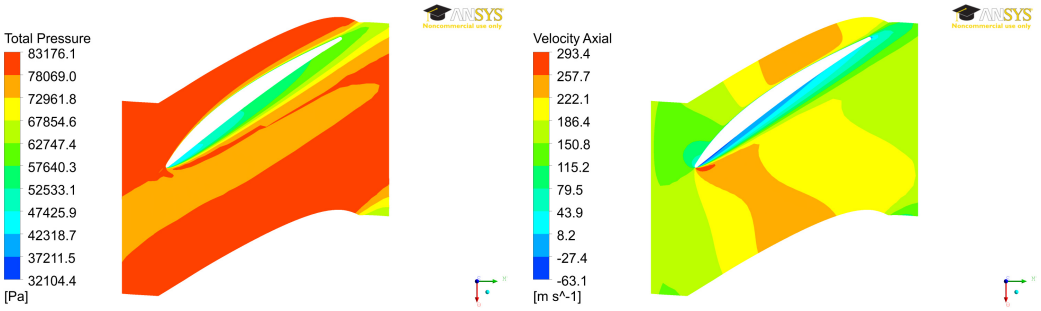

Figure 6.13: Blade to blade view for the zone 3 at 0.5 span height

The pressure losses area change between the solutions modifying the minimum value of the pressure and the wide of the vortex. In the axial velocity monitor it's clear how the different operating points work with different axial speed at the inlet but also how the effect of the vortex on the axial velocity on the outlet. The maximum velocity in the solution belonging to the zone 3 is located near the vortex which works as a venturi tube.

Chapter 7

Surge line definition

In a compressors the surge line is defined as the curve obtained by the interpolation of the last stable points for the different geometrical configurations[11]. Before showing the results obtained with the simulations is important to present the instabilities which occur over the surge line. Three kind of instabilities can occur in an axial compressor: the rotating stall, the surge and modified surge. These depend on the compressor's geometry and on its operating conditions. The rotating stall is a three-dimensional instability that is located in the compressor's rotors. The stalled cell is a region in the blade channel where the flow is separated this vortex rotates with a lower speed with respect to the rotor, so it rotates in the reverse direction of the rotor in a relative frame. In a rotor can take place one or more stalled cells, here the flow is decelerated by the vortex effect and this change the incidence on the blades next to the stalled cells. The movement of the rotating cell is time dependent and is the result of the non uniform velocity distribution in the circumferential direction. Referring to blade to blade view of the picture the blades above are mainly loaded than the blades beyond, hence the stalled cell move frome the bottom to the top of the row. The blades are moving

from the top to the bottom referring to a stationary frame, while the rotating cell is moving referring to the rotating frame from the bottom to the top. The rotating speed of the stalled cell has the same direction of the rotor but the speed value usually between the 20% and the 80% of the rotor speed. The speed of the rotating cells is depending on the compressor's geometry, operating conditions and number of stalled cells.

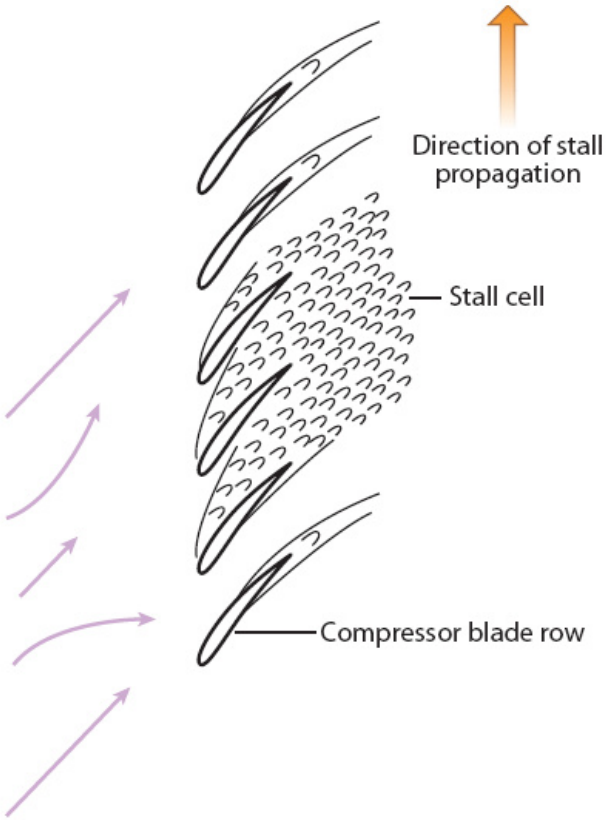

Figure 7.1: Blade to blade view of a stalled cell's propagation

The surge is an axisymmetric oscillation of the mass flow along the axial length of the compressor. When the pressure at the compressor outlet is too high for the compressor performance this become unstable. Some compressor's stage stall and the pressure ratio drop down with the generation of a

pressure wave or a reverse mass flow along the compressor. The pressure at the outlet of the compressor is reduced and the mass flow and the axial speed increase working with an operating condition next to the choke. The incidence on the stalled rotor is reduced and the the pressure ratio increase again moving along the operating line next to the surge line. If the pressure ratio at the outlet is still too high the cycle happens again creating a pumping cycle which load and unload the blades in the axial direction.

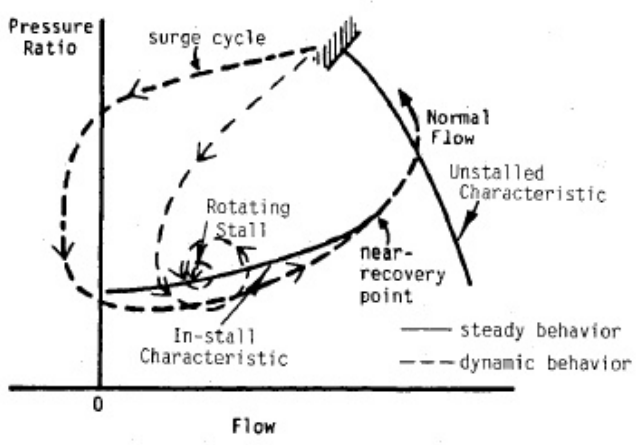

Figure 7.2: Surge pumping cycle in a compressor

The third phenomena, the modified surge, is a combination of the rotating stall and surge. The flow in the compressor show some channels similar to the stalled cells where reverse flow happens, while the other parts of the compressor are working in a normal condition. The channels with reverse flow are rotating too inside the compressor with a speed lower than the rotor speed, generating a variable load on the blades. These different instabilities depend on the compress characteristic as summarized by the Greitzer parameter[12]:

$$B = \frac{\frac{1}{2} \cdot U^2 A_c}{\rho \omega U L_c A_c} = \frac{U}{2a}\sqrt{\frac{V_p}{A_c L_c}} \tag{7.1}$$

Where a is the speed of sound U is the tangential speed of the compressor V_p is the volume of the rear plenum A_c is the area of the compressor duct and L_c is the length of the compressor and the duct as presented in picture.

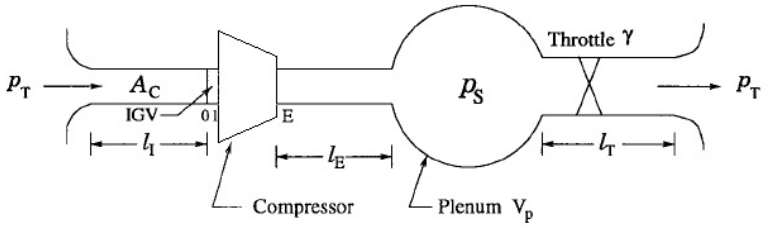

Figure 7.3: Schematic of compressor showing nondimensionalized lengths

The Greitzer parameter is nowadays the parameter which allows to predict the kind of instability for the compressor. High value of the parameter requires the surge as unstable behaviour while low value requires the rotating stall, between them there is a zone where the modified surge occur. The limit of the Greitzer parameter are function of the compressor and can divide the three behaviours of the machine. All the instabilities are triggered by the rotating stall before developing in the different manners, except for the machines with very high rotational speeds and very high pressure ratios where the surge can occur immediately after the last stable operating point. The studied compressor has a pressure ratio lower than two and the design rotational speed is 11500 [rpm], with these parameters the compressor can be classified as high speed but not high pressure ratio compressor. There are two different types of local instabilities which precede the rotating stall and they depend on the compressor configuration. The first type of inception is referred to a modal stall inception, which is is characterized by the growth of small-amplitude, two-dimensional, long-length-scale (approximately equal to the compressor circumference, π multiplied by the compressor diameter)

wavelike disturbances extending axially through the compressor. These disturbances, referred to as modes, can often be detected tens or hundreds of rotor revolutions prior to stall onset and propagate in the circumferential direction at speeds ranging from 20% to 50% of the rotor speed [13]. The second type of stall inception, referred to as spike-type inception[14], is characterized by the formation of three-dimensional, finite-amplitude disturbances (after Day 1993b) localized to the tip region of just one rotor row in a multistage compressor. Spike-type stall inception is distinctly different from modal-stall inception in both timescale and length scale. The short length and long length disturbance exist in the compressor at the same time but the mode which first get unstable is the origin of the rotating stall. The two instabilities existing in the compressor are showed below, there the small length instabilities, spike-type inception, bring the compressor to the stall.

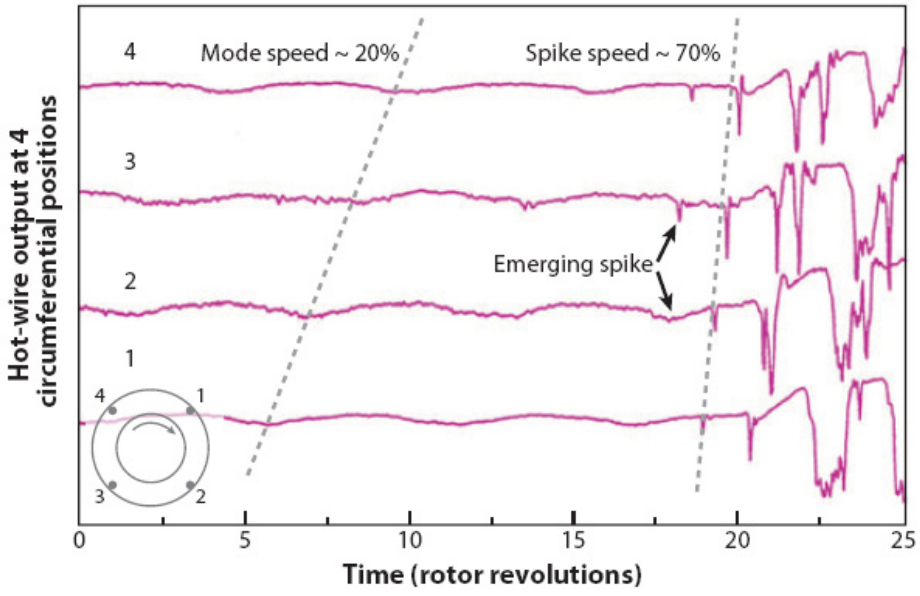

Figure 7.4: Blade row with a stalled cell

In the early years the usage of the CFD codes allows to analyse the flow features for the stalling flow. The spikes are located in the blade circumfer-

ence and near the tip clearance where instabilities develop from. To detect the stall inception two conditions are required, first the flow at the inflow of the blade has to be parallel to the plane defined by the trailing edge of the blades. This happens when the flow cross the tip clearance and is spilled by the adjacent blade ahead of the trailing edge. The second inception is the suction of reverse flow in to the rotor. Fluid originating from the tip-clearance region of one blade moves across the blade passage into the neighboring passage by passing around the trailing edge. The trajectory of this fluid is such that there is impingement on the pressure surface of the adjacent passage. This reversal of the tip-clearance fluid from the first blade passage (essentially an end-wall separation with a circumferential relative velocity component) is referred to as tip-clearance backflow.

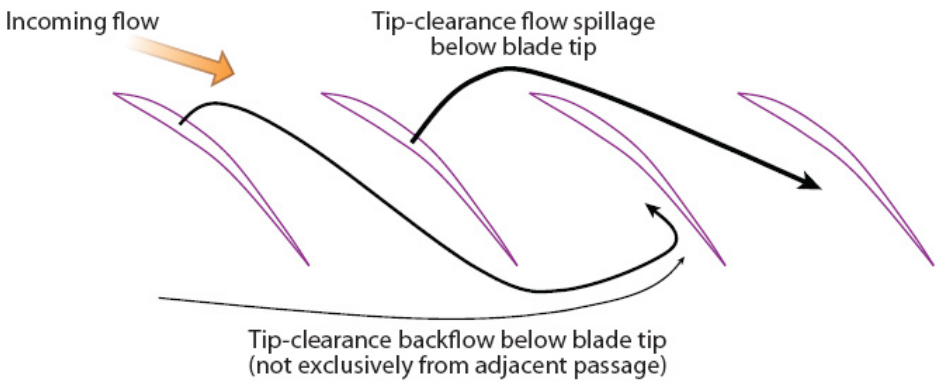

Figure 7.5: Critical condition for the stall triggering near the blade's tip

For a compressor with adjustable geometry is possible to find both of the inception instabilities because changing the matching of the stage also the stalled stage can change. Some critical conditions can trigger the stall and reveal if there are some common features for the different IGV's orientations. The short scale instabilities (spikes) are usually detected with a critical incidence angle while the long scale instabilities (modal) become unstable when

the static pressure ratio curve has a zero slope.

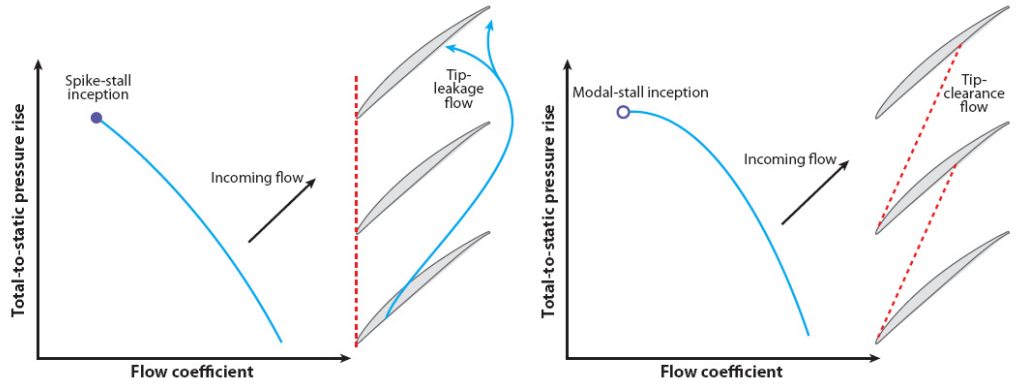

Figure 7.6: Comparison between the two stalling cause

The CFD simulations can't reproduce the real compressor's behaviour because the simplifications of the model don't allow to reproduce exactly the flow in the compressor when it approaches the stall. From the experiments is known that the rotating stall is transient and not-axisymmetric and the pressure disturbance move along the compressor. In the simulations a single blade channel is modelled, this supposes that the flow is the same in every blade channel. The analysis is steady state, not time dependent, while the real phenomena is transient because the position and the dimension of the disturbances are function of the rotations thereby of the time. The last hypothesis used in the model is to have a perfect mixing of the flow at the interface between the rotors and the stators. So the incoming flow in a successive blade row is the result of the circumferential average made on the flow coming out from the previous blade row. The flow disturbances are circumferentially located and they move all along the compressor affecting the rear stages. These passing thought the mixing plane are completely deleted. To model the stall inception is necessary to use a transient simulation and use the complete compressor row with all the stage's blades, solution not available

with the usable computational power. The prediction of the CFD simulation can not discover exactly the stall inception but with the experimental result validation can give some interesting information about the local flow in a stalling compressor and close off some critical conditions.

7.1 Simulations result and discussion

The simulation's results are obtained using the following set-up as the boundary conditions, the total pressure inlet to 101325 [MPa] and the temperature are fixed while at the compressor outlet the mass flow is fixed as the second boundary condition. These conditions make the convergence process slower compared to the simulations with the static pressure at the outlet, but because of the shape of the operating line next to the surge this solution is necessary to avoid high uncertainty in the results. For the simplified configuration without the fillet in the simulations the flow field features are compared for the different configuration at the last stable point. The stall in a rotor can propagate in other rotor where the critical condition are not reached yet. The stall vortex has different effects on the other stages, the wake effect which pass through the rear stages and the potential effect which act on the forward stages. The effects however don't have the same magnitude and when a compressor stage stall all the rear stage stall too because of the vortex wake, while the stage forward are still working in a normal manner. For the configuration with a positive IGV's angle the first stage is unloaded and the rear stage are making the main part of the compressor's work while with a negative IGV's angle the first stage is strongly loaded. The comparison of the performance maps of the compressor allows to predict the stage which stall first, in the simulation however the uncertainty is

high because the results are depending on the mesh size as seen in the mesh independence study, so the prediction can not be quantitative but only give a qualitative idea of the stall phenomena.

IGV's angle	mass flow	π_c	$\pi_{c\,stage1}$	$\pi_{c\,stage2}$	$\pi_{c\,stage3}$	$\pi_{c\,stage4}$
-15°	14.4	1.884	1.221	1.173	1.159	1.139
-10°	14.6	1.892	1.229	1.176	1.157	1.137
-5°	14.2	1.891	1.219	1.177	1.159	1.14
0°	13.8	1.873	1.201	1.179	1.161	1.143
10°	13.0	1.818	1.159	1.180	1.164	1.146
20°	12.4	1.739	1.115	1.183	1.166	1.148
30°	11.6	1.616	1.048	1.190	1.170	1.151

The pressure ratio in the configuration with positive IGV angle is maximum in the second stage while in the other configurations it's in the first stage. The enthalpy difference follow the same trend suggesting that the stall occur in the second stage for positive IGV angle while in the first one for the other orientations.

IGV's angle	mass	ΔH_{stage1}	ΔH_{stage2}	ΔH_{stage3}	ΔH_{stage4}
-15°	14.4	21115	16735	15737	14536
-10°	14.6	20205	16373	15478	14331
-5°	14.2	18909	16454	15653	14589
0°	13.8	17302	16547	15831	14823
10°	13.0	14114	16542	16047	15139
20°	12.4	10686	16701	16172	15243
30°	11.6	5468.1	17065	16366	15340

The stage pressure ratio is not always growing but with positive IGV's angle the pressure ratio in the stage behind the first one decrease for the

operating points next to the surge. While with negative and zero IGV's angle the pressure ratio is always increasing when the mass flow decreases. The stage which become unstable is not the same for all the IGV's angle. The last stable point are the points with the maximum pressure ratio, which states the compressor is still working without deep losses. The streamline in the first rotor has a zone with high speed on the suction side of the blade and next to the trailing edge the flow start to separate. The high speed on the suction side is linked with the loading of the blade because the lift force on a blade is directly proportional to the flow circulation around the blade. The vortex next to the trailing edge is a consequence of the high pressure difference between suction side and pressure side, the pressure is a continuous function around the blade so in the suction side where the pressure is less the flow next to the trailing edge has to decelerate. The deceleration is directly linked to the pressure difference on the two blade sides, if the difference is to big the flow can't be attached to the surface and generate a vortex. These effects are the consequence of the IGV loading but they are not the only cause of the compressor stall because there are different size of the vortex and of the velocity gradient but the points are still stable.

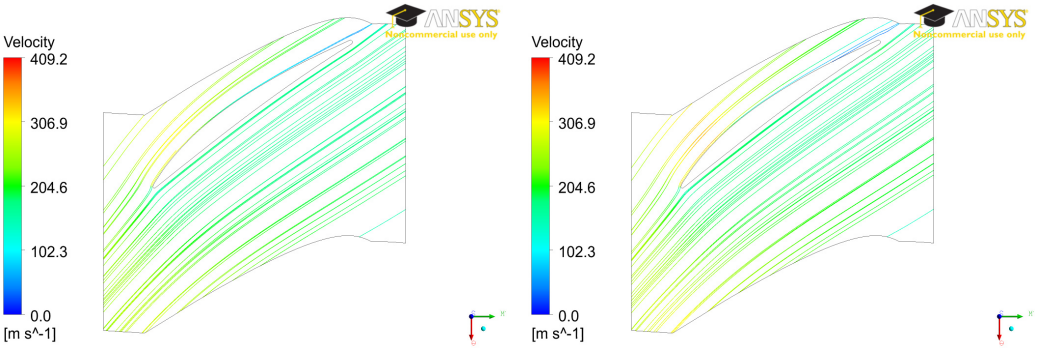

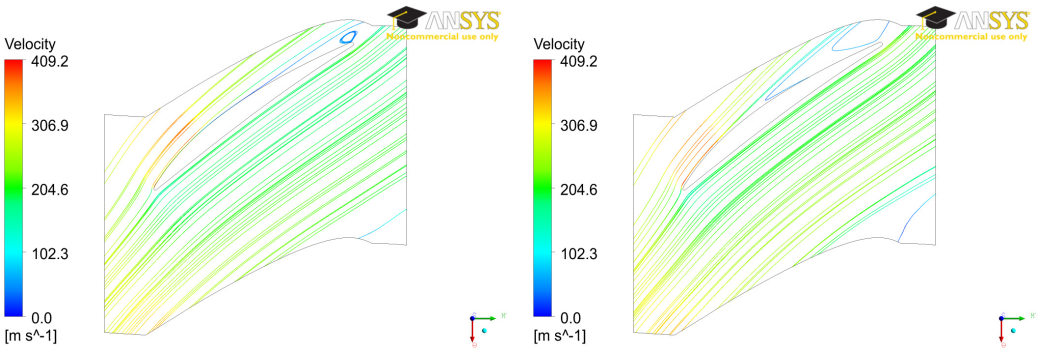

The flow close to the tip clearance of the blade is fundamental to trigger the stall inception because in the stalling rotor the angle of the flow is 180° and there is a spillage of flow from the outflow. The complete phenomena cover more than one blade and it is transient but it's still possible to find some qualitative informations on the flow near the tip clearance. The plot of the flow angle along the span is compared for the different IGV configurations, the maximum flow angle at the tip clearance changes its position in the stages. For the configurations with IGV's negative angle the maximum incidence is in the first rotor while for the positive configurations the maximum incidence move to the second stage. For the 00° configuration the angles at the blade inflow are the same but the angle of the blade is not the same in the tip region. The axial compressor use the same blade in all the stages which are copied and trimmed in the tip zone. The solid angle reduces increasing the blade radius thus the incidence angle changes too $i = \alpha_{in} - \alpha_{blade}$. The fluid angles in the first and second stage are the same in the tip region but the incidence angles are different. For the transition configuration 10° 00° -5° the angle is plotted showing the three different behaviour.

The difference of the angle is between 1 and 2 degree but this difference changes the behaviour of the entire machine. The flow characteristic for the

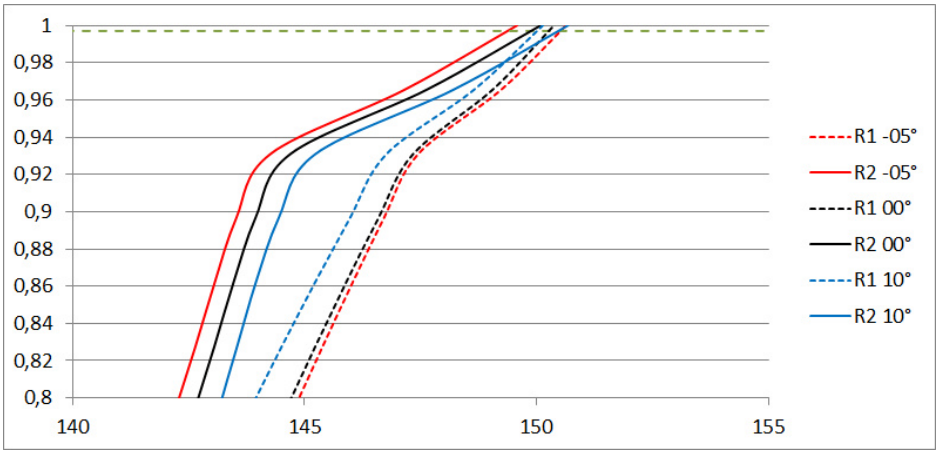

configuration with positive angle are compared in the second rotor where is supposed the stall start. The angle profile for the first stage and the second stage are compared and for the three configuration the solutions show almost the same curve for the second rotor.

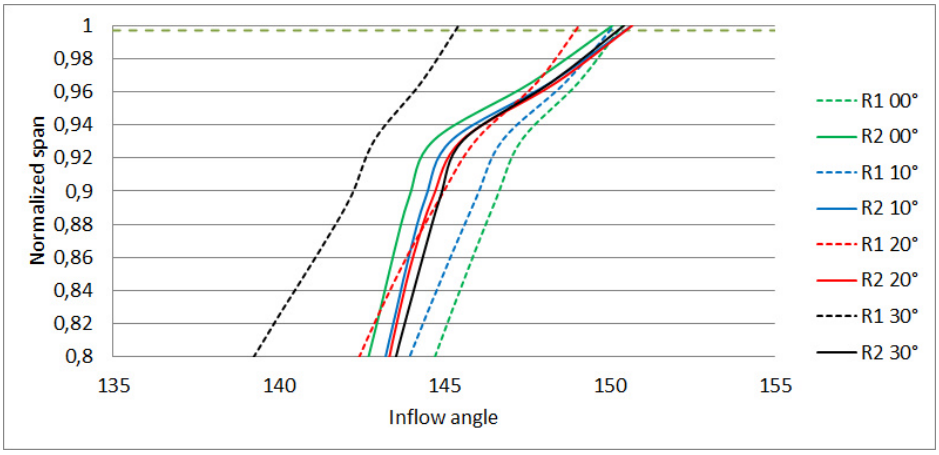

In the second rotor near the tip clearance there are also the same value for the meridional velocity and the circumferential velocity. The speed distributions in the machine configuration with positive IGV's angle show the same trend in the tip region, while the 00° configuration is still different. This result confirm how the stall is for positive IGV angle configurations in the second rotor instead of the first. At the same time there is another

important result, all the flow field considering the meridional velocity and the circumferential velocity are the same. The stall in the second rotor is triggered by these flow condition for the region close to the blade tip. These result can have only a qualitative meaning because of all the simplifications in the model but is still helpful because for these geometrical configuration a common condition for the stall inception is founded.

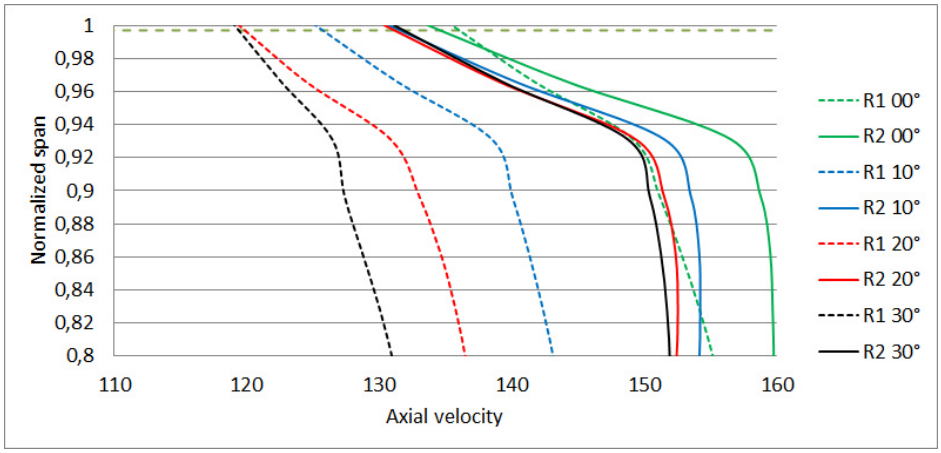

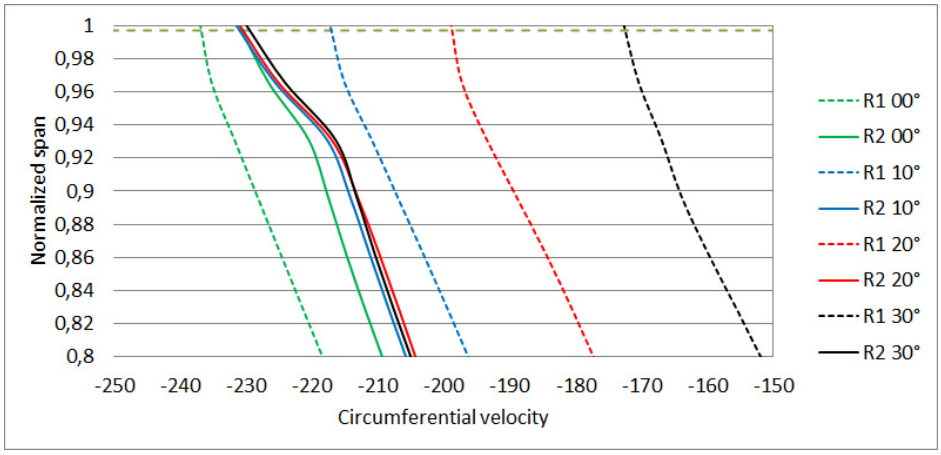

For the configurations with the negative IGV's angle the flow features are also compared but the flow is not the same as happened in the previous configuration, the velocity angle and the speed component are different. At the surge line the last stable point for the -15° configuration is between the

-10° and the -05°ones because the operating line are crossing each other as discussed in the previous chapter. Hence for the negative angle configurations there isn't a common feature for all the configuration but is still clear that the vortex on the blade suction side and the incidence angle are not the only causes of the stall. The different characteristic of the last stable point suggest also that the stall inception is different. The compressor can have a modes stall inception or a spike stall inception as seen in the experimental investigation carried out by Day. The negative angle configuration have a modes stall inception while the positive angle configuration show a spike stall inception. For the simulations this is only an hypothesis because of the simulation uncertainty, but this can explains why there is no a unique feature for the stall inception.

Chapter 8

Compressor map for the geometry with fillets

Normally in the CFD simulations the fillet are not counted in the geometrical representation of the blade because they request more time and more effort to generate the mesh and their effects are usually ignored. The new geometrical model is closer to the real geometry of the real machine, without being the exact copy. The rotor's blade has the same geometry of the real machine with a constant radius fillet, while the stator's blade ant the IGV's blade have a constant radius too instead of the real fillet, placed only around the blade's shaft. The new simulations allow to monitor the effect of the real geometry on the machine behaviour comparing the new results with the previous. In the geometry with the fillet there is a unique surface between the blade and the hub, rotors, or the shroud, stators.

This smooth surface prevent the usage of the Turbogrid mesh which require two different surfaces with a sharp corner between. A new mesh structure is generated using another meshing program, ICEM. The mesh still has a structured topology, but it require also a O-grid all around the blade. The

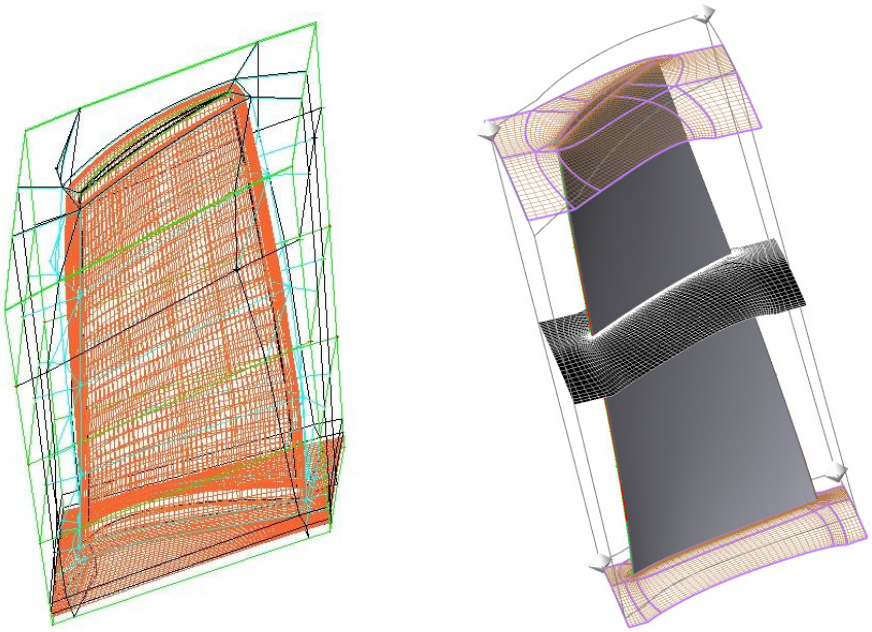

Figure 8.1: Mesh with O-grid for the blade with fillets(left) and conventional mesh without O-grid for the blade without fillets (right)

O-gird allows to mesh the smooth fillet using the Hexahedrons has mesh elements. Instead of the mesh configuration ATM-optimized performed by Turbogrid a H mesh is generated. The new mesh is defined in order to have the same number of elements distributed in the different stages. In the literature the fillet were not widely and deeply investigated mainly because their effects were considered negligible and the results are hard to explain. These is furthermore another problem connected with the experimental results, it's not possible to run a compressor without fillet otherwise the blade will break after few rounds[15]. The experimental data are refereed only on linear cascade[16] where the flow has not the same three dimensional characteristic of the one in a rotating blade row. The fillet are used in the compressor for a structural reason, the stress distribution in the blade root is influenced by the blade shape[17]. If there is a sharp edge between the machine's hub and the blade

surface the stress will have theoretically infinite value. When the blades are forced by a swinging load fatigue can break the blades, the fillets reduce the stress peak in the blade and the avoid the extension of the crick inside the blade. The stress damping depends on the fillet's radius, a bigger radius decreases more the stress in the blade, on the other hand it blocks the mass flow and change more the machine's geometry.

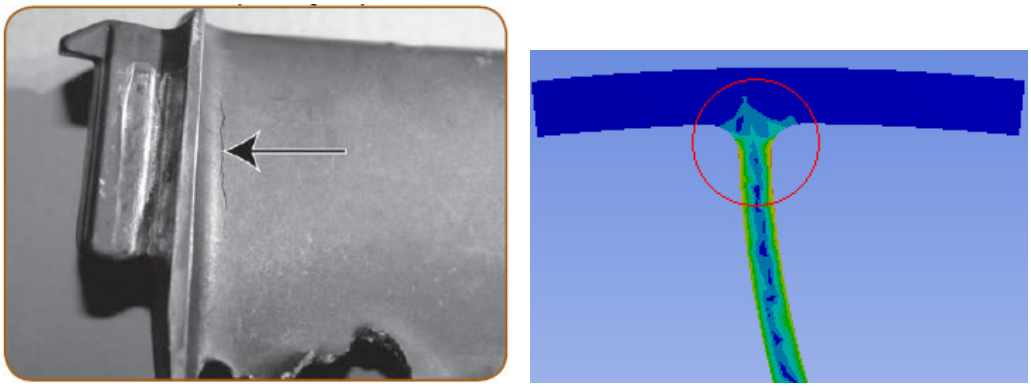

Figure 8.2: Blade's crick near in the fillet(left) and stress distribution near the fillet of a blade (right)

Some investigation were carried out about the influence of the fillet on the fluidynamics machine performance, but not a unique answer was founded. The incidence angle changes near the blade root because there is a new profile in these blade's part thus the profile's load is modified. The endwall losses increase near the root because of the larger surface where the air flows. These two aspect of the fillet fluid interaction are clear and they can be easily evaluated also with simplified experiments, while it's harder to close off effect of the secondary flow. Different authors with experimental and numerical researches didn't find the same results and a unique explanation comparing the blade's behaviour with and without fillet. Normally in the blades with fillet the losses are greater and they are mainly located near the

root, decreasing the total total pressure ratio. The pressure losses depend also on the size of the fillet because decreasing the cross flow area the speed increases as the endwall losses. Experimental investigation showed also that the total pressure usually decreases, but with small radius fillet the static pressure increase. The fillet decreasing the cross flow section increase flow deceleration and the static pressure rise also if the total pressure is reduced. Different experiments were made on different profile shape and they assert that the losses distribution depends on the profile and on the operating point. Some profile work better with fillet while others work better without them as well for some operating point the profile with fillet work better while for some others the profile without fillet work better. Because of the difficulty to find a explanation for the fillet influence on the secondary flow and because of the other approximations used in the CFD there fillet effect is not completely understood yet. In the CFD simulations all the stages increases the pressure ratio and the enthalpy difference for all the simulated operating points, this is in contrast with the previous investigation but this can depend on the profile shape but also on the meshing. However the effect of the fillets is closed off in the choke region where it change the mass flow in the throat area.

8.1 Effect of the fillet near the choke line

The main effect discovered studying the simulations with and without fillet is the deep effect on the choke limit. As mentioned in the previous chapter all the simulations without fillet don't reach the convergence for the points next to the choke because of a transient vortex near the root of the fourth rotor. The new simulations with the fillet reach the convergence for all the IGV configuration and show a important difference in the mass flow for the

choked solution. In the following picture the compressor mas is presented showing the new choke limit for all the configurations As founded in the

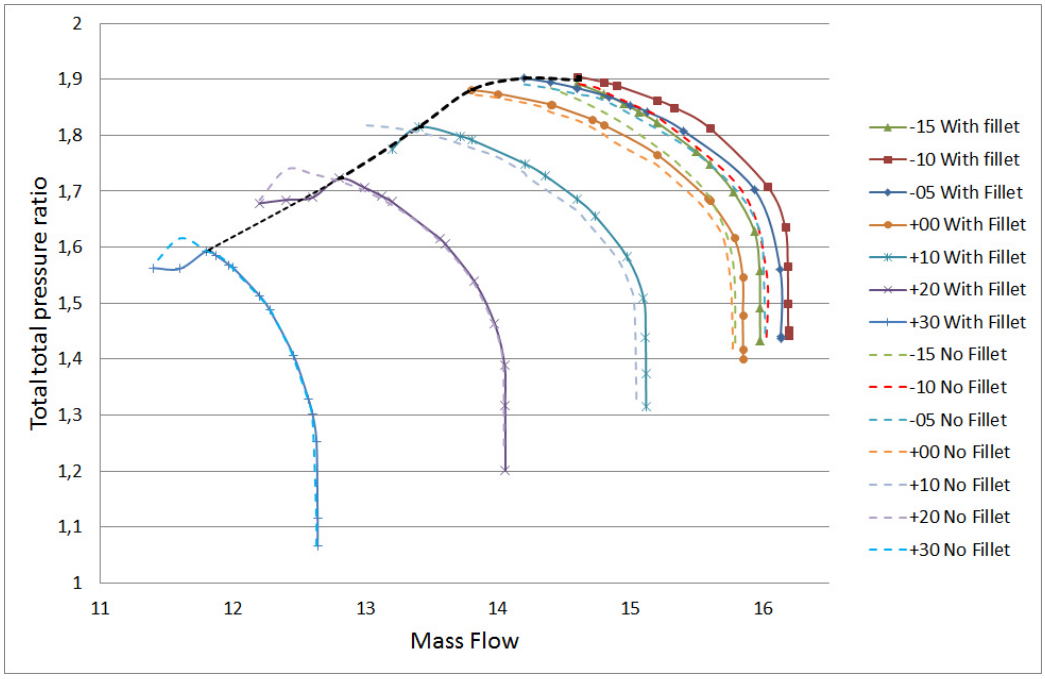

simulations without fillet the choke occur in the last stator where the Mach number is equal to one and the stator stage behaves like a De Laval nozzle. To understand why the compressor has a greater mass flow when the fillet are added the results at the choke line for the 00° configuration are compared. The boundary condition for the simulation are the same total pressure inlet 101325 [Pa] and static pressure outlet 50662.5 [Pa] the independent variable in the simulation is the mass flow. In the simulation with fillet there is a big vortex on the suction side of the fourth rotor, because of the vortex the total pressure decrease at the last stator inlet where there is throat area. If the total pressure drop down due to the vortex losses the density in the vortex region decrease and the temperature increases following the first low of the thermodynamic and the low of the ideal gas. The losses transform the pressure energy in thermal energy and in kinetic energy maintaining the

rothalpy constant. The mass flow incoming into the last stator is the product of different factors which are linked with the vortex in the rotor blade.

$$\dot{m} = A \cdot \rho \cdot v \tag{8.1}$$

The area is the same for the two solution but the density and the speed are the result of the flow in the rotor.

00 IGV	$\dot{m}$ [kg s^{-1}]	ρ [kg m^{-3}]	v_{ax} [m s^{-1}]	P° [Pa]	T [K]
with fillet	15.85	1.2951	219.4	151230	308.7
without fillet	15.77	1.2906	220.7	150572	307.6

From the table the quantities look be the same because they are averaged with respect with the mass flow, so it's expected the averaged speed times the average density times the area is not equal to the mass flow. The mass flow is the integral of the local quantities so the two calculations give different results. The density and axial speed profile are plotted at the rotor outlet in order to show the mass flow distribution.

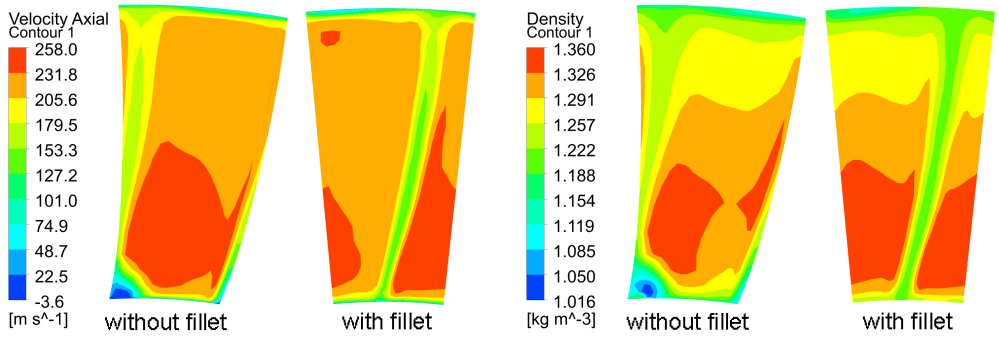

Figure 8.3: Axial speed comparison without and with fillet(left) and density comparison without and with fillet(right)

In all the IGV's configuration the same trend was founded because the mass flow for the simulations with the fillet have always greater mass flow at

the choke line. The difference between the simulations with the fillets and without is not constant but it's depending also on the angle. The mass flow are compared for the different IGV's configurations evaluating the absolute and the normalized difference between the mass flow.

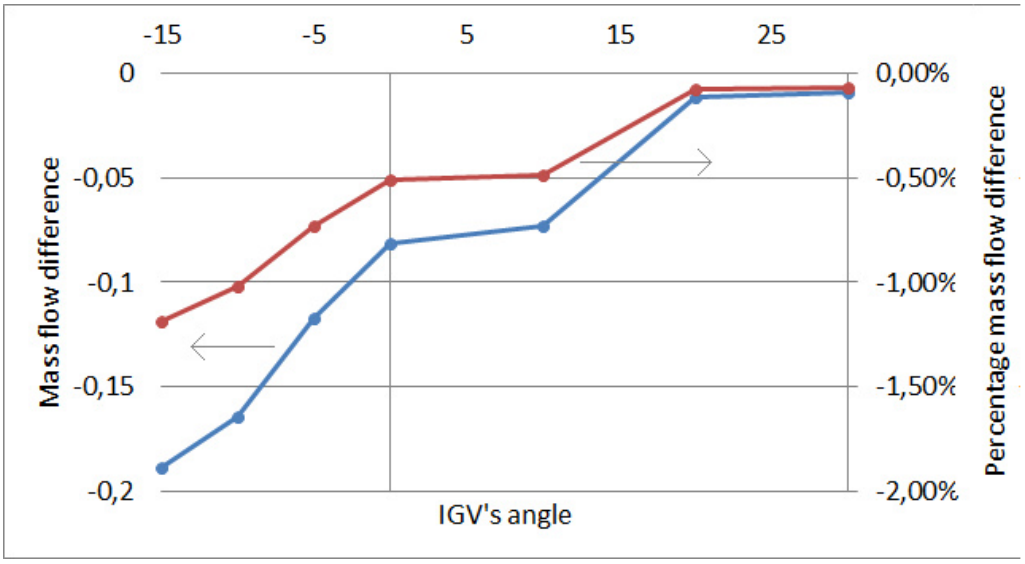

The relationship between the mass flow and the angle is not linear so is necessary to analyse in the flow field how the losses operate in the different configurations. The -15 configuration show the maximum difference between the mass flow in the geometry with fillet and the geometry without fillet. The vortex in the last rotor is founded only for the simulation without fillet as happened in the previous analysis but in the entire machine the pressure ratio and the enthalpy difference are always greater for the simulation with the fillets that the simulation without.

-15 IGV	$\dot{m}$ [kg s^{-1}]	ρ [kg m^{-3}]	v_{ax} [m s^{-1}]	P$^{\circ}_{tot}$ [Pa]	T [K]
with fillet	15.98	1.2947	220.98	152240	314.44
without fillet	15.79	1.2838	220.99	150260	312.94

So the difference between the simulation is all along the machine thus the result is influenced also by the matching of the first stage and by the IGV's

orientation.

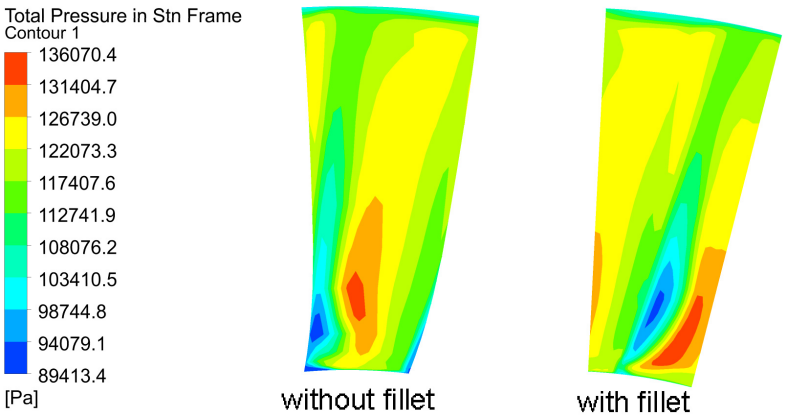

Figure 8.4: Total pressure distribution at the first rotor outlet, blade without fillet (left), blade with fillet (right)

The pressure distribution at the outflow of the first rotor show a difference in the vortex location. For all the operating point in the -15° on the suction side of the blade there is a vortex which decrease its size from the blade's root to the tip. The main losses are located behind blade in both configurations but the fillet moves the low pressure zone to higher radius. The fillet reduces also the losses near the machine's hub increasing the averaged value of the total pressure, for the configuration with fillet this is 119525 [Pa] while for the configuration without fillet it is 118997 [Pa]. The two simulations have the same inlet condition as density and temperature but being the mass flow different the velocity will be different too. In the machine with fillet the flow deceleration can be greater because of the lower losses. In the rear stages the effect of the fillet is not so clear because there isn't any vortex on the blade surface in both configurations but all the stages with fillet work with a greater pressure ratio and a grater enthalpy difference. The difference can depend on the geometry and its action on the flow field or on the mesh which

is different from the previous case without fillet. At the last rotor outflow the two machines have the same axial velocity meaning the fillet decelerate the flow better as mentioned also in the previous section. The density due to the grater pressure ratio in all the stages is greater in the configuration with the fillet so the resulting mass flow is greater too. Comparing the pressure ratio of the different rotors along the span the effect of the fillet changes in the different stage. In the first rotor the pressure ratio in the machine with the fillet is greater near the blade root because of the vortex on the suction side is smaller and is mainly located in the middle span zone, with a greater overall pressure ratio. In the second and third stage the effect of the fillet is different from the previous stage because the pressure ratio decrease a little near the blade root but the stage is working better in the middle span zone. In the last stage the vortex on the suction side in the configuration without fillet prevent a good pressure ratio in the stage with a total pressure drop near the hub.

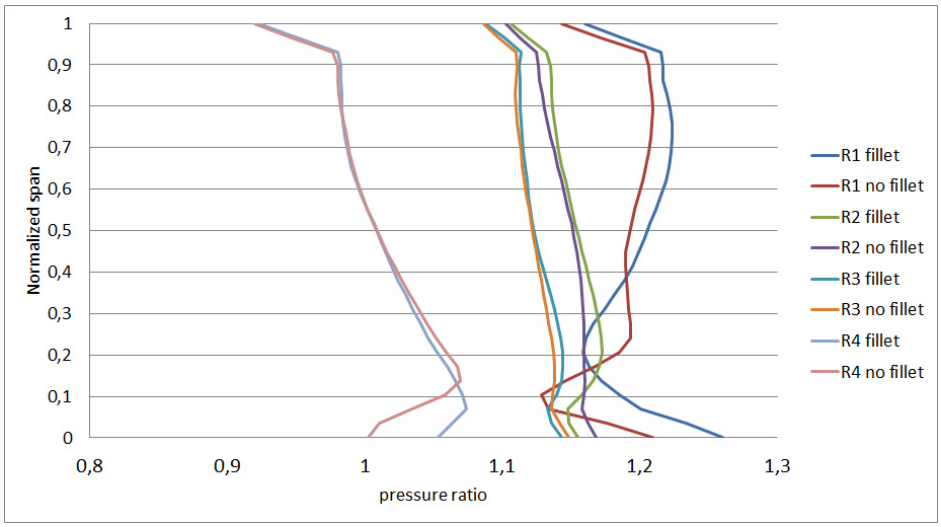

Figure 8.5: Total pressure distribution at the first rotor outlet, blade without fillet (left), blade with fillet (right)

From the literature background it was supposed to have a greater pressure loss with the fillet so a lower pressure ratio, but the simulations result don't confirm that. Probably the effect of the mesh size and the element distribution can affect the pressure ratio in the machine. The -15°configuration shows the greater difference between the choked mass in the simulation with fillet and the one without.

For positive IGV's angle the mass flow difference is reduced and the smaller difference occur with +30° configuration. The pressure ratio distribution in the stages along the compressor is different with respect to the -15° configuration because the pressure ratio is greater in the rear stage as previously founded but is lower in the first stage. For this IGV orientation the fillet decrease the pressure ratio changing the flow feature in the rear stages.

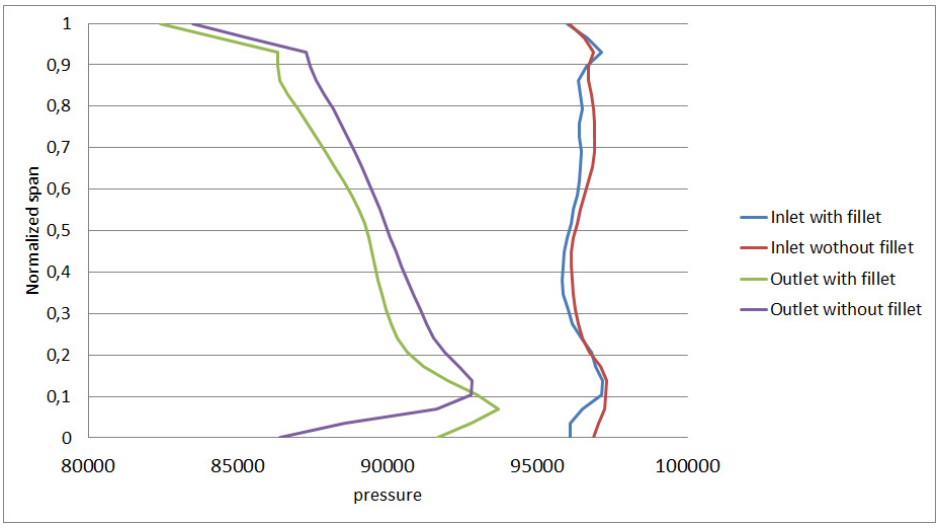

Figure 8.6: Total pressure distribution at the first rotor

In the fist stage as founded in the previous configuration there is a vortex in the fist rotor, due to the new stage matching. The vortex near the hub region is bigger in the configuration without fillet and the minimum total

pressure in the vortex core is lower however the pressure distribution along the span is greater. The pressure ratio in the first stage is greater for the configuration without fillet because the fillet reduce the vortex size on the suction side but decrease also the pressure distribution along the blade span. In the last rotor there is another vortex in the configuration without fillet, as founded in the other configurations. The pressure ratio in the rotor is affected by the pressure drop but the mass flow in the machine is depending on the complete machine performances.

+30 IGV	$\dot{m}$ [kg s^{-1}]	ρ [kg m^{-3}]	v_{ax} [m s^{-1}]	P$^{\circ}_{tot}$ [Pa]	T [K]
with fillet	12.638	1.0515	217.9	88161	293.16
without fillet	12.629	1.0526	215.6	88552	293.92

The difference between the mass flow in the machines is smaller with respect to the other configurations because the pressure ratio and the density decrease in the fist stage with fillets. The fillet has the same effect in the rear stages as founded previously it increases the pressure ratio and the enthalpy exchange. Also if the pressure and the density at the second stage inlet are lower the rear stages with the fillet reduce the gap stage by stage and at the last rotor outflow the mass flow is greater in the configuration with fillet. The same reasoning can be carried out also for the +20° configuration because there is a vortex in the first stage on the pressure side of the blade which interacts with the fillet and reduce the pressure ratio while in the other stages the pressure ratio for the configuration with the fillet is always greater. It's possible to watch how the vortex in the first stage change its shape because of the fillet, in the configuration with fillet the vortex is more compact and close to the hub while the vortex in the other configuration develops along the blade span. This distribution confirm what showed by the pressure distribution where the losses for the configuration near the fillet

are bigger but the don' t affect all the blade.

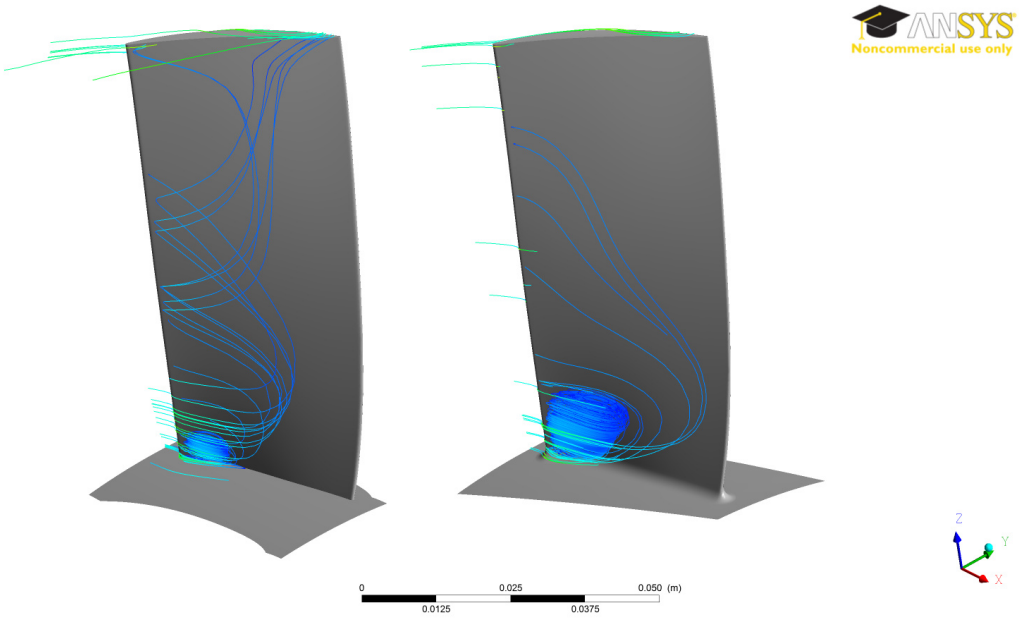

Figure 8.7: Total pressure distribution at the first rotor

8.2 Effect of the fillet near the surge line

The fillet modify also the compressor map near the choke line which moves to greater mass flow reducing the compressor operating range for all the configurations with positive IGV angle and -15°. The surge line is affected by the new geometry but can be also influenced by the new mesh, because as seen in the mesh independence study the difference between the solutions approaching the surge line increase. The angle distribution are monitored in order to find a common condition which trigger the stall inception. The angle near the tip clearance of the rotor is monitored for the first second and third stage. In these solution also the third rotor is monitored because some points over the surge line where simulated and these show big vortexes in the

third and fourth stators. The stall is always a phenomena starting from the rotors, thus the result are not believable except to define the last stable point and suggest the stall cell location. When a rotor falls in stall in a multistage compressor the rotors behind the stalled one fall also into stall. Following this reasoning the stall is supposed to take place in the third rotor and not in the second as founded for the configuration without fillets.

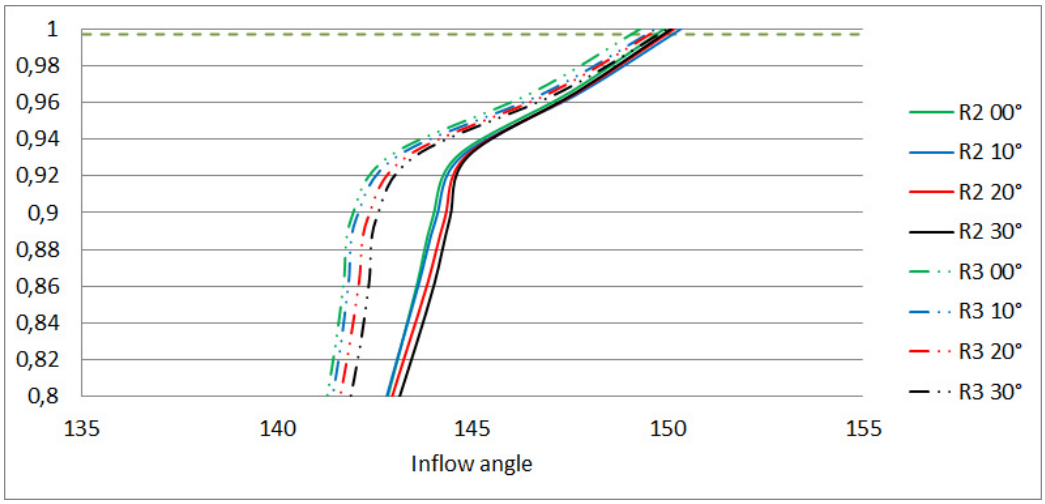

Figure 8.8: Angle distribution near the blade tip for the second and the third rotors

Near the tip blade also the velocity components are compared, the axial speed near the tip are almost the same for the configuration with positive angle at the inlet of the second rotor while they are distributed in a wider range in the third rotor. The circumferential speed show for the second and third rotor almost the same distribution, but the second rotor has for all the configurations a greater absolute value of the speed component. In the second rotor the axial speed for the 00° configuration in greater and is not so close to the other three lines. This can mean the stall condition as seen in the configuration without fillet are different because the phenomena of stall

inception can be different.

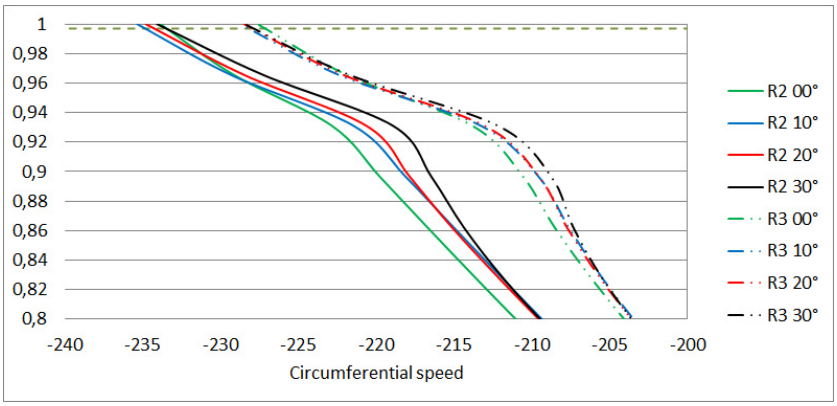

Figure 8.9: Circumferential speed distribution along the span near the tip on the second and the third rotor

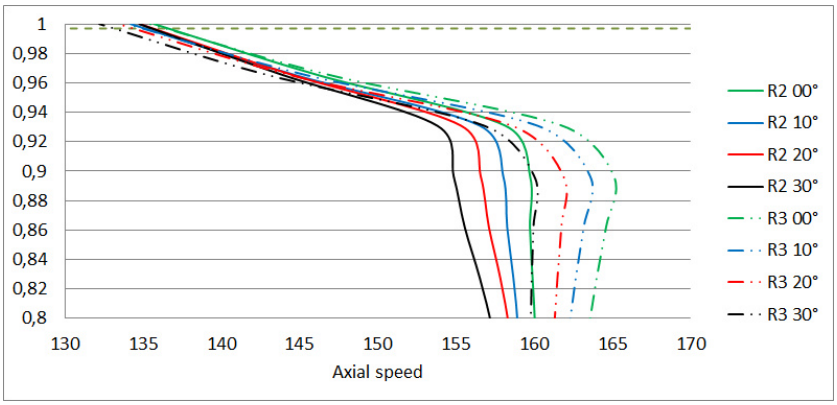

Figure 8.10: Axial speed distribution along the span near the tip on the second and the third rotor

From the analysis of the results is possible to suppose the stall happens in the second rotor as happened in the machine without fillet. In the machine configuration with negative IGV angle only the -15° operating line change the last stable point to a greater mass flow. The flow feature as done in the machine without fillet are compared in order to find some common flow conditions which predict the stall inception. For the negative IGV orientations

only the inlet conditions in the first stage are monitored but the velocity components don't show the same agreement that was founded for the positive configuration near the surge line.

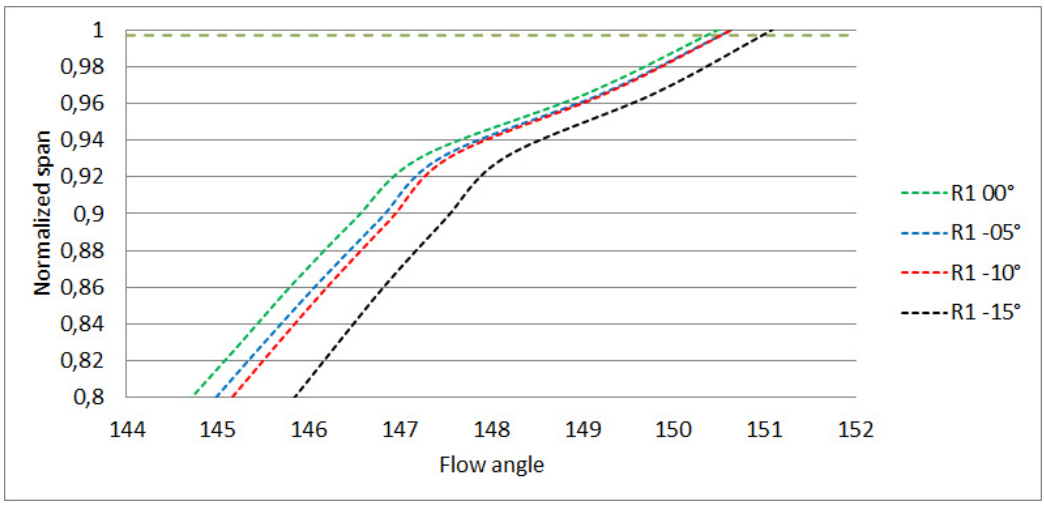

Figure 8.11: Angle distribution near the blade tip for the second and the third rotors

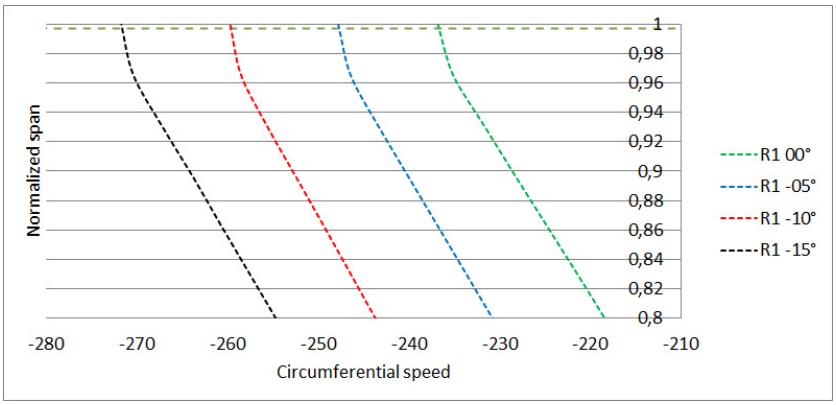

Figure 8.12: Circumferential speed distribution along the span near the tip on the second and the third rotor

The different surge limit founded in the compressor move the last stable point to greater mass flow so to lower pressure ratio. All the simulations with

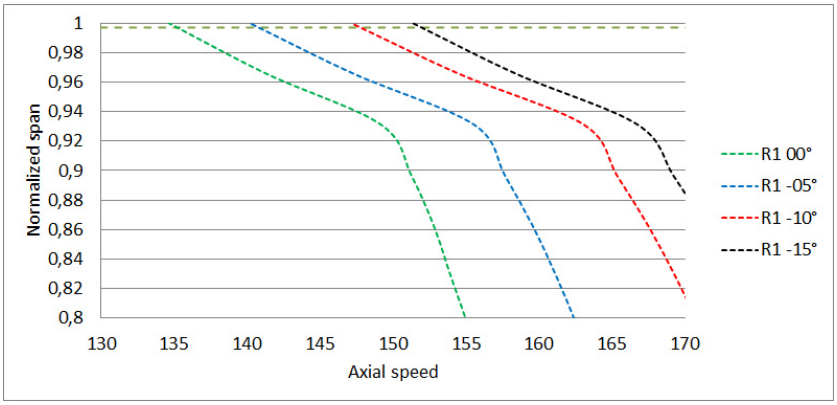

Figure 8.13: Axial speed distribution along the span near the tip on the second and the third rotor

the fillet usage increased the machine pressure ratio and enthalpy exchange hence the same critical conditions such pressure ratio and maximum flow incidence are reached with greater mass flow. Unfortunately this explanation can be only qualitative because also comparing the flow angle distribution along the span in the tip region there isn't a good agreement for the results with fillet and without fillet.

Chapter 9

Structural analysis for the axial compressor

The axial compressor has been widely studied regarding the aerodynamic performances in the different operating configurations. This is a prediction of the machine's behaviour which will be tested in the reality and which will confirm on not the prediction carried out until now. To run the compressor in a safe manner is request a structural analysis where the deformations and the stress are controlled. The risks are the seizing of the blade on the casing ans the failure because of the maximum stress. To model the stress in the compressor is necessary to use the second geometry with the fillet because this is closer to the real model than the initial geometry. This has a sharp corner between the blade surface and the frame surface and here the stresses rise until infinite value giving us some false prediction.

The analysis investigates all the geometrical configuration and different operating points on the compressor's line, hence a new compressor map are generated where the maximum stress and the maximum deformation are plotted. For the different configurations also the most loaded configuration

are investigated in order to understand how the blade work under the effect of the loads.

9.1 Theoretical introduction

The mechanical analysis is based on the theory of the linear elasticity which give as result the stress and the deformation distribution for a solid stressed by some prescribed loadings. The theory consider a linear elastic material, hence the stress is lower than the yielding limit and a linear relation connect the stress and the strain. To solve the problem of the elastic behaviour of the material is necessary to write the equations which rule the motion of the solid, the strain displacement and the constructive equations[18]. The motion equation is an expression of the newton second law of dynamic.

$$\rho \frac{d^2u}{dt^2} = \nabla \cdot \sigma + F \tag{9.1}$$

The analysis is steady state as the previous fluid-dynamic one but the acceleration of the body is not equal to zero because some blades are rotating. In the stator's blades the acceleration is null while in the rotors the acceleration is the result of the their motion.

$$du = d\theta \times R(t) \tag{9.2}$$

The radius is not time depending because the study is carried out ignoring the transitory from the compressor start and the until it reaches the normal operating conditions. Deriving the previous equation by the time we get:

$$\frac{du}{dt} = \frac{d\vec{\theta}}{dt} \times \vec{R} = \vec{\omega} \times \vec{R} \tag{9.3}$$

The acceleration is the derivative of the speed by the time, where the ω is depending on the time but also direction of the $\vec{R}$ is changing so the

acceleration become.

$$\frac{du}{dt} = \frac{d\vec{\theta}}{dt} \times \vec{R} = \vec{\omega} \times \vec{R} \tag{9.4}$$

The stress at the body surface have to be in equilibrium with the pressure field generated by the flow and F is the body force but it's equal to zero because the centrifugal force is counted in the body acceleration and the gravity force is not counted.

$$\frac{d^2u}{dt^2} = \frac{d\vec{\omega}}{dt} \times \vec{R} + \vec{\omega} \times \frac{d\vec{R}}{dt} \tag{9.5}$$

The first term is equal to zero because the shaft is rotating at the constant speed 11500 [rpm], while the second one is the derivative of a vector by the time. The modulus of $\vec{R}$ is constant, but in a stationary frame the direction is changing and $\vec{R}$ can be written as —R— $\vec{i}$. Deriving the direction i by the time the result is ($\omega times \vec{i}$) and the acceleration become:

$$\frac{d^2u}{dt^2} = \vec{\omega} \times (\vec{\omega} \times \frac{\vec{R}}{dt}) = -\omega^2 \vec{R} \tag{9.6}$$

The equation of the motion can be written in a easiest way suitable for the studied case:

$$-\rho\omega^2 \vec{R} = \nabla \cdot \sigma \tag{9.7}$$

The stress are contained in the Cauchy stress tensor where all the components of the tensor represent a stress on the surfaces of a elementary solid cube to which the motion equation is applied:

$$\sigma = \begin{pmatrix} \sigma_x & \tau_{xy} & \tau_{xz} \\ \tau_{yx} & \sigma_y & \tau_{yz} \\ \tau_{zx} & \tau_{zy} & \sigma_z \end{pmatrix} \tag{9.8}$$

The stress components on the main diagonal are the stresses normal to the surfaces, while the other component are the shear stresses. The tensor because of the momentum equilibrium is symmetrical and $\sigma_{i,j} = \sigma_{j,i}$.

The displacement equation unites the internal strain with the body deformations

$$\epsilon = \frac{1}{2}\left[\nabla u + (\nabla u)^T\right] \tag{9.9}$$

The strains are, as the stresses, summarized in a tensor and every component is defined as the ratio between the deformation of the solid and its initial dimension.

$$\epsilon = \frac{l - l_\circ}{l_\circ} \tag{9.10}$$

A body can deform in different manner there are normal components which stretch or constrict the size of the elementary element and there are also shear deformations which change the angle between the faces of the elementary element.

$$\epsilon_x = \frac{dx + \frac{\partial u_x}{\partial x}dx - dx}{dx} = \frac{\partial u_x}{\partial x} \tag{9.11}$$

The engineering shear strain is defined as $\gamma_{xy} = \alpha + \beta$ the angle between the two surface of the solid element. For small angle the tangent of the angle can substitute the angle.

$$\alpha = \frac{\frac{\partial u_y}{\partial x}dx}{1 + \frac{\partial u_x}{\partial x}dx} = \frac{\partial u_y}{\partial x} \; ; \; \beta = \frac{\frac{\partial u_x}{\partial y}dy}{1 + \frac{\partial u_y}{\partial y}dy} = \frac{\partial u_x}{\partial y} \tag{9.12}$$

The angle γ_{xy} is equal to the sum of the partial derivatives and it can be used in the tensor definition:

$$\epsilon = \begin{pmatrix} \epsilon_x & \gamma_{x\,y}/2 & \gamma_{x\,z}/2 \\ \gamma_{y\,x}/2 & \epsilon_y & \gamma_{y\,z}/2 \\ \gamma_{z\,x}/2 & \gamma_{z\,y}/2 & \epsilon_z \end{pmatrix} \tag{9.13}$$

Form the definition of the single terms of the tensor it possible to write the previous matrix in a compact form using the derivatives of the displacements.

The constructive equation relates the stress and the strain and it's a feature of the used material. The relation is written supposing a linear behaviour of the material and the properties of the material are constant with the stress.

$$\sigma = C\epsilon \tag{9.14}$$

The constructive equation is the extension to a general case of the Hooke's law. For a spring or a body with linear behaviour for small loads the relation between the force and the deformations $F = k\Delta x$. The constructive equation is related with the local features of the material. For a constructive steel as the one used for the compressor manufacturing the properties of the material are supposed to be homogeneous in the different points and in the different directions. The C tensor for a generic material relates the stress and the strain in the different direction. If the material is homogeneous the tensor is constant in every point while if the material is isotropic the tensor has a simplified form:

$$\frac{E}{(1+\nu)(1-2\nu)} \begin{pmatrix} 1-\nu & \nu & \nu & 0 & 0 & 0 \\ \nu & 1-\nu & \nu & 0 & 0 & 0 \\ \nu & \nu & 1-\nu & 0 & 0 & 0 \\ 0 & 0 & 0 & (1-2\nu)/2 & 0 & 0 \\ 0 & 0 & 0 & 0 & (1-2\nu)/2 & 0 \\ 0 & 0 & 0 & 0 & 0 & (1-2\nu)/2 \end{pmatrix} \tag{9.15}$$

The relations between the stresses and the strain can be clarified for the normal stress and the shear stress:

$$\sigma_i = \frac{E}{(1+\nu)(1-2\nu)}[(1-\nu)\epsilon_i + \nu\epsilon_j + \nu\epsilon_k] \tag{9.16}$$

$$\tau_{i\,j} = \frac{E}{(1+\nu)}\epsilon_{i\,j} \tag{9.17}$$

The relations between the stress and the strain are local and referred to a elementary solid with infinitesimal dimensions. The solution for the complete body is obtained with the integration of the local deformation requiring the the distribution of the strain in the body. To solve the stress and strain field in the solid two way are possible the analytical way or the numerical way. With some hypothesis the stress and the strain field is defined by analytical functions but this kind of solutions are available only for some easy problems. The Euler-Bernoulli beam theory is the most important example where the geometrical constrain are the dimension and the loading. For a beam the one dimension have to be much bigger than the others while the loading have to be applied only on the beam tip. The beam theory can still give us some qualitative information about the behaviour of the blade under the centrifugal and pressure loading but to solve the complete problem is necessary a fully three dimensional model with a general solution. The solution is obtained using a finite element model hence numerical techniques. The finite element methods (FEM) starts from differential equations and some boundary conditions as founded for the fluid-dynamic problem.

9.2 Mesh generation and loading definition

A structural analysis was already carried out during the design of the compressor, but that one was simplified and gave only some partial results. The previous analysis considers only the first rotor because the blade is the longest and only the centrifugal force was counted because the pressure data were missing. The structural design presented an uncertainty, but the stresses and the deformation in the first rotor blade were much smaller than the limit. A complete structural analysis is necessary to have a correct result and to

know also the stresses in the other blades and to see the effect of the different pressure load induced by the fluid. To carry out the complete study is necessary to connect the structural solver and the CFD solver, this is done in Ansys workbench where the structural and the fluid dynamic solver are coupled together. The structural tool start from the material data of the used steel:

density	7700 [kg m^{-3}]
Young modulus	206 [GPa]
Poisson's ratio	0,29

When the properties are defined a geometrical model is imported, the geometry used for the structural analysis is generated in CREO 2 because the blade will be meshed instead of the flow field around the blade. The blade and the hub in the rotors, the blade and the casing in the stator are the volume model which are imported in the step format. In the Mechanical tool the first steep is the mesh definition, this is automatically generated by the program, the latter generates a unstructured mesh using tetrahedral elements to split the domain. The mesh features are the same for all the geometrical configurations.

Use Advanced Size Function	Off
Relevance Center	Fine
Element Size	Default
Initial Size Seed Active	Assembly
Smoothing	Medium
Transition	Fast
Span Angle Center	Coarse

To increase the number of elements on the blade surface and increase the quality of the result a mesh refinement is attached on the blade surfaces. This

avoids to lose some information of the pressure field in the data transferring because also the pressure field is defined not as a continuous function but using the points of the mesh.

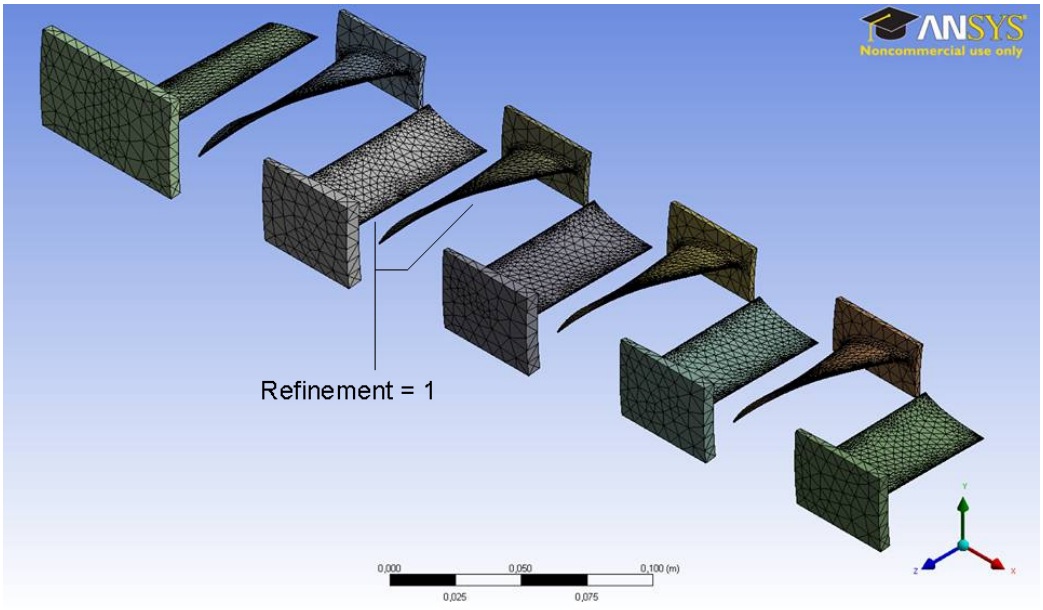

Figure 9.1: Element distribution in the different stages

After the mesh definition is necessary to define the loading and the boundary conditions. The constrains are necessary at the blade root to fix the boundary conditions of the problem. In the blade five surfaces are fixed so the deformation of the solid in this model is equal to zero. The rotors are setted in motion because they have a rotational speed of 11500 [rpm], the rotation induce a centrifugal force on the blade. The centrifugal force generates traction and bending moment in the blade since it is twisted and the normal traction force in the local element passing thought adjacent mass induce a complete three dimensional stress. The second load on the blade is the pressure field on the blade's surface imported from the CFD result.

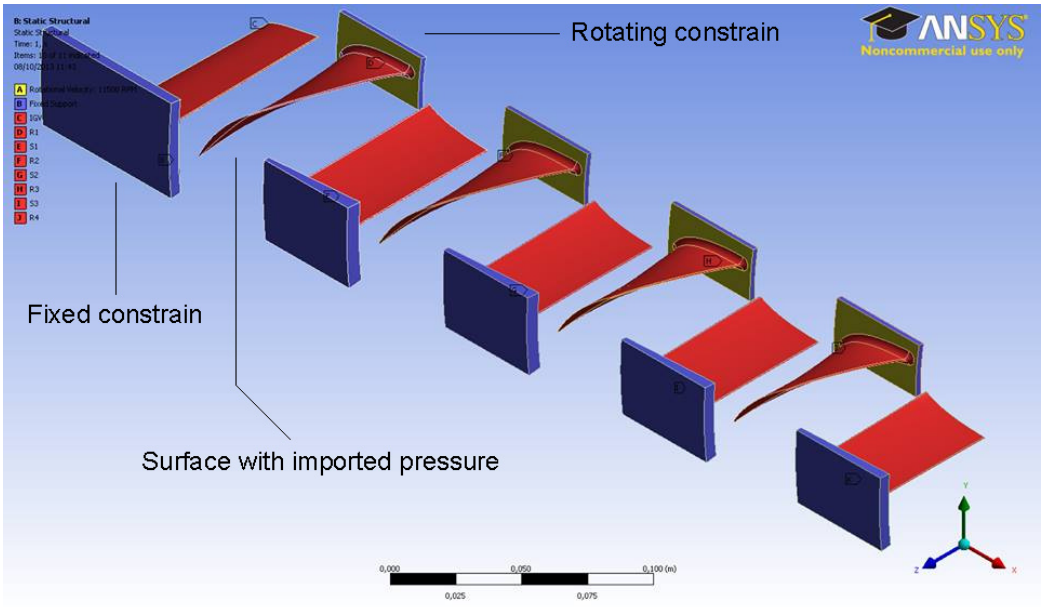

Figure 9.2: Element distribution in the different stages

The main effect of the pressure is the blade's bending because the pressure side normally works with greater pressure than the suction side. The flow deflection induces the pressure difference between the blade's sides and this changes with the operating conditions of the compressor and the geometrical configuration.

9.3 Results

For all the geometrical configurations and for different operating points the structural analysis is carried out, the monitored parameters are the total deformation the maximum stress and deformation in the z direction. The tip clearance between the blade and the casing is 0,25[mm] for stators and rotors, this limit is important mainly for the rotating blade. The rotor's blades are loaded by the fluid load as the stators but there is also the centrifugal force

which stretch the blade as well. The length of the blade influences the stress and the deformation too, if we sketch the blade as beam with a fixed end, centrifugal load and the pressure field which bends and stretch the blade increases the stress and the deformation increasing the blade's size. The bending moment if the pressure is uniform on the surface is a parabolic so the its maximum value is located at the beam root and it's proportional to L^2. As well also the centrifugal force increases its effect increasing the length of the blade because the strain is constant along the blade but the it's size and the deformation at the tip change. The different motion of the blades and the different size suggest that the most loaded and the most deformed blade are in the first rotor. The blade loading change with the operating point and if the pressure difference between the blade's side is connected with the pressure ratio the most loaded configuration is the one with maximum pressure ratio in the first rotor.

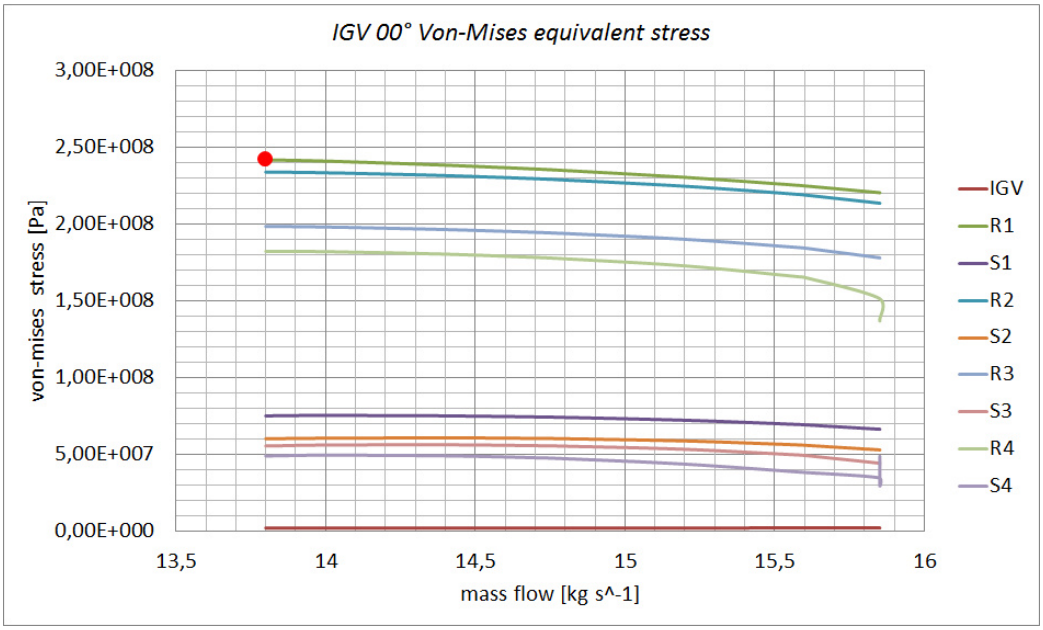

Figure 9.3: Maximum stress in the different rows for the base configuration

This simple analysis is proved by the result in the base configuration with the IGV's angle equal to zero the most maximum stress occur in the last stable point with mass flow equal to 13,8 [kg s^{-}1]. The maximum stress is located in the first rotor and the most loaded zone is near the blade root where the bending moment has the maximum effect and the fillet influence the stress distribution.

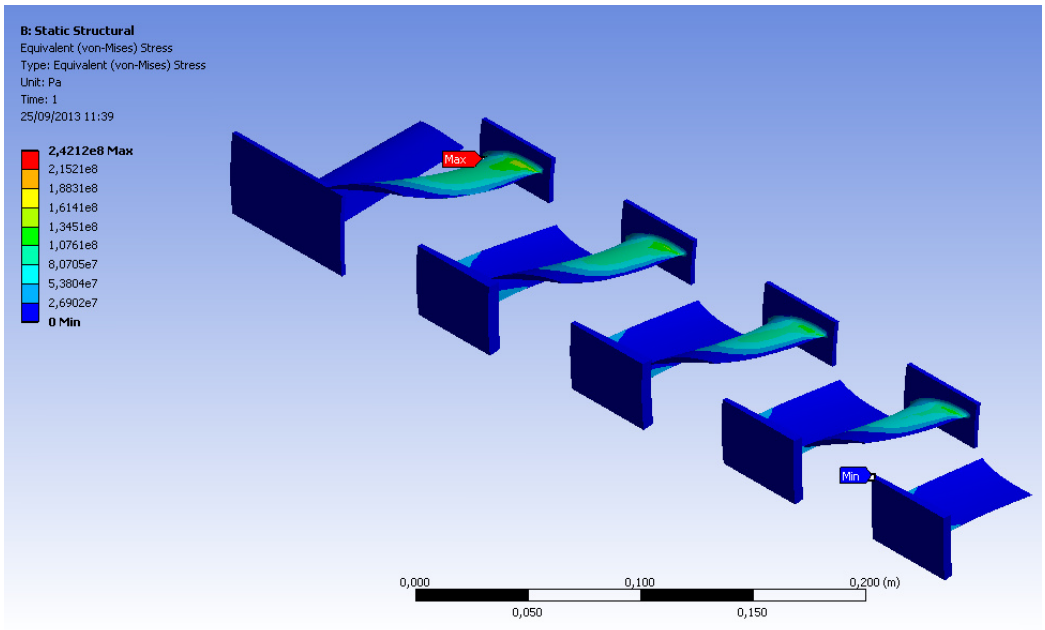

Figure 9.4: Von - Mises stress distribution for the last stable operating point

The maximum total deformation is located at the tip of the blade but it's important to control the component in the radial direction. In the first rotor occur the maximum z deformation which is equal to 0,048 mm while the tip clearance is 0,25 mm so it stands the test. Also the stress test is standed because the maximum stress is 242,1 MPa while the maximum stress available for the material is 500 MPa. For the other configuration the new matching between the blade change also the loading on the stages and the position stress pick.

IGV's angle	Max z def. [m]	Max Von-Mises [Mpa]	Max total def. [m]
-15°	0,0539	290,5	0,5801
-10°	0,0523	290,3	0,5592
-5°	0,0498	285,2	0,5197
0°	0,0481	242,1	0,4805
10°	0,0403	255,2	0,3720
20°	0,0466	234,9	0,3215
30°	0,0651	231,0	0,4615

The data from the table show how the maximum load increases for negative IGV angle this is the consequence of the greater load induced by the IGV. The total deformation has the same trend meaning the configuration with the higher failure risk because of the stress is the -15° where the maximum stress is located in the blade root in the first rotor as expected.

The maximum stress is not obtained at the surge line but it occur with mass flow 15,2 [kg s^{-1}] and pressure ratio 1,8229. The maximum z deformation has in turn an unexpected position since the deformation increases decreasing the IGV angle but for the +30° configuration the maximum occur. The maximum z deformation doesn't occur for the most loaded configuration when the compressor operates near the surge line but critical point is next to the choke line when the machine work with the first stage as a turbine. The pressure side and the suction side are inverted and this changes the deformation of the blade. Also the point with the maximum z deformation changes because in the other configurations this is located at the blade's leading edge while here is close to trailing edge.

The maximum value founded for the +30° allows to run the compressor since the deformation is 0,0651[mm] almost one fourth of the tip clearance.

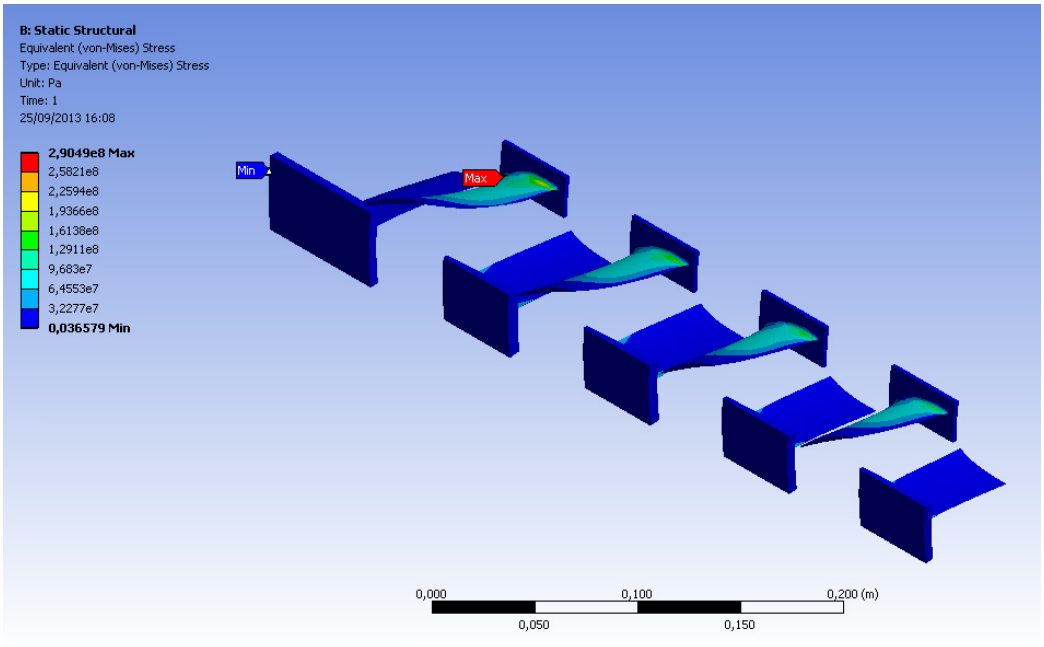

Figure 9.5: Von - Mises stress distribution for the configuration with the highest stress

The result in the analysis present an uncertainty because of the difference between the imported load and the load in the CFD result. For the two critical configuration the effect is investigated considering the possible effect of the different imported load. The stress and the deformation are the consequence of the centrifugal force and of the pressure field. The first is not affected by uncertainty since the load is evaluated on the model in Mechanical while for the fluid dynamic load the small difference between the CFD and the Mechanical geometries induces some errors.

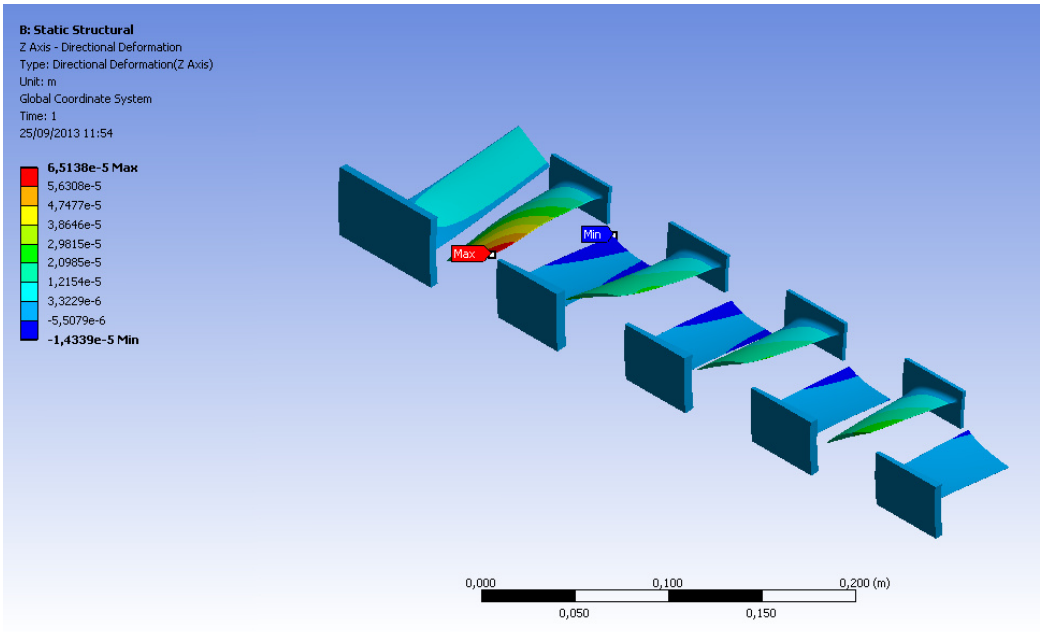

Figure 9.6: Z deformation distribution for the configuration with the greater deformation

	Force CFD [N]	Force mechanical [N]	Δ F %
F_x	-48,443	-49,019	1,189
F_y	52,474	51,412	2,024
F_z	-22,333	-26,825	20,11
F_{tot}	74,818	75.932	1,457

Because model is linear and the force has a direct effect on the stress the uncertainty is added to the maximum Von - Mises equivalent stress. This is wrong because the error in the force affect only the fluid load, but the most loaded point with the complete load is not the same with the two different loads added separately.

$$\sigma = 290,5 \pm 4,25 MPa \tag{9.18}$$

The same reasoning is carried out for the maximum z deformation where the

imported forces are:

	Force CFD [N]	Force mechanical [N]	Δ F %
F_x	14,495	14,231	1,821
F_y	-8,122	-8,435	-3,853
F_z	-17,874	-21,987	23,011
F_{tot}	24,404	27,488	11,291

The maximum z deformation is thus increased of the uncertainty but it is still lower than the tin clearance:

$$\Delta_z = 0,0651 \pm 0,0074mm \tag{9.19}$$

Adding the uncertainty to the results these are still usable because during the design the elimination of the fluid load on the blade forced the designer to use high factor of safety and a great space between the blade tip and the casing. When the IGV unload the first stage are also reduced the stress and the deformation, hence for the positive IGV configuration the failure risk decreases in the first stage. The second rotor for the $+20°$ and $+30°$ configurations become the most loaded and here occur the maximum equivalent stress and the maximum deformation. The IGV have a different behaviour respect to the other blades, IGV increase the maximum stress and the maximum deformation changing the angle from the zero position. As well increasing the the mass flow the blade load increase while normally for the other blades the maximum stress occur when near the surge line.

Chapter 10

Conclusion

The carried out study is a preliminary investigation before the experimental analysis, which have to predict the compressor behaviour, analysing the risk during the real run. For this reason the structural analysis is carried out after the fluid dynamic one, this allows to obtain the results regarding all the performance of the machine. The lack of experimental results, also on the base configuration, subtracts credibility on the computational results. Thus the complete mesh independence study is carried out all along the operating line for the base configuration and not only in one operating point. It show well agreement between the results whit different mesh size, hence these waiting for experimental confirm give us interesting qualitative informations on the machine behaviour and on the flow inside. The four stages compressor is designed in order to work with IGV in a neutral position with a stagger angle equal to zero, this doesn't induce any flow deflection. The new orientation of the blades generate two kind of effects, primary and secondary effects. The primary effect is the new load of the fist rotor, decreasing the IGV's angle the incidence increases and the blade is more loaded, but the load is not uniform. The secondary effect are the consequences of the new matching on the rear

stages. As seen the incidence distribution is not constant along the span, on the first rotor the incidence angle is negative and it increases along the span for positive IGV's angles while the incidence is positive and it decreases along the span for negative IGV's angle. The non uniform distribution on the first rotor induce a vortex rising at the first rotor root, with negative IGV angle the vortex grows on the suction side while with positive angle it grows on the pressure side.

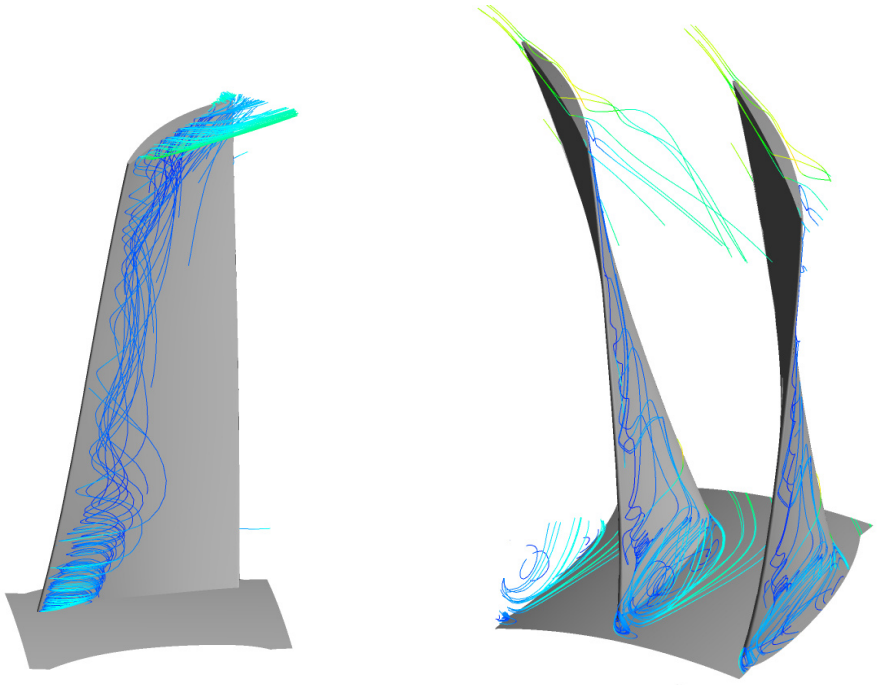

Figure 10.1: Vortex in the first rotor for the +30° configuration (left) and the -15° configuration

The new distribution of the speed changes also the performance in the rear stages which don't work any more as designed with constant axial speed along the span and flow in the axial direction at the stator outflow. The incidence distribution at the rear rotor's inlet has the same trend of the

first rotor outlet as seen previously. For a not stalled profile the deflection at the profile outlet increases with the incidence angle because the pressure difference between the blade's surface is greater. The outflow angle thus is proportional to the inlet angle both in the rotor and in the stator. Supposing a two dimensional flow in the rear stages has the same distribution founded in the first rotor inlet:

$$\tan(\beta_{in}) = \frac{u - c_u}{c_{ax}} = \frac{u}{c_{ax}} - \tan(\alpha_{out}) = \frac{u}{c_{ax}} - \tan(m\,\alpha_{in}) \tag{10.1}$$

$$\tan(\alpha_{in}) = \frac{c_u}{c_{ax}} = \frac{u}{c_{ax}} - \tan(\beta_{out}) = \frac{u}{c_{ax}} - \tan(m\,\beta_{in}) \tag{10.2}$$

Where m is a coefficient almost constant if the blade is not stalled, if in the first rotor the incidence increases and the angle increases in the rear stator the blade load decreases while in the second rotor the incidence increases again. The inflow angle distribution are almost the same in all the rotors and stators, but the stages damp the not uniform speed profile inducing the distribution defined in the design conditions. The new speed distribution have some positive effect as seen in the configurations with positive IGV angle where the maximum performance of the rear stages are greater than the one obtained in the base configuration. The incidence distribution in the first rotor increase the blade load in the tip region and unload the blade root, this allow to obtain with the same averaged inlet angle a greater energy exchange.

The new development for the compressor could be the movement of the first stator, the new matching between IGV and first rotor can be corrected by the first stator. The compressor already changed geometry generating six different machines now is necessary to find for the new configuration the better solution regarding pressure ratio and energy exchange, which can be obtained moving the first stator. The new aim is the logical consequence of

this investigation, the compressor has to increase its operating range as already obtained but it can still work better because of the matching correction which are not optimized.

Appendix

In order to provide detail about the compressor usage and about its performance the maps of every single stage are plotted:

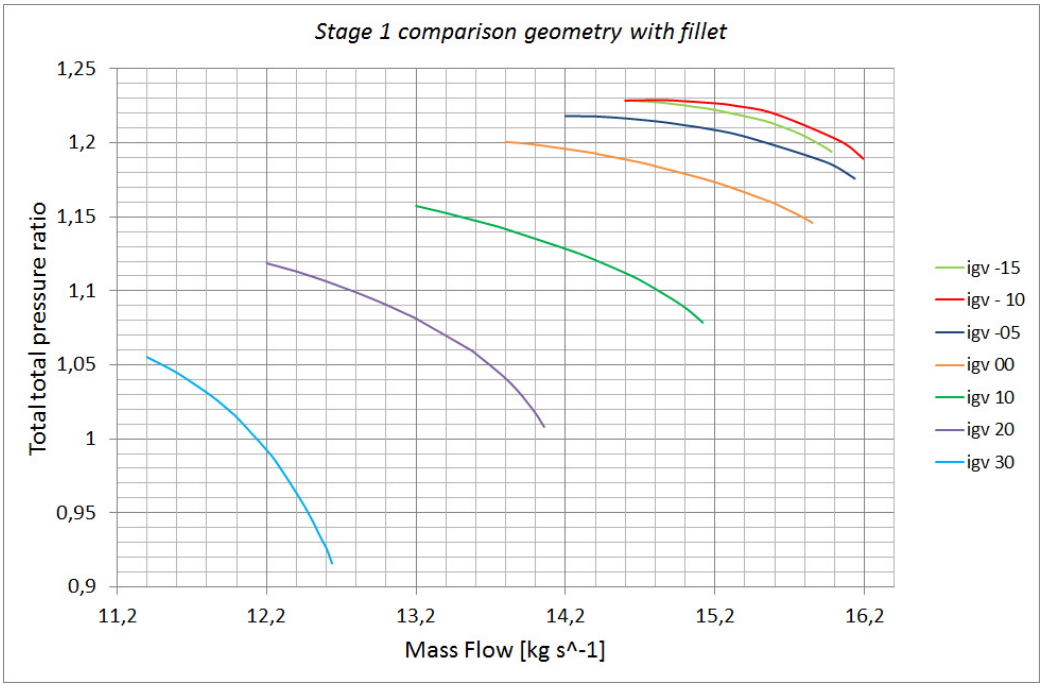

Figure 10.2: Pressure ratio for the first stage

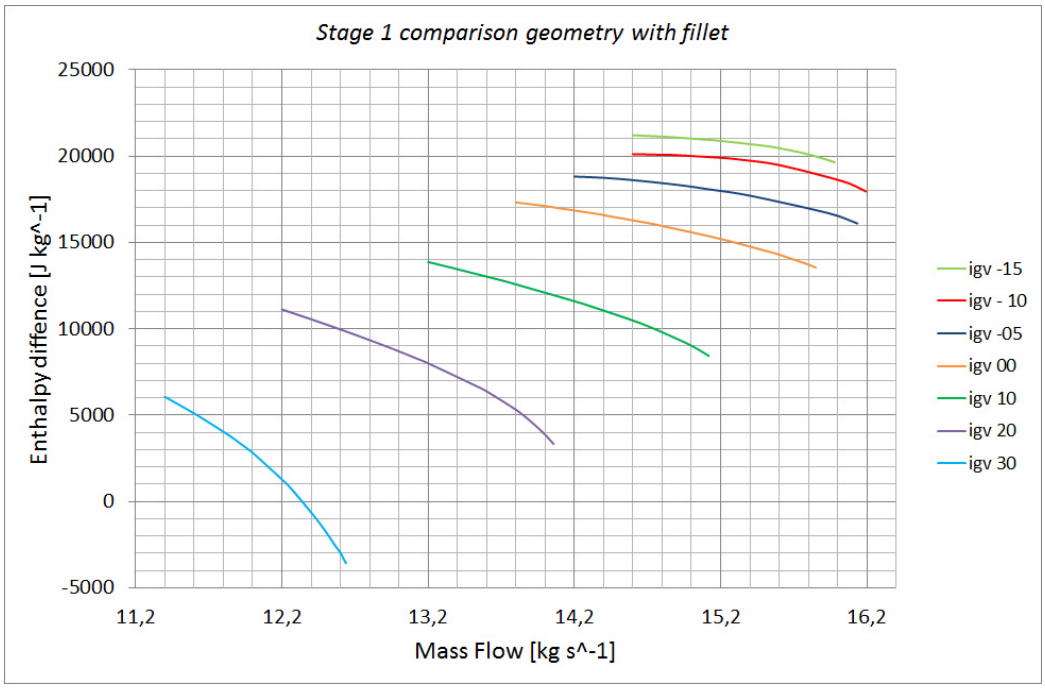

Figure 10.3: Enthalpy difference for the first stage

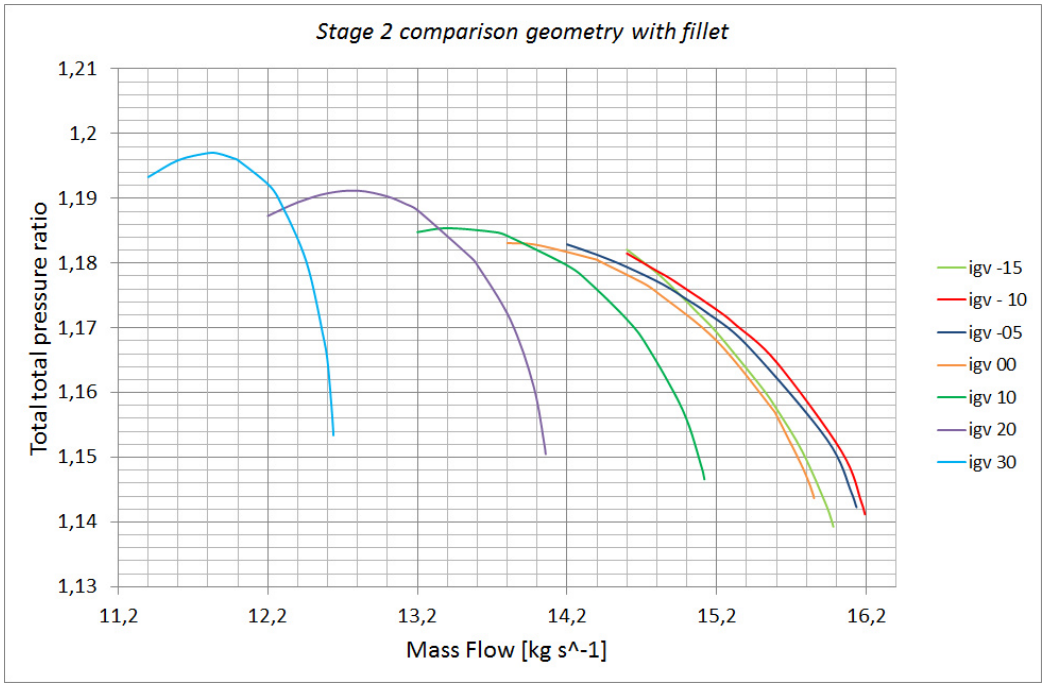

Figure 10.4: Pressure ratio for the second stage

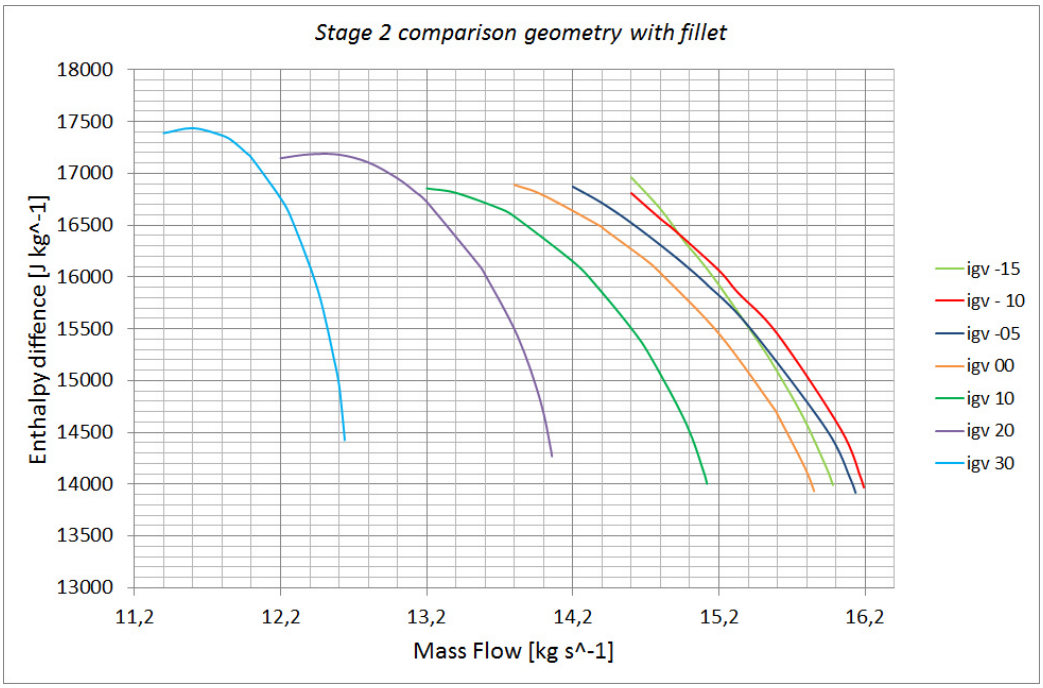

Figure 10.5: Enthalpy difference for the second stage

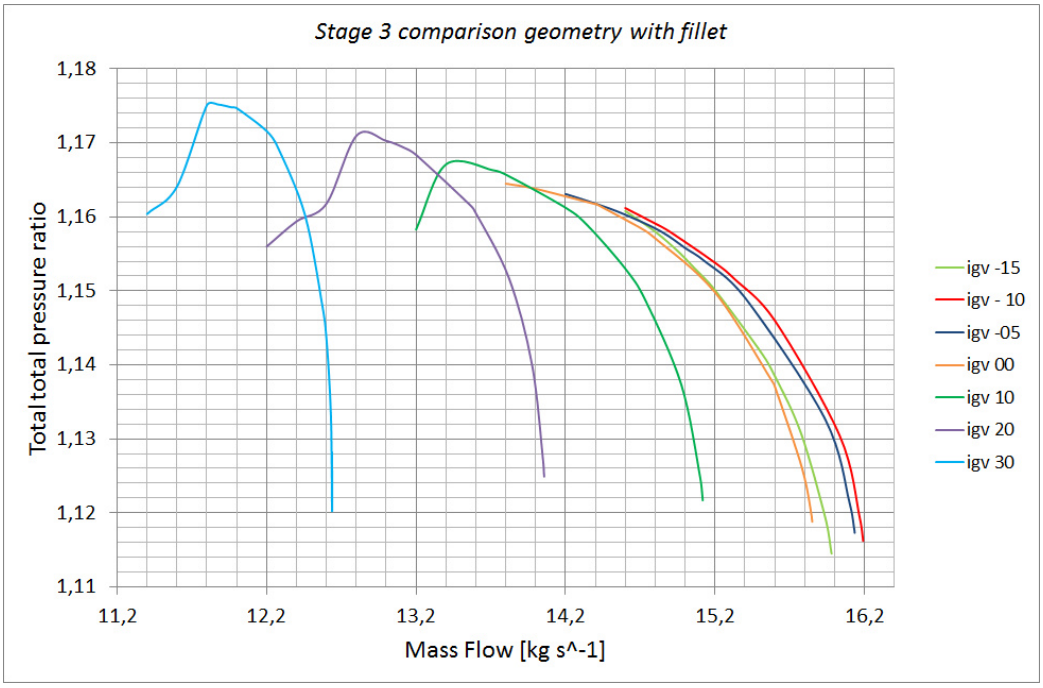

Figure 10.6: Pressure ratio for the third stage

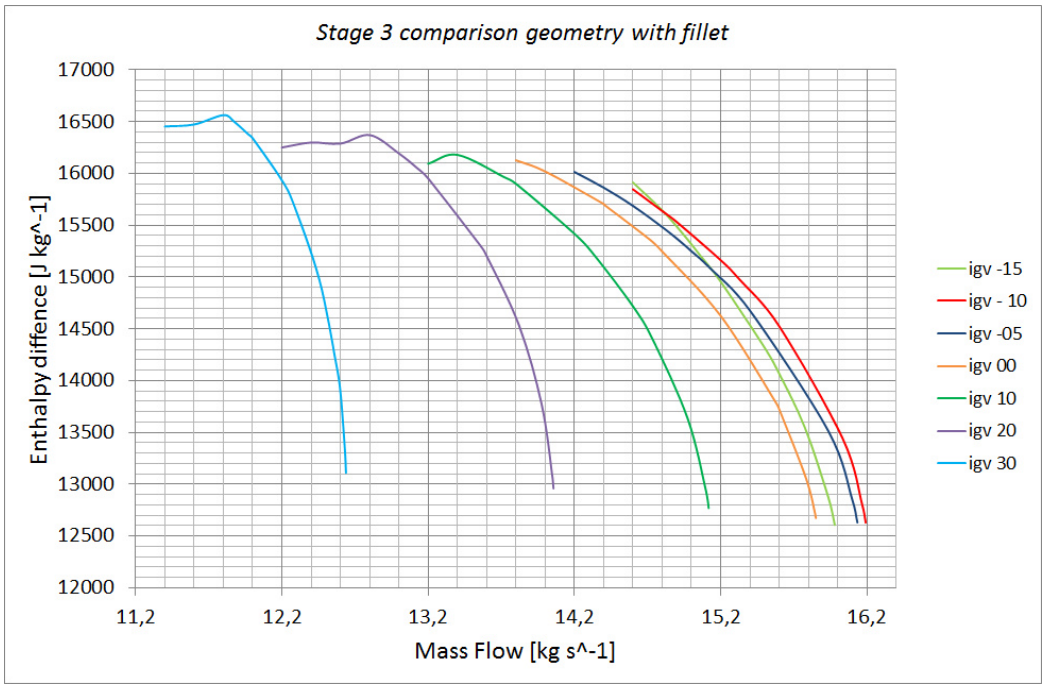

Figure 10.7: Enthalpy difference for the third stage

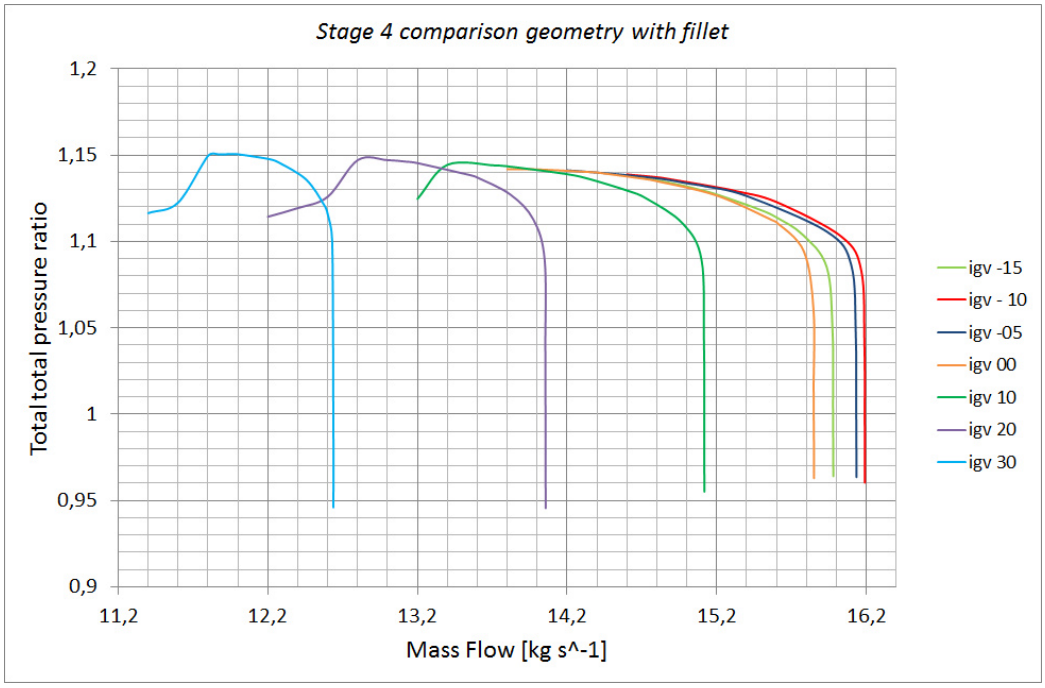

Figure 10.8: Pressure ratio for the fourth stage

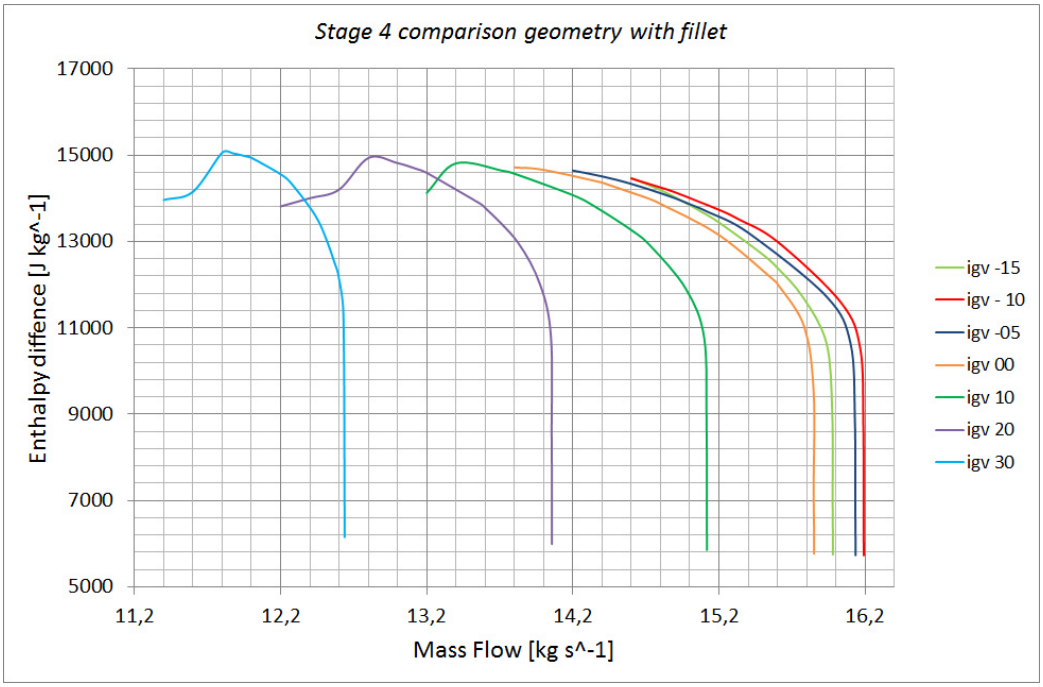

Figure 10.9: Enthalpy difference for the fourth stage

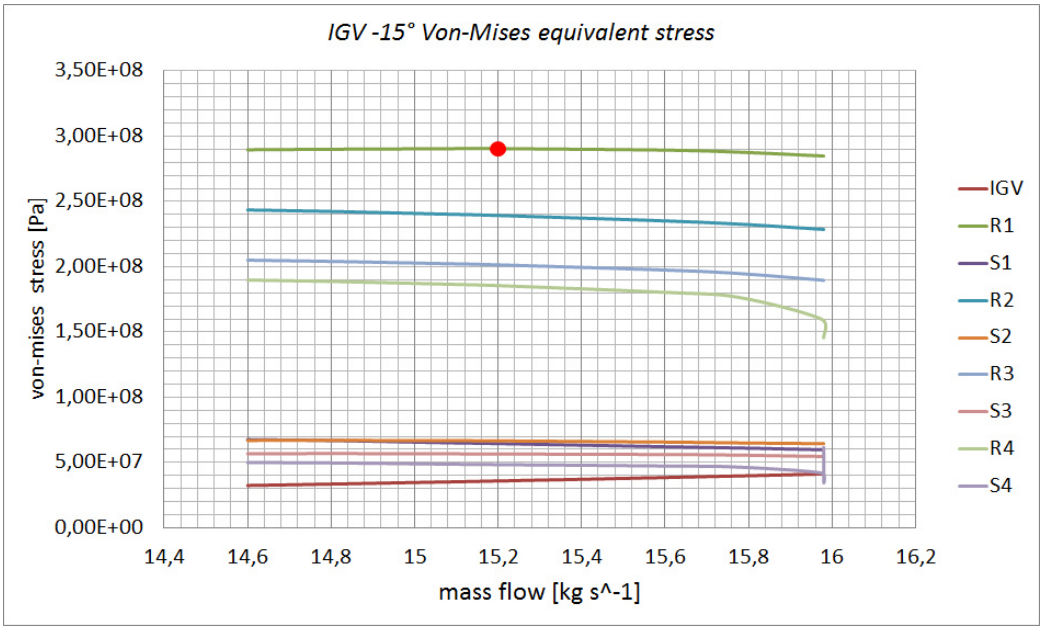

Figure 10.10: Maximum Von-Mises for the -15° configuration

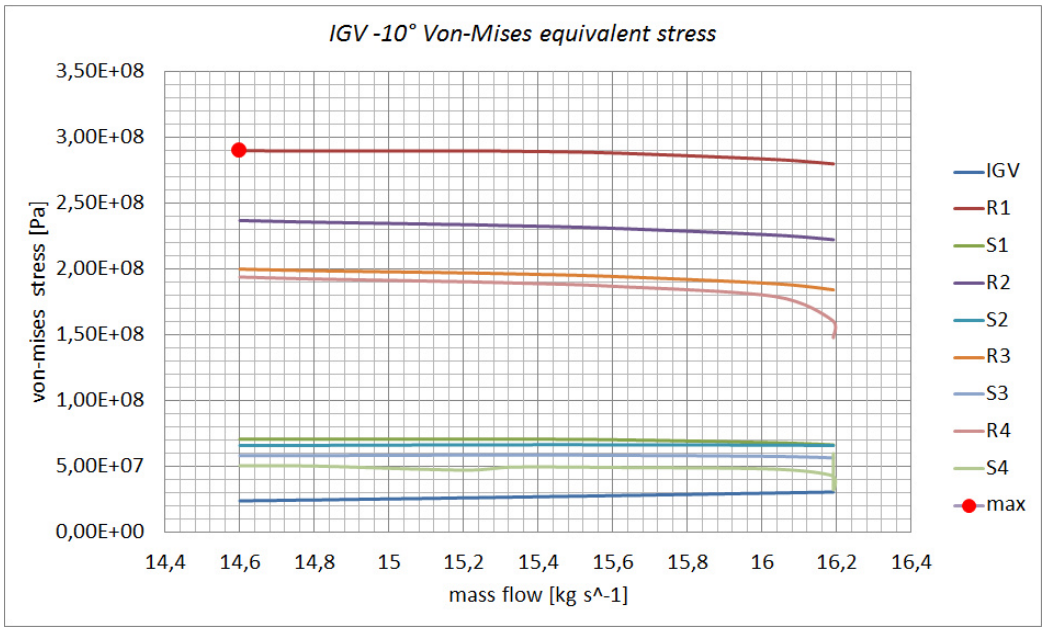

Figure 10.11: Maximum Von-Mises for the -10° configuration

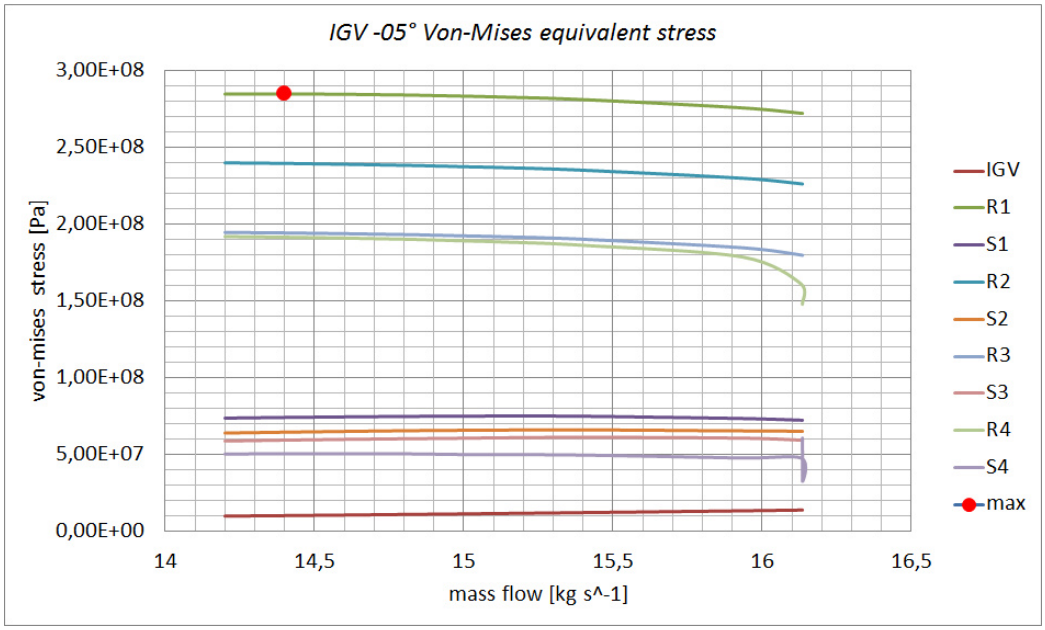

Figure 10.12: Maximum Von-Mises for the -05° configuration

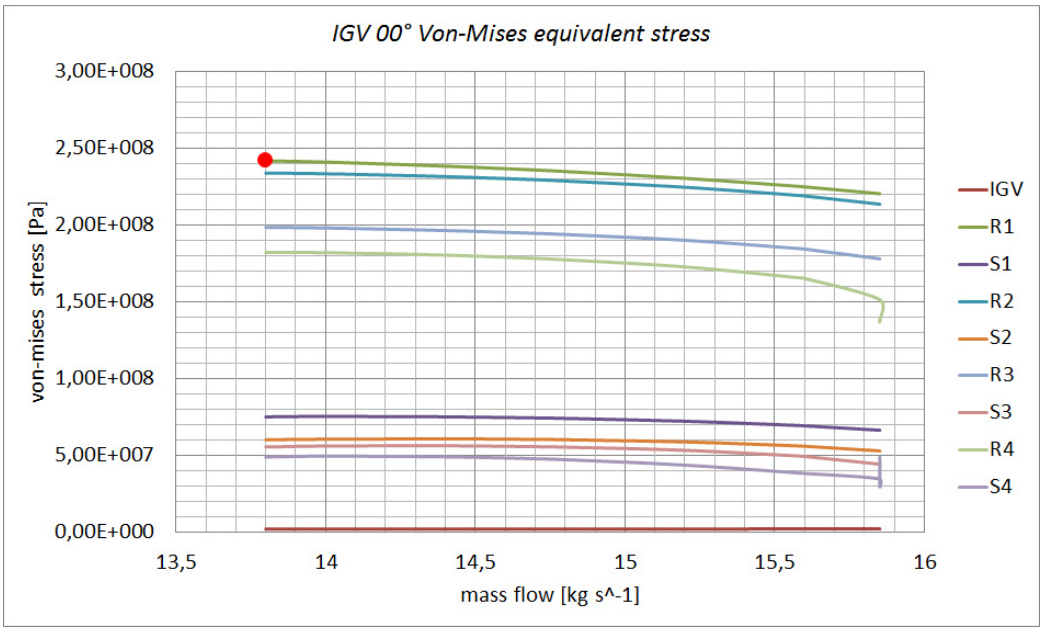

Figure 10.13: Maximum Von-Mises for the 00° configuration

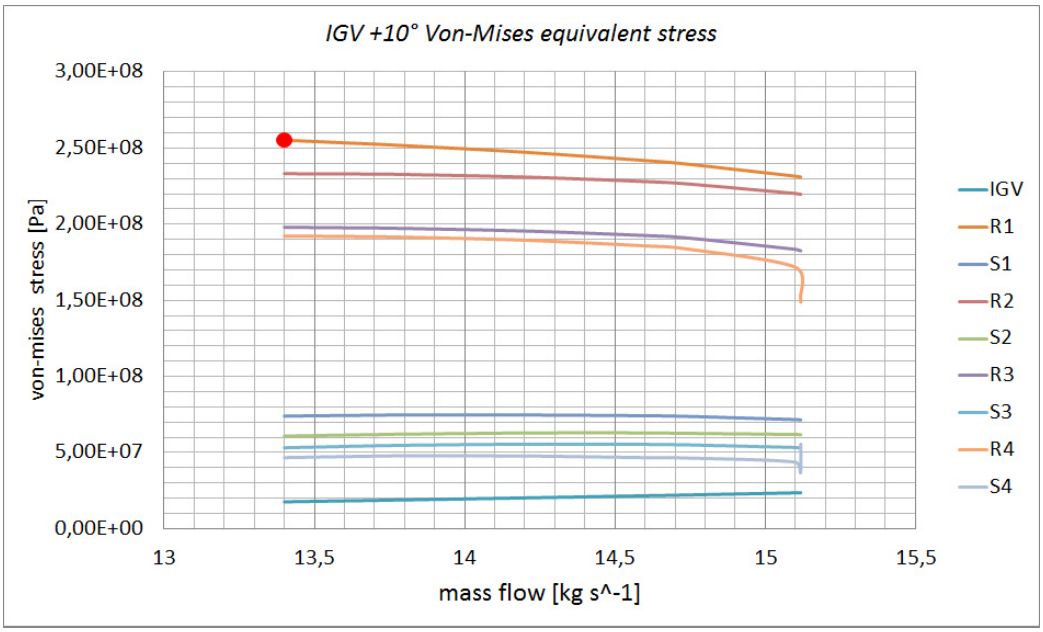

Figure 10.14: Maximum Von-Mises for the +10° configuration

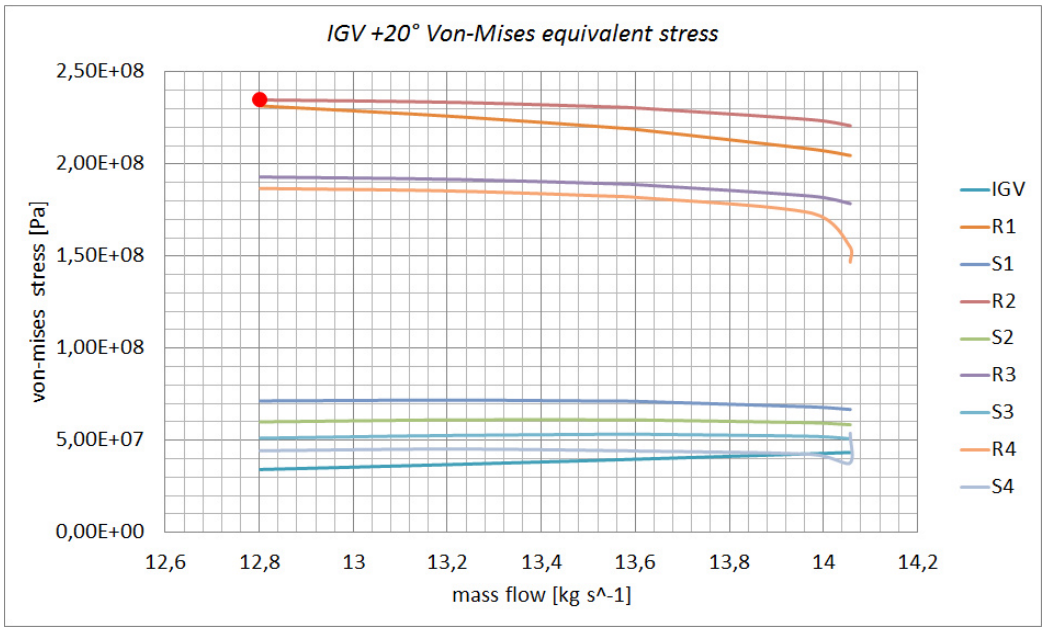

Figure 10.15: Maximum Von-Mises for the +20° configuration

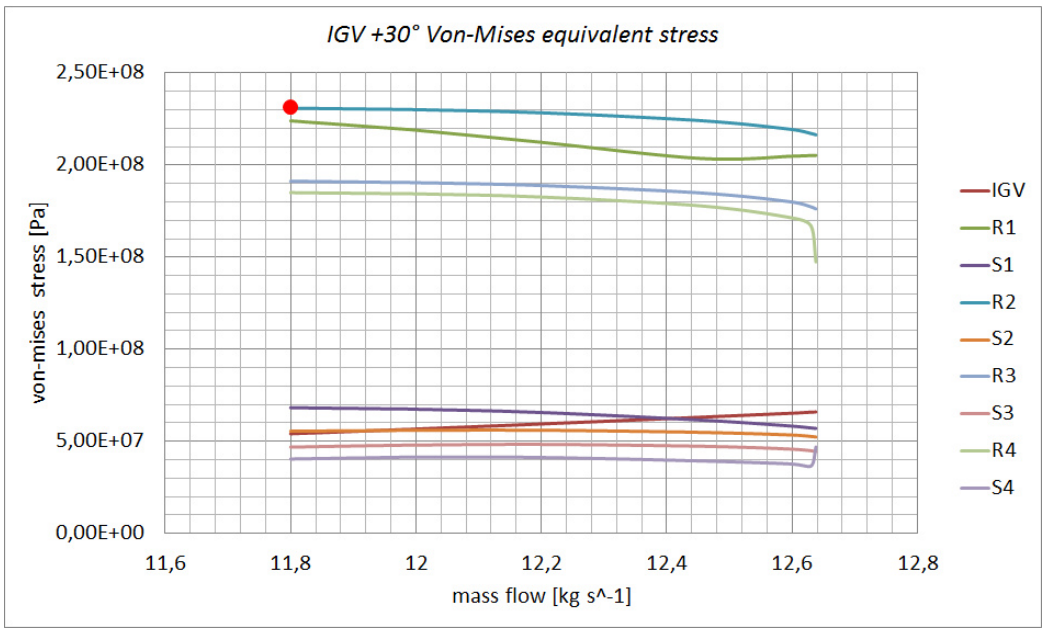

Figure 10.16: Maximum Von-Mises for the +30° configuration

Bibliography

[1] Perry, R.H. and Green, D.W. *Perry's Chemical Engineers' Handbook*. McGraw-Hill Companies, 2007.

[2] Meinhard T. Schobeiri *Turbomachinery Flow Physics and Dynamic Performance*. Springer, 2012.

[3] Dixon S.L. *Fluid Mechanics, Thermodynamics of Turbomachinery* . Pergamon Press, 1978.

[4] Nagabhushan P. S. *Design and Numerical Investigation of an Axial Compressor Repeating Stage*. Master's thesis 2011.

[5] Navier C. L. M. H. *Memoire sur les lois du mouvement des fluides*. Mem. Acad. Sci. Inst. France 1822.

[6] Wilcox D.C. *Re-assessment of the scale-determining equation for advanced turbulence models*. AIAA Journal vol.26 no. 11 1988.

[7] Jones, W. P., and Launder, B. E. *The Prediction of Laminarization with a Two-Equation Model of Turbulence*. International Journal of Heat and Mass Transfer 1972.

[8] Menter, F. R. *Zonal Two Equation k-ω Turbulence Models for Aerodynamic Flows*. AIAA Paper 93-2906 1993.

[9] Taylor J. R. *An Introduction to Error Analysis*. University Science Books, 1997.

[10] Chen, L-Y., Drew, D. A., and Lahey, Jr. R. T. *An Analysis of Wave Dispersion, Sonic Velocity and Critical Flow in Two-Phase Mixtures*. NUREG/CR-3372, 1983.

[11] C.S. Tan, I. Day, S. Morris and A.Wadia *Spike-Type Compressor Stall Inception, Detection and Control*. Annu. Rev. Fluid Mech. 2010.

[12] Greitzer EM. *Surge and rotating stall in compressors. Part 1 and 2.*. ASME J. Eng. Power 98:190-217, 1976.

[13] McDougall NM, Cumpsty NA, Hynes TP. *Stall inception in axial compressors.*. Turbomach. 112:116-25, 1990.

[14] Vo HD, Tan CS, Greitzer EM. *Criteria for spike initiated rotating stall.*. ASME J. Turbomach. 130:1-8 2008b.

[15] Robert Meyer, Sebastian Schulz, Karsten Liesner *A PARAMETER STUDY ON THE INFLUENCE OF FILLETS ON THE COMPRESSOR CASCADE PERFORMANCE*. JOURNAL OF THEORETICAL AND APPLIED MECHANICS, 2010

[16] Curlett B. P. *The Aerodynamic Effect Of Fillet Radius in a Low Speed Compressor Cascade*. Von Karman Inst. for Fluid Dynamics (NASA), 1991

[17] Di Walter D. Pilkey,Deborah F. Pilkey *Peterson's Stress Concentration Factors*. A Wiley-lnterscience Publication, 2008

[18] Slaughter, W. S. *The linearized theory of elasticity*. Birkhauser, (2002).

[19] Symon, Keith R. *Mechanics*. Addison-Wesley, (1971).